Master Thesis

Implementation of an Automotive-Grade Time-of-Flight Camera Demonstrator

conducted at the
Institute for Electronics
Graz University of Technology, Austria

in cooperation with
Infineon Technologies Austria AG
Graz, Austria

by
Matthias Brückler, BSc.

Supervisor
DI Krum Beshinski

Assessor
Univ.Prof. DI Dr. Bernd Deutschmann

Graz, June 17, 2020

Statutory Declaration

I declare that I have authored this thesis independently, that I have not used other than the declared sources/resources, and that I have explicitly marked all material which has been quoted either literally or by content from the used sources.

Date

Signature

Abstract

Time-of-flight is a 3D-imaging method that collects the z-distance based on propagation delay measurements. Over the last years more and more use cases for this technology were developed. In automotive market this includes in-cabin sensing for gesture control, driver drowsiness detection, people recognition and a lot of others. These tasks need an automotive grade, robust, efficient and precise camera system.
The most important outcome of this master thesis is a demonstrator for such a camera system. For low complexity in the car connections a serializer-deserializer approach was chosen. To get confident with this approach evaluation boards were ordered and adopted to work with existing consumer-cameras. Then a first prototype was developed and tested successfully. To evaluate the best performance, systems with different iltuminations and camera interfaces were built and tested.
Out of these results the finalized demonstrator was built and characterized. To speedup future serializer-deserialzer projects from *Infineon Technologies*, an Application-Note with a design description was written.
For sufficient evaluation also a basic calibration was performed, this includes lens focus, lens parameters, offset, temperature drift and wiggling error. The results indicate the good performance of the demonstrator for automotive in-cabin 3D-sensing.

Acknowledgment

I would like to thank Dipl.-Ing. Krum Beshinski at Infineon Austria AG for supervising my thesis, his experienced feedback and the support of my ideas.

Futhermore I would like to thank Univ.Prof. DI Dr. Bernd Deutschmann, from the Institute for Electronics at the TU Graz for his support and remarks especially during the writing process.

I would like to acknowledge the company Infineon Austria AG, in particular Dipl.-Ing. Dr. Vjekoslav Matic, for the pleasant working atmosphere and the chance to deeply investigate this interesting topic.

Special thanks be due my parents and all the people who have supported me during my master thesis.

Matthias Brückler
Graz, June 17, 2020

Contents

1 Introduction

This chapter gives a general overview about 3D-imaging, where it can be used and some state of the art applications. At least the motivation for this thesis is given.

1.1 3D-Imaging introduction

T*he first portable camera was designed by Johann Zahn in 1685. Not much progress was made in the development for up to approximately 130 years later. Most of the attempts to make cameras in between were futile. It was not until the year 1814 when Joseph Nicephore Niepce clicked the first photograph.* [Mis17] Since this years camera development rose rapidly, from analog to digital and in the last decades to 3D-images. 3D-pictures add a third parameter, additional to the standard 2D-image also the distance to the sensor is measured. The data can be displayed in different ways, as shown in **Figure 1.1** and **Figure 1.2**. But different to 2D-images the main use case for 3D-images is machine vision. Due to increased importance of automation, world sensing became a very important topic. A accurate world sensing is necessary for a lot of applications, for example:

- Gesture control
- Automated driving
- Augmented reality
- Face recognition
- and many more

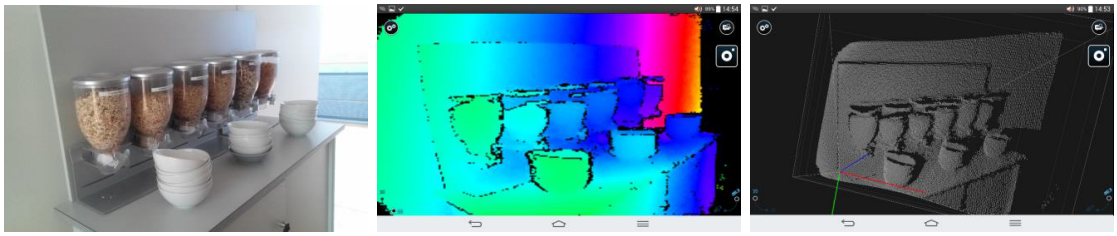

(a) Original scene (b) 2D color coded picture (c) Point cloud

Figure 1.1: Possibilities to display a 3D-picture [Kre16, Page 17]

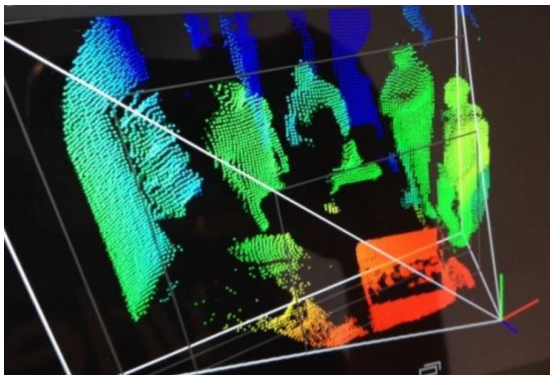

Figure 1.2: Combined point cloud and color code [Kre16, Page 17]

The next chapter will show some state of the art products for this applications.

1.2 3D-Imaging applications

Some already existing solutions for 3D-imaging are:

- ***iPhone X* by *Apple*:** The *iPhone X* uses the 3D-imager mainly for face recognition, this means the camera detects the unique face-shape to unlock the phone (see **Figure 1.3**).

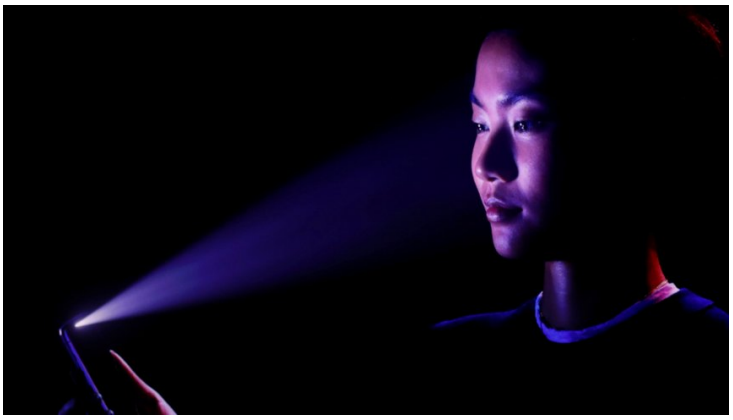

Figure 1.3: iPhone X by Apple [Onl17]

- ***G8 ThinQ* by *LG*:** In contrast to the *iPhone X* the *LG G8 ThinQ* (**Figure 1.4**) uses its 3D-imager for gesture control and hand unlock. Hand unlock uses the front camera together with the 3D camera to detect the hand shape, thickness, veins and other individual characteristics for a safe unlock method.

Figure 1.4: G8 ThinQ by LG [LG19]

- ***Microsoft Kinect*:** The *Microsoft Kinect* (**Figure 1.5**) was initially made for gaming but got very popular in the developer scene for a cheap and easy world sensing implementation.

Figure 1.5: Microsoft Kinect [Car13]

- ***Pico S* by *pmdtechnologies*:** The *pico S* (**Figure 1.6**) is a consumer evaluation camera made by pmdtechnologies.

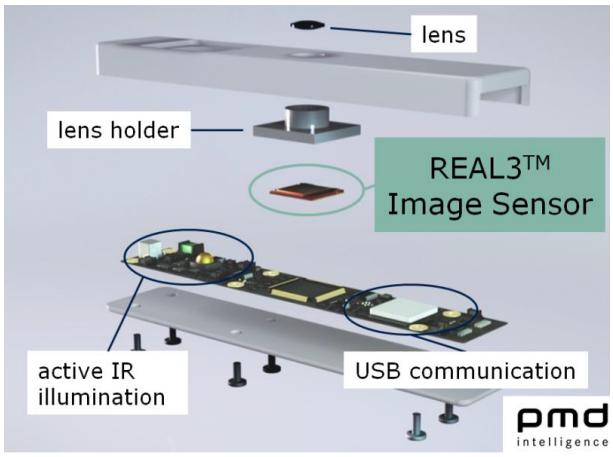

Figure 1.6: pico S by pmdtechnologies [Kre16, Page 16]

- ***Pico Monstar* by *pmdtechnologies*:** In opposite to the *pico S* the *pico monstar* (**Figure 1.7**) is a reference camera for automotive and industrial applications.

Figure 1.7: pico monstar by pmdtechnologies [pmd]

1.3 Motivation

3D-imaging includes a wide field of applications. Time-of-flight is one of the most researched 3D-technologies of the last years. Every use case has different and special requirements and challenges. One of the most challenging markets is the automotive market. A proper automotive grade Time-of-flight camera demonstrator must be suitable to demonstrate the technology, evaluate use cases, evaluate products and should have a detailed functional and performance characterization.
Because of these reasons a demonstrator must fulfill strict requirements regarding precision, robustness, operation temperature and complexity.
A fitting image sensor is provided by *Infineon Technologies*, based on this sensor the demonstrator was developed.
To connect cameras in automotive environment there are two established companies: *Texas Instruments*, with its *FPD-Link* and *Maxim Integrated*, with its *GMSL*-family. One of the most important steps for the demonstrator development is to choose the best fitting link matching the camera requirements.
But for a complete demonstrator there are much more important design considerations, like the proper illumination, power management, thermal management, optical parameters and a sufficient casing including special optical windows.
At least there is also a camera calibration needed, including lens focus, lens parameters, offset, temperature dependency and wiggling error.

1.4 About this Thesis

This Master Thesis is conducted as a collaboration between *Infineon Technologies Austria AG* and the *Institute for Electronics (IFE)* at the *Technical University Graz*.

The structure follows the process of the taken investigations. The first three chapters are the outcome of a literary study and the last three chapters describe the development of the demonstrator.
Chapter 1 explains what 3D-imaging is and for what it is used for. Further on the chapter explains the motivation for the thesis.
Chapter 2 gives an overview over the common optical distance measurement techniques with a comparison between them, this includes interferometry triangulation, structured light, and Time-of-flight.
Chapter 3 afterward describes the Time-of-flight measurement more in detail, starting with the functional principle, later the different optical signals, then the detectors with the demodulation and at least the calculation of the phaseshift.
Chapter 4 mentions the requirements for the automotive Time-of-flight demonstrator and explains the different design-steps to the finalized demonstrator.
Chapter 5 shows the characterization of the demonstrator, including LTS measurements, optical waveforms, voltage- respectively current-measurements and the dimensions of the demonstrator.
Chapter 6 completes the thesis with a summary and an outlook for future developments.

2 Optical distance measurement techniques

This chapter gives a general overview over optical distance measurement methods and describes their function principle. All of this methods have advantages and disadvantages so they are better qualified for different fields of applications. At first a very precise 1D-distance measurement, the Interferometry, is introduced. Afterward the most common technique Triangulation will be described, with the special cases Stereo Vision and Structured Light. Then the basics behind Time of Flight are mentioned and at the end of the chapter an overview of the benefits and drawbacks is given.

2.1 Interferometry

Starting with an 1D-distance measurement, the Interferometry. This method will be described by the Michelson interferometer (**Figure 2.1**).
The basic principle, is the split of one monochromatic light wave, into two parts. They pass different distances, which leads to a phase shift between these two. Then the two light waves get merged and a interference pattern accrues.
At the Michelson interferometer a monochromatic light wave get split at a half transparent mirror. One wave travels straight through the mirror U_2 and one wave is reflected by 90° U_1. The 90° reflected wave U_1 get reflected back to the half transparent mirror by a fixed mirror. The other wave U_2 get reflected back by a moveable mirror or object. Behind the half transparent mirror the two waves interfere with each other.
If the distance between the half transparent and the moveable mirror changes the phase from the wave U_2 shifts. So the interference changes. The amplitude from the interfered wave $U_1 + U_2$ has a maximum at 0° phase difference and a minimum at 180° phase difference. With this method also very small length changes can be detected and measured [Kar09, Page 1].

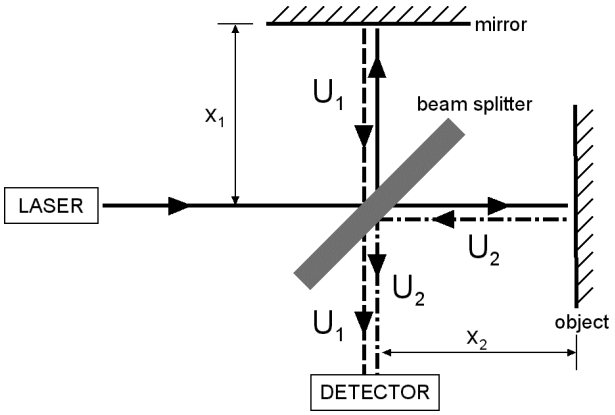

Figure 2.1: Michelson Interferometer [Lan00, Page 14]

Such interferometers can only measure distance changes but no absolute distances. For these relative distance changes the unambiguous range is given by half of the wavelength (half is caused by the way to the object and back) of the used wave.
There are also interferometers working with two different wavelengths, called multiple-wavelength interferometers, these can also measure absolute distances with an accuracy of $\lambda/100$ [ZSD96].

2.2 Triangulation

Triangulation is a geometrical approach for optical distance measurement. There are two types of Triangulation, active- and passive-Triangulation. Both of them are based on a triangle calculation with two known points and at least one angle. Referred to them, the distance can be calculated.

- **Passive Triangulation**
  This technique is used by nature over millions of years, for example by the human eye. As shown in **Figure 2.2** the determining point is observed from two points (eyes), with known distance x (called base) to each other. By measuring the angles α and β, the distance z to the observed point can be calculated by [Lan00, Page 11]:

$$z = \frac{x}{\frac{1}{\tan\alpha} + \frac{1}{\tan\beta}}. \tag{2.1}$$

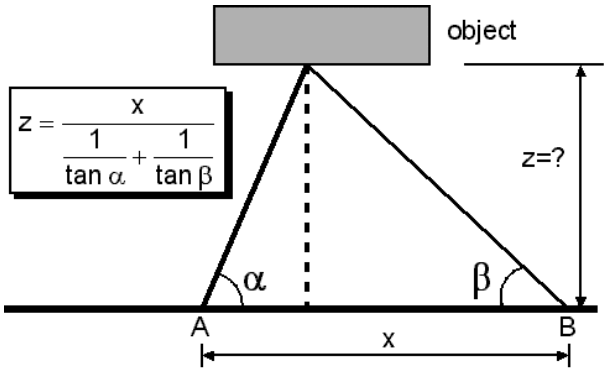

Figure 2.2: Principle of passive Triangulation [Lan00, Page 11]

Each determining point must be identified unambiguously, therefore passive Triangulation require a scene with high contrast and good light conditions. A common application for passive Triangulation is Stereovision.

- **Active Triangulation**
  At active Triangulation one observing point is replaced by a light source. This light source projects a point or a structure (for example a grid or a point cloud) on the determining object. In case of a point source the projection is detected by a position sensitive detector (**Figure 2.3**). The distance can be calculated by the angle α (determined by the focal length h and the position of the point projection x') and the distance between light source and detector, the base x [Lan00, Page 12]:

$$z = \frac{x}{\tan\alpha} = h\frac{x}{x'}. \tag{2.2}$$

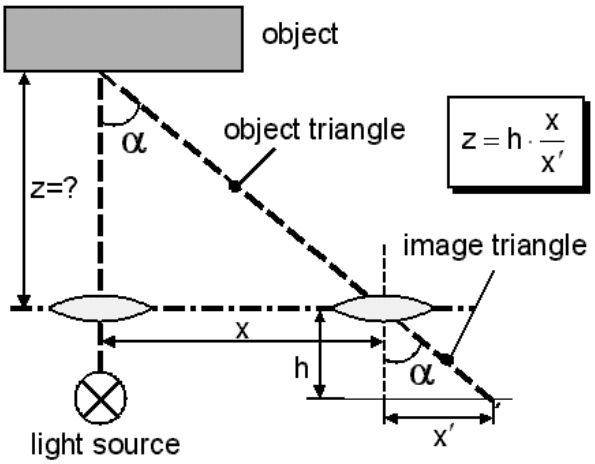

Figure 2.3: Principle of active Triangulation [Lan00, Page 11]

In case of a light structure at least one 2D-detector is required instead of the position sensitive detector. By the use of more detectors shadowing effects can be reduced (**Figure 2.4**). The method of using 2D-detectors for active Triangulation is called Structured Light and will be described more in detail in the next chapter (**Chapter 2.3**).

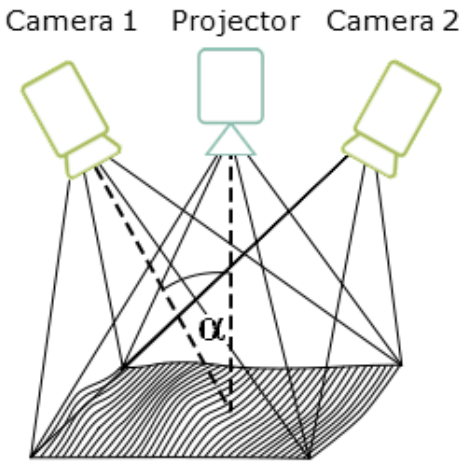

Figure 2.4: Principle of Structured Light [Kre16, Page 6]

2.3 Structured Light

Structured Light is beside Time of Flight (**Chapter 2.4**) one of the most common optical distance measurement techniques in consumer electronics. As mentioned before it is a special case of active Triangulation, it can use a point cloud, a grid or other light shapes projected on an object. The 2D detector observes this shape distorted, caused by the different viewing position (see **Figure 2.4** and **Figure 2.5**).

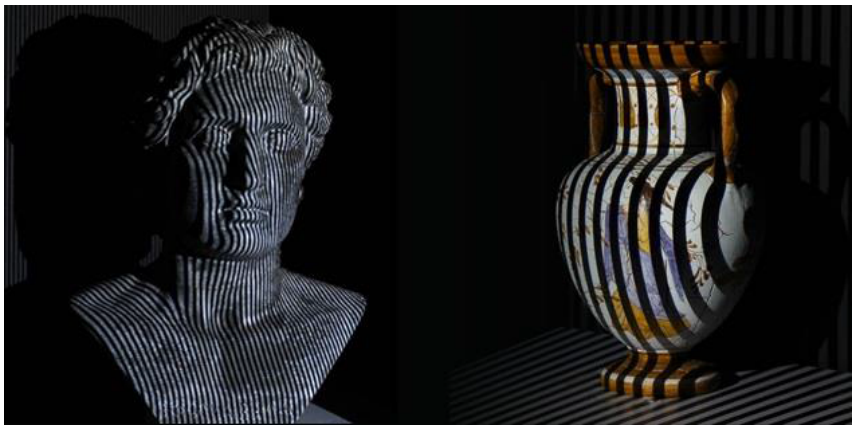

Figure 2.5: Distorted Structured Light [Kre16, Page 5]

Based on this distortion the shape of the object can be calculated. The reconstruction requires complex algorithms and a lot of calculation power. One of the most popular structured light systems is the *Microsoft Kinect*. The *Kinect* uses a infrared point cloud as light structure, as shown in **Figure 2.6**[Kre16, Page 5-7].

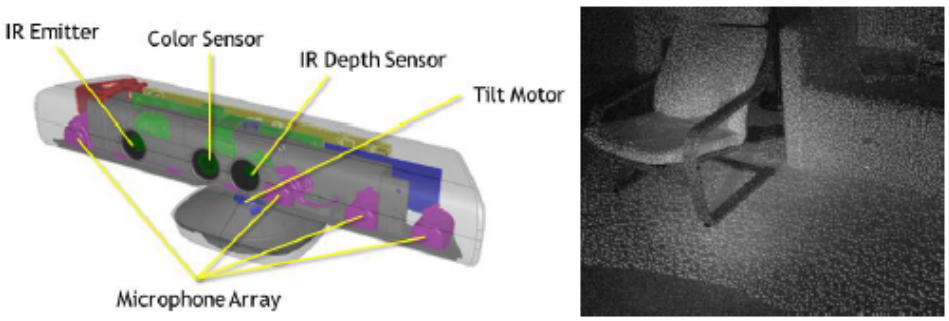

Figure 2.6: Microsoft Kinect (left) point cloud pattern (right) [Kre16, Page 7]

2.4 Time of Flight

The basic principle behind **Time of Flight** (ToF) is to measure the time t_d a light pulse needs to pass the distance from the light source to the target and back to a detector, the speed of light is known as $c \approx 3 \cdot 10^8 m/s$, so the distance can be calculated:

$$d = (c \cdot t_d)/2 \tag{2.3}$$

The factor 2 is caused by the light path to the target and back, the emitter and detector have to be very close together for this approximation, otherwise geometrical calculations have to be added.
For this method a very precise time measurement is necessary. The time needed by the light is very short, for example in *Equation* (2.4) the time needed for 1m distance is calculated:

$$t_d = \frac{2d}{c} = \frac{2 \cdot 1m}{3 \cdot 10^8 m/s} = 6.67ns. \tag{2.4}$$

By this fact most ToF Systems use a different way for the measurement of small distances (**Figure 2.7**). Instead of one light pulse a **continuous wave** (CW) is emitted from the light source. Caused by the time, light needs to travel to the target and back, the

received light is phase shifted to the emitted signal. These two signals get compared in the detector and depending on the phase shift φ_d the distance to the target can be calculated by [Gru13, Page 3]:

$$t_d = \frac{\varphi_d}{2\pi f_{mod}}, \qquad f_{mod} \text{ is the modulation frequency of the CW.} \tag{2.5}$$

Combining *Equation* (2.5) and *Equation* (2.3) results in:

$$d = \frac{c}{4\pi f_{mod}} \cdot \varphi_d. \tag{2.6}$$

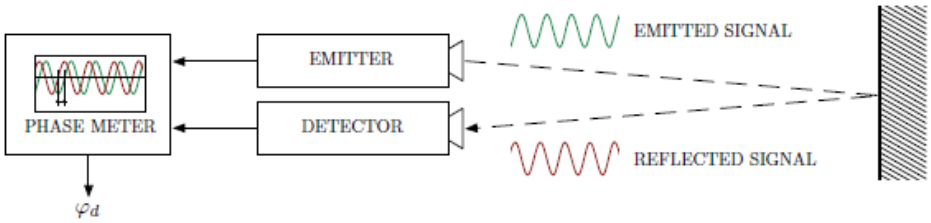

Figure 2.7: ToF principle [Gru13, Page 4] [Lan00, Page 11]

Due to the periodicity of the CW such a ToF system has a limited unambiguous range of $c/(2f_{mod}) = \lambda/2$. After this range the CW is repeating and it is not possible to differentiate between a distance of $0 - \lambda/2$ or $\lambda/2 - \lambda$.
To measure directly the time delay, of a sent and received light pulse, is called **direct Time of Flight**, the measurement of the phase-shift, from a continous wave signal, is called **indirect Time of Flight**. **Chapter 2** gives only a short introduction in all systems. ToF with CW modulation is the used distance measurement technique for this Masterthesis, so a more detailed explanation will be given in **Chapter 3**.

2.5 Conclusion

In the chapters above the different optical distance measurement techniques were explained. This leads to special advantages and disadvantages of every method [Kre16, Page 11]:

Interferometry:

Advantages:

- best accuracy
- low calibration effort
- low power consumption
- low computation needs
- no shadowing
- fast response time

Disadvantages:

- 1D measurement
- low range

Passive Triangulation (especially Stereovision):

Advantages:
- low cost
- no illumination needed
- good accuracy
- good resolution

Disadvantages:
- a lot of computation needed (increasing power and measurement time)
- reduced accuracy under low light conditions
- no possibility to scale the range
- for good accuracy big baseline needed
- shadowing effects
- big calibration effort

Active Triangulation (especially Structured Light):

Advantages:
- good accuracy
- good resolution
- good low light performance

Disadvantages:
- a lot of computation needed (increased Power and Time needed)
- fixed illumination pattern needed
- very high power consumption (computation and illumination)
- high costs
- for good accuracy big baseline needed
- shadowing effects
- big calibration effort

ToF:

Advantages:
- high system compactness
- low costs
- low computation needed
- practical no shadowing
- fast response time
- scalable range
- good low light performance
- good ambient light performance
- low calibration effort
- power consumption scalable

Disadvantages:
- limited accuracy
- for good accuracy or big range high illumination power needed
- limited resolution

Summarizing **Figure 2.8** shows the measurement uncertainty $\frac{\partial z}{z}$ in dependency of the distance z, from the optical distance measurement techniques.

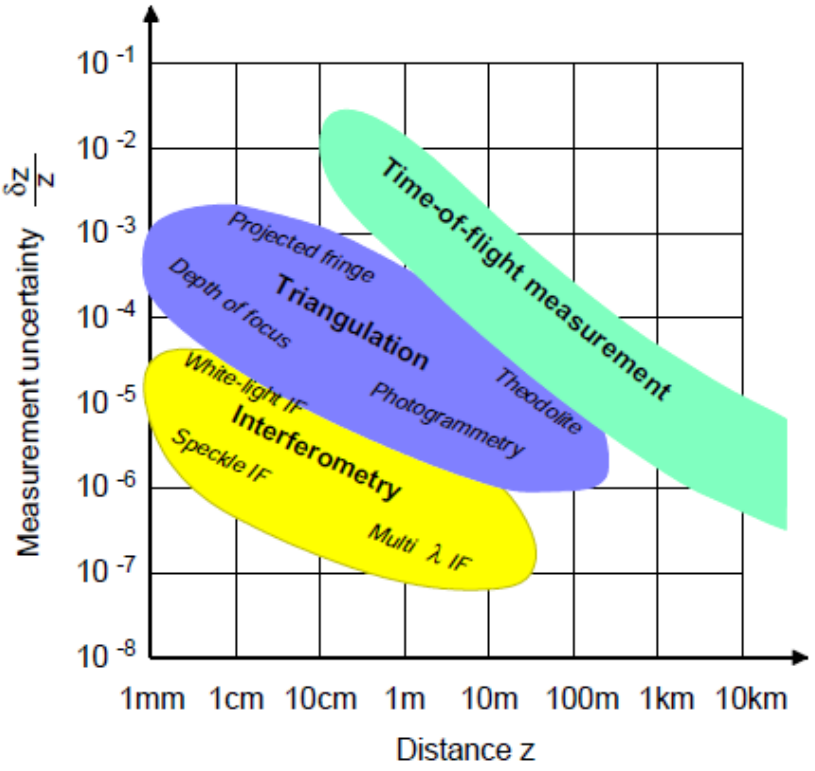

Figure 2.8: Comparison of distance measurement techniques [Sch99][Lan00, Page 25]

Over all Structured Light and ToF are the competing techniques for sensing applications in mass products like smart phones, notebooks or cars. In 3D photographing and filming usually Stereo Vision is used [Kre16, Page 11]. Interferometry is the preferred technology for 1D distance measurements with a high accuracy.
Because of the smaller form factor (for a good accuracy, especially at higher distances a big baseline is needed for structured light), the good low- and high- ambient light performance, the scalable range together with the scalable power consumption, the low shadowing, the lower calibration effort and the fact that a change of the baseline (can happen due to warming of the car chassis) renders the data, from structured light systems, useless, Time of Flight is chosen as the best matching technology for the efforts of the automotive-demonstrator.

3 Time-of-Flight measurement method

3.1 Overview

As explained in **Chapter 2.4** light propagates with a constant speed of $c = 3 \cdot 10^8 m/s$. Related to this fact a emitted light pulse can be detected after a certain time (*Equation* (2.4)) or in the case of a CW modulated signal with a certain phase shift (*Equation* (2.5)) (the setting is shown in **Figure 2.7**). Based on the time needed, respectively the occurred phase shift, the distance can be calculated (*Equation* (2.3) and *Equation* (2.6)). It is important to remind that these calculations only accords, if the sensor and detector are very close together in relation to the measured distance, otherwise some geometrical calculations must be added. The choice, which optical signal, pulsed (direct ToF) or CW (indirect ToF) is used, depends on some considerations explained in **Chapter 3.2**. **Figure 3.1** shows a scheme for a complete indirect ToF-system.

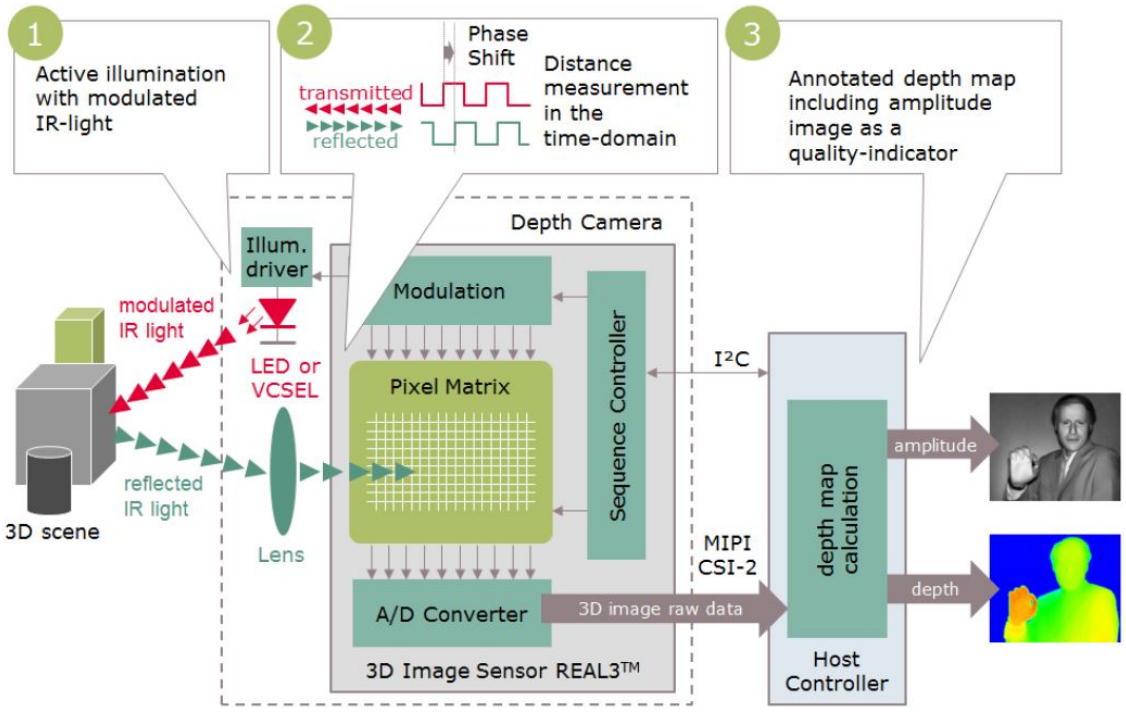

Figure 3.1: Scheme of an indirect-ToF 3D system[Kre16, Page 14]

The system consists of five parts:

- **Image sensor:** There are two main ToF sensor-types available, the Current Assisted Photonic Demodulator and the Photonic Mixing Device.
- **Illumination unit:** For the most applications an **infrared** (IR)-LED or IR-**Vertical Cavity Surface Emitting Laser** (VCSEL) is used to emit the CW-signal.
- **Optics:** To focus the incoming light a lens is located on the top of the sensor. Additionally an optical bandpass filter could be integrated in the lens to suppress the ambient light. This leads, by noise reduction, to a higher SNR.
- **Drive electronics:** The drive electronic controls the illumination and the image sensor over synchronized high speed signals.

- **Computation/interface units:** The image sensor provides the raw 3D image data, they are transformed into a **Mobile Industry Processor Interface-Camera Serial Interface-2** (MIPI-CSI-2) or parallel interface signal and are delivered to the host controller. For a better performance the data can be corrected with the use of device related calibration data.

The optical signal from the illumination unit and the different kinds of image sensors are described more in detail in the following chapters, **Chapter 3.2** and **Chapter 3.3**

3.2 Optical Signal

Basically there are two modulation types for the optical ToF signal, Pulsed modulation [Mor89] and CW modulation[BF86]. In this chapter the characteristics of these two are outlined [Lan00, Page 16-19].

- **Pulsed modulation**
  At this modulation type light pulses are sent and a stop watch is started. After the reflection on the target the pulse returns to the detector and stops the watch. So the time of flight can be measured directly.
  A light pulse can transmit a high amount of energy in a very short time. This leads to the advantages and also to the challenges of this modulation type.
  A high energy in short time means a high **signal to noise ratio** (SNR) nevertheless the average power can stay low, which is important for power limited devices or eye safety. A high SNR leads to better ambient light robustness and larger range respectively better accuracy.
  Otherwise a pulse modulation requires a large bandwidth of the receiver. Air leads to dispersion of the pulse, which makes it difficult to detect the exact arrival time. The transmitter has to create pulses with very short rise/fall times and high power. This is currently only possible with lasers or laser diodes, but these have a limited repetition rate, in the kHz range, which limits the frame rate.

- **Continuous Wave modulation**
  A CW modulated signal is sent. The shape of this signal can vary from sinusoidal to square. In difference to pulsed modulation, CW modulation is not a direct time measurement. This modulation relies on phase measurement, therefore its called indirect ToF.
  CW modulation does not need such a high bandwidth and rise/fall times as pulsed modulation. So many types of light sources can be used, for instance **Light Emitting Diodes** (LED).
  Otherwise the SNR is less and the average power is higher than at pulsed modulation. With only one modulation frequency f_{mod}, the unambiguous range is limited by half of the wavelength. For a common modulation frequency of $30MHz$ this means:
  $$d_{max} = \frac{\lambda}{2} = \frac{c}{2f_{mod}} = \frac{3 \cdot 10^8 m/s}{2 \cdot 30MHz} = 5m. \tag{3.1}$$
  This unambiguous range can be increased by the use of two different modulation frequencies, called **Extended Unambiguity Range Sequence** (EURZ) [Inf16b, Page 10], also known as *heterodyn operation* or *frequency shifting* [SHXH95]. The big advantage of this method is the increase of the unambiguous range and simultaneously the maintain of the same accuracy. The absolute unambiguous range

increases, by the use of a second modulation frequency of $20MHz$ to [Tex14a, Page 25]:

$$\begin{aligned} d_{max} &= \frac{c}{2gcd(f_{mod,1}, f_{mod,2})} = \frac{3 \cdot 10^8 m/s}{2\,\mathrm{gcd}(30MHz, 20MHz)} \\ &= \frac{3 \cdot 10^8 m/s}{2 \cdot 10MHz} = 15m. \end{aligned} \tag{3.2}$$

3.3 Detectors and Demodulation

For a simple 1D distance measurement any fast and sensitive optical sensors can be used, for example photo diodes.
In contrast a 3D scene measurement is more complicated. A point wise scanning from the scene with one or more photo diodes is not effective. Therefore the whole scene is illuminated and the reflected light is observed by a 2D electro optical detector [Lan00, Page 20-22] (see **Figure 3.2**).
In this section two types of this 2D electro optical detectors are described, the **Photonic Mixing Device** (PMD) and the **Current Assisted Photonic Demodulator** (CAPD). These can observe a few thousands, up to hundred thousands points at the same time. The **PMD** will be **used in this master thesis**, so it will be described more in detail, nevertheless also CAPD is used from many companies, so it will be shortly mentioned.

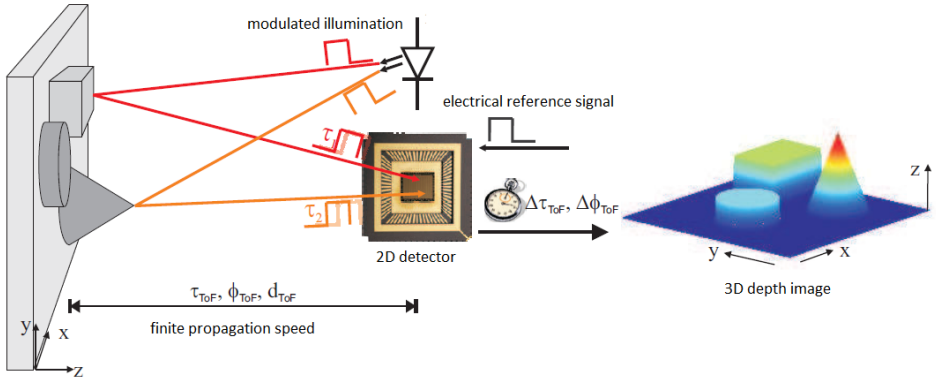

Figure 3.2: ToF 3D measurement [Alb07, Page 7]

Similar to a simple **charge-coupled device** (CCD)-sensor, PMD and CAPD are based on the photo electric effect. Therefore this effect is described in the next section.

3.3.1 The Photo Electric Effect

All kinds of photo electric sensors, such as CCD, PMD, CAPD, LDR (Light depending Resistor) or photo diodes, are based on the photo electric effect.
The **photo electric effect** (PEE) is separated in three types [Wik17]:

- **External PEE**
  External PEE or also called Photo Emission occurs when a photon hits a surface with high energy. If the energy is high enough, respectively the binding energy of the electrons in the surface are low (especially in conductors or semiconductors), some electrons are released from the surface. This effect is used for photomultipliers or photo electronic spectroscopy.

- **Photo Conductive Effect**
  This is the main effect needed for ToF sensors. The photo conductive effect is a inner PEE, caused by the energy, of an in a material penetrating photon, an electron-hole-pair is generated. The generated electron is lifted from the valence band up to the conduction band. This increases the conductivity of the material. With an applied electrical field the generated electrons can be separated before they recombine and get stored and preprocessed. Some typical applications are CCD, PMD, CAPD, LDR or photo diodes.
- **Photovoltaic Effect**
  The photovoltaic effect is also an inner PEE. In the depletion region (pn junction) generated electron hole pairs gets separated in p- and n-zone. The electrons move in the n-zone, the hole in the p-zone. This results in a current called photo current. This effect is used in photovoltaic cells.

3.3.2 Photonic Mixing Device

Figure 3.3 shows the principle structure of a PMD pixel. PMD uses the PEE in deep threshold region and applies an electric field to prevent an immediate recombination of the generated electron-hole pairs. The electric field is controlled by the modulation signal, applied to the two modulation gates, driven in a differential manner. In this way the generated charges get separated in relation to the phase shift between the modulation signal and detected light. These separated charges get stored and integrated to a voltage in two capacitors. This relation is shown in **Figure 3.4**.

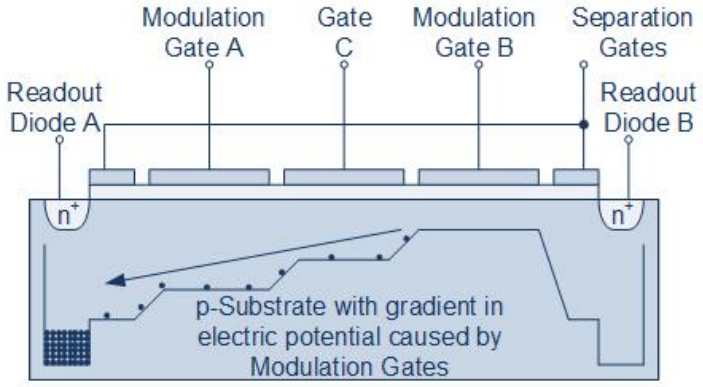

Figure 3.3: PMD pixel structure [Inf16b, Page 7]

Is the phase shift φ, between the signals, equal 0° or equal 180° the whole photo current is guided to one side. At $\varphi = 90°$ or $\varphi = 270°$ the photo current splits up equal to both sides. At all other phases the current splits up in ratio of the phase. This process is equivalent to a mixing of two analog signals.

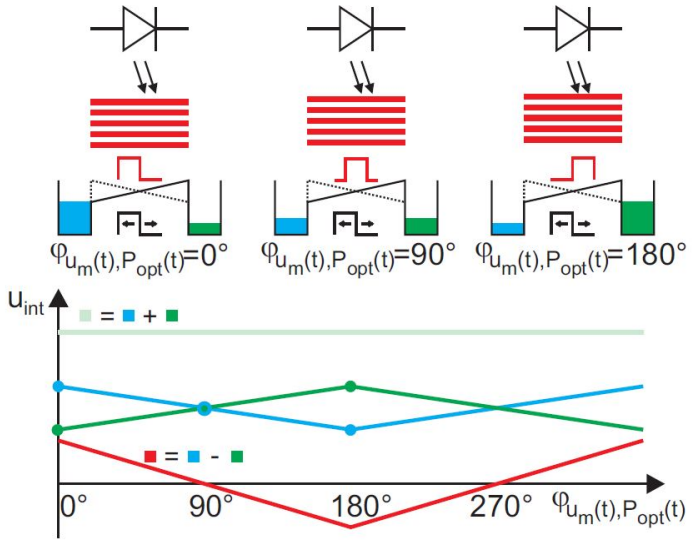

Figure 3.4: PMD pixel charge separation [Alb07, Page 9]

The mixing of two signals with following integration is defined as cross correlation of two functions. This means the output of a PMD pixel, $c(\varphi)$ is the cross correlation between the electrical $r(t)$ a received optical signal $s_\varphi(t)$, also called the **sensor response function** (SRF) [Alb07, Page 9-10]:

$$c(\varphi) = \int_0^{T_{int}} s_\varphi(t) r(t) dt, \qquad T_{int} \text{ is the integration time.} \tag{3.3}$$

Figure 3.5 shows the mathematical correspondence of the ToF System with PMD pixel.

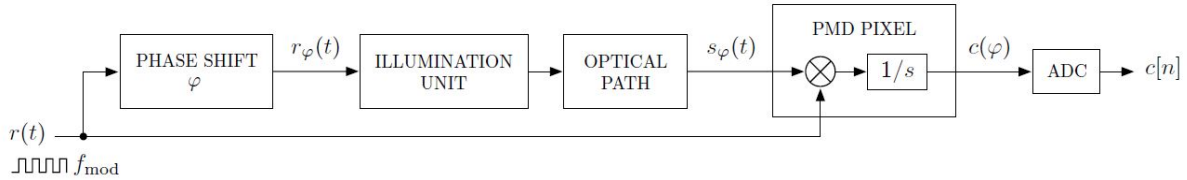

Figure 3.5: Mathematical correspondence to ToF [Gru13, Page 3]

The derivation of the SRF will be performed in phase domain, for a clearer view of the phase changing parameters. The first block of **Figure 3.5** represents a certain phase shift applied to the modulation frequency f_{mod}. The reason for this additional phase shift will be described in the **Chapter 3.4**. The resulting electrical signal $r_\varphi(t)$ is applied on the illumination unit, which can be modeled as:

$$h_{ill}(t) = \delta(t). \tag{3.4}$$

Take care that this model doesn´t include distortions caused by the temperature drift or the low pass behavior of the light source.
The following optical path can be represented by:

$$h_{opt}(t) = g(d)\delta(t - t_d). \tag{3.5}$$

This equation represents the signal attenuation $g(d)$ in relation to the distance d, $g(d \propto 1/d)$ and t_d is the, to the ToF related, upcoming time delay.
The phase shifted electrical signal $r_\varphi(t)$ together with *Equation* (3.4) and *Equation* (3.5) results in the detected optical signal:

$$s_\varphi(t) = g(d) r_\varphi(t - t_d). \tag{3.6}$$

Now the detected signal will be mixed, in the PMD pixel, with the original modulation signal, as mentioned above. So the SRF is calculated by:

$$\begin{aligned} c(\varphi) &= g(d) \int_0^{T_{int}} r_\varphi(t - t_d) * r(t) dt \\ &= g(d) \int_0^{T_{int}} r_\varphi(t - t_d - \frac{\varphi}{2\pi f_{mod}}) * r(t) dt. \end{aligned} \tag{3.7}$$

In the second step of *Equation* (3.7) the additional phase shift is inserted. Now it is clear that this integral maximizes if t_d and $\frac{\varphi}{2\pi f_{mod}}$ cancels out. So the phase shift between the received and the original signal can be calculated by:

$$\varphi_d = -argmax(c(\varphi)). \tag{3.8}$$

Phase shifting of the optical signal is equivalent to sampling the SRF. This leads to the discrete SRF:

$$c[n] = Q_B(c(\varphi))|_{\varphi=\varphi_n} \qquad \text{,with } n \in \{0, ..., N-1\}. \tag{3.9}$$

Q_B denotes the ideal B-bit quantization of the **analog to digital converter** (ADC). This is called the **N-point sampling**, N samples are taken from the SRF with a stepsize of $2\pi/N$:

$$\varphi_n = \frac{2\pi}{N} n. \tag{3.10}$$

[Gru13, Page 13-15]

3.3.3 Current Assisted Photonic Demodulator

Figure 3.6 shows a typical CAPD pixel structure. Modulation is achieved by applying a modulation voltage between DMIX0 and DMIX1. This voltage generates a hole-current, between the modulation nodes. The resulting field guides the PEE generated electrons to pin A or B. Due to the field also electrons generated deeper in the substrate ($> 4\mu m$) can be collected. This leads to a better responsivity and demodulation contrast of CAPD in contrast to PMD.
With increasing demodulation voltage [Tex14a, Page 13-14]:

- Demodulation contrast increases
- Responsivity increases
- Substrate current increases ⇒ higher power dissipation ⇒ higher heat generation in the sensor

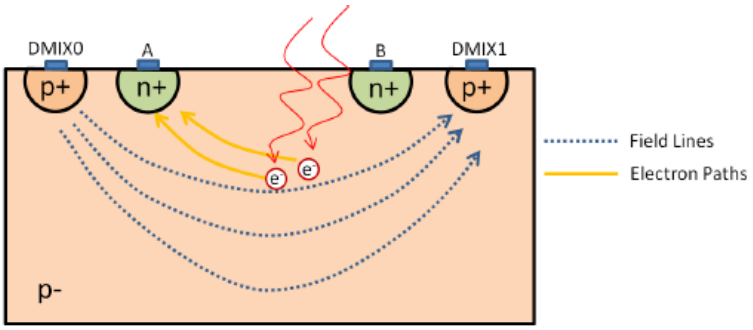

Figure 3.6: CAPD pixel structure [Tex14a, Page 14]

3.4 Calculation of the phase-shift

In this chapter the derivation of the phase and amplitude calculation will be performed. As basis the **Equivalent Circuit Diagram** (ECD) of a pixel is shown in **Figure 3.7**.

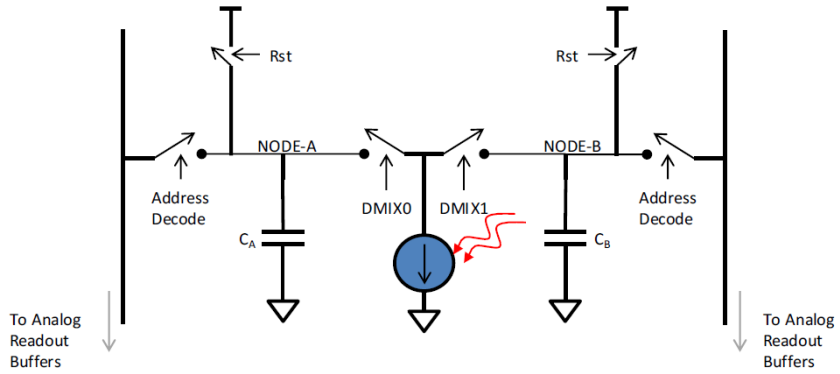

Figure 3.7: ECD of a pixel [Tex14a, Page 8]

In comparison to **Figure 3.6** and **Figure 3.3** the switches with the control signals $DMIX0$ and $DMIX1$ represent the effect of the modulation gates in case of PMD respectively the modulation pins in case of CAPD. The current source represents the current, generated by the PEE and the capacitors C_A and C_B are equivalent to the storage of the integrated mixed charges. With the switches Rst these capacitors can be discharged. The capacitor voltages $Node - A$ and $Node - B$ can be readout over the Address Decode switches.
A full readout circle consists of four parts:

1. **Reset:** The capacitors C_A and C_B get discharged to a known voltage V_R.
2. **Integration:** During integration time C_A and C_B are charged over the current source, controlled by the modulation signals $DMIX0$ and $DMIX1$ driven in a differential manner.
3. **Readout:** $DMIX0$ and $DMIX1$ are opened and the voltage of $Node - A$ and $Node - B$ get readout over the address decode switches.
4. **Dead time:** All switches are opened.

Node voltage calculation for ideal pixel and no ambient light

On base of **Figure 3.7** discussed above and under the assumption that the pixel is ideal (infinity short switching time, perfect matching, ...) the timing diagram in **Figure 3.8** can be used.

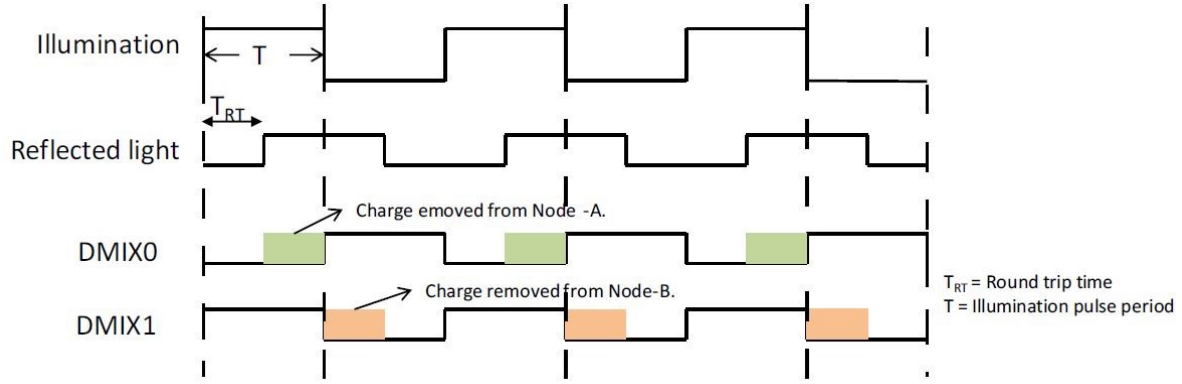

Figure 3.8: Timing Diagram for illumination[Tex14a, Page 8]

V_A and V_B are defined as the voltage on the notes, K is a constant factor and under the assumption $T_{RT} < T$ this voltages can be calculated by:

$$V_A = V_R - (T - T_{RT})K, \tag{3.11}$$

$$V_B = V_R - T_{RT}K. \tag{3.12}$$

Node voltage calculation for real pixel and ambient light

Now ambient light ($V_{A,A}$ and $V_{A,B}$) and a difference in the reset voltages ($V_{0,A}$ and $V_{0,B}$) will be considered:

$$V_A = V_{A,A} + V_{0,A} + V_R - (T - T_{RT})K, \tag{3.13}$$

$$V_B = V_{A,B} + V_{0,B} + V_R - T_{RT}K. \tag{3.14}$$

Summarizing there are four unknowns ($(V_{A,A}+V_{0,A})$, $(V_{A,B}+V_{0,B})$, K and T_{RT}). To solve this problem a second measurement must be introduced. The easiest way is to run the second measurement without illumination. So there are two additional equations:

$$V_{off,A} = V_{A,A} + V_{0,A} + V_R, \tag{3.15}$$

$$V_{off,B} = V_{A,B} + V_{0,B} + V_R. \tag{3.16}$$

Substracting this four equations (*Equation* (3.13)−(3.15) and *Equation* (3.14)−(3.16)) leads to two equations with two unknowns:

$$V_A = -(T - T_{RT})K, \tag{3.17}$$

$$V_B = -T_{RT}K. \tag{3.18}$$

If the capacitors C_A and C_B are not perfect matched, another factor, the gain have do be added:

$$V_A = -G_A(T - T_{RT})K, \tag{3.19}$$

$$V_B = -G_B T_{RT}K. \tag{3.20}$$

Now again four unknowns are in the two equations, so another measurement have to be added. This leads to the standard four phase ToF measurement. Therefore the phase for the illumination signal will be delayed (**Figure 3.5**) by 0°, 90°, 180° and 270°. If the modulation signal and the detected signal are perfect squares, the difference between V_A and V_B has a triangular form (**Figure 3.9a**). In practice the waveform looks more like a sinus (**Figure 3.9b**), caused by distortions of the optical signal.

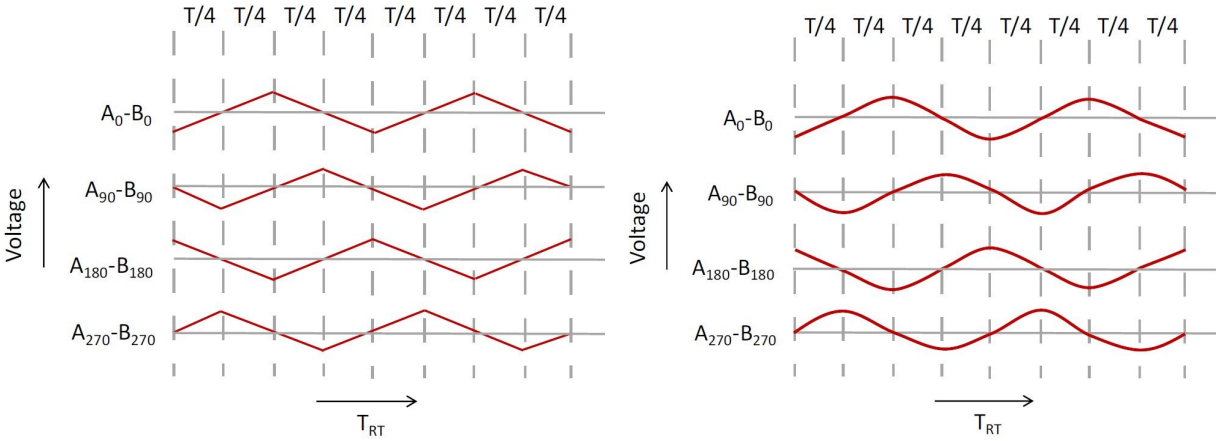

(a) ideal signal shape

(b) practice signal shape

Figure 3.9: Four phase signal shapes of $V_A - V_B$ [Tex14a, Page 10]

Under this conditions the calculation can be performed by:

$$V_{A,0} - V_{B,0} = (V_{A,A} + V_{0,A} + V_R) - (V_{A,B} + V_{0,B} + V_R) - (G_A + G_B)2\cos(\frac{T_{RT}}{T}), \quad (3.21)$$

$$V_{A,180} - V_{B,180} = (V_{A,A} + V_{0,A} + V_R) - (V_{A,B} + V_{0,B} + V_R) + (G_A + G_B)2\cos(\frac{T_{RT}}{T}), \quad (3.22)$$

$$V_{A,90} - V_{B,90} = (V_{A,A} + V_{0,A} + V_R) - (V_{A,B} + V_{0,B} + V_R) - (G_A + G_B)2\sin(\frac{T_{RT}}{T}), \quad (3.23)$$

$$V_{A,270} - V_{B,270} = (V_{A,A} + V_{0,A} + V_R) - (V_{A,B} + V_{0,B} + V_R) + (G_A + G_B)2\sin(\frac{T_{RT}}{T}). \quad (3.24)$$

Finally the phase and the amplitude can be calculated with the I/Q method (in-phase/quadrature method).

$$I = (V_{A,0} - V_{B,0}) - (V_{A,180} - V_{B,180}) = -(G_A + G_B)4\cos(\frac{T_{RT}}{T}), \quad (3.25)$$

$$Q = (V_{A,90} - V_{B,90}) - (V_{A,270} - V_{B,270}) = -(G_A + G_B)4\sin(\frac{T_{RT}}{T}). \quad (3.26)$$

Phase φ:

$$\varphi = \arctan 2(\frac{Q}{I}). \quad (3.27)$$

Amplitude A:

$$A = \sqrt{I^2 + Q^2}. \quad (3.28)$$

[Tex14a, Page 8-11]

4 Time-of-Flight camera design

This chapter describes the way from the specification to the finalized demonstrator. Starting with the block diagram of the required system, including the minimum requirements. Based on them, the key components are chosen. Then a prove of concept with available evaluation boards was made. This lead then, with some design steps between, to the finalized demonstrator, described in the end.

4.1 Block Diagram and Specifications

The required demonstrator consists of three main parts (**Figure 4.1**), the ToF-camera, an **electronic control unit** (ECU) and a link between them.

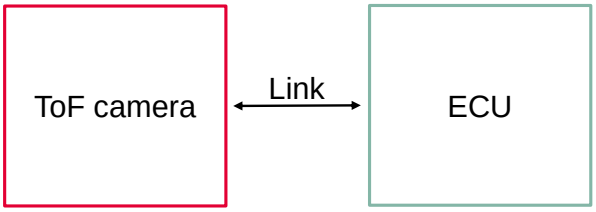

Figure 4.1: ToF application block diagram

- **ToF Camera**:
  An image-sensor controls the illumination, compares the received light with the control signal and generates the 3D-image. The image data are sent over the **Parallel Interface** (PIF) or the **Camera Serial Interface-2** (CSI-2) to a converter, which delivers the data to the link.

- **Link**:
  The link connects the ToF camera with the ECU. For low connection complexity a **Low Voltage Differential Signal** (LVDS) or a **Low Voltage Coaxial** (COAX) cable is demanded.

- **ECU**:
  The ECU converts the image data from the Link to CSI-2 data and delivers them to the USB converter. Further it provides the control signal, for the ToF camera, to the Link. The CSI-2 to USB converter acts as an interface between ECU board and the PC, which controls the imager and processes the 3D-raw-data.

Figure 4.2 shows the block diagram for the evaluation.

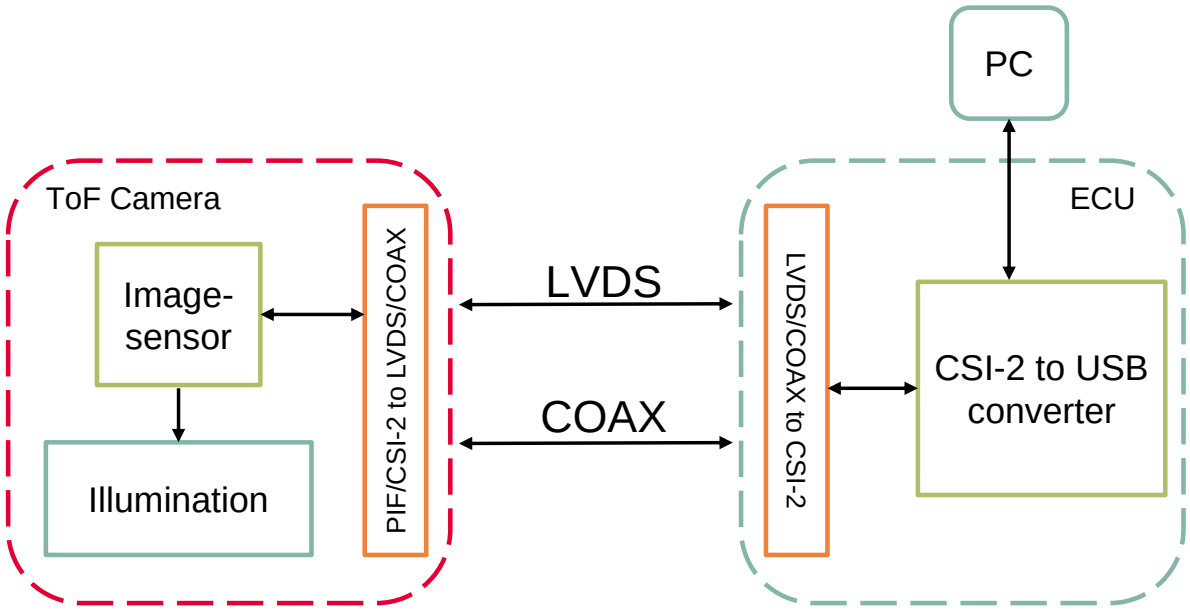

Figure 4.2: ToF evaluation block diagram

This evaluation setup must meet the following requirements:

- **ToF Camera**
  - $12V$ supply voltage delivered from the link
  - compatible with the *Infineon IRS1125A REAL3*^{TM}, this means CSI-2- or PIF-image data interface and **Inter-Integrated Circuit** (I^2C) and **General Purpose Input/Output** (GPIO) control interface.
  - approx. 100° field of view
  - up to 45fps(basic four sequence image)
  - Illumination: 4xVCSEL and 4xLED with 850nm or 940nm wavelength, modulation signal over **single ended** (SE)- or LVDS-interface, up to $80MHz$ modulation frequency,
  - $> 1Mbit$ flash memory for calibration data
- **Link**
  - LVDS or COAX
  - capable to deliver $10W$ power
  - capable to deliver the control and image data over at least $2m$ cable length
  - automotive standard interface
- **ECU**
  - compatible with the *Infineon CX3 interface-board*, this means CSI-2 data interface, I^2C and GPIO control interface
  - $12V$ power delivery for the ToF camera suitable for at least $10W$

To fulfill these requirements a setup, as shown in **Figure 4.3**, is necessary.

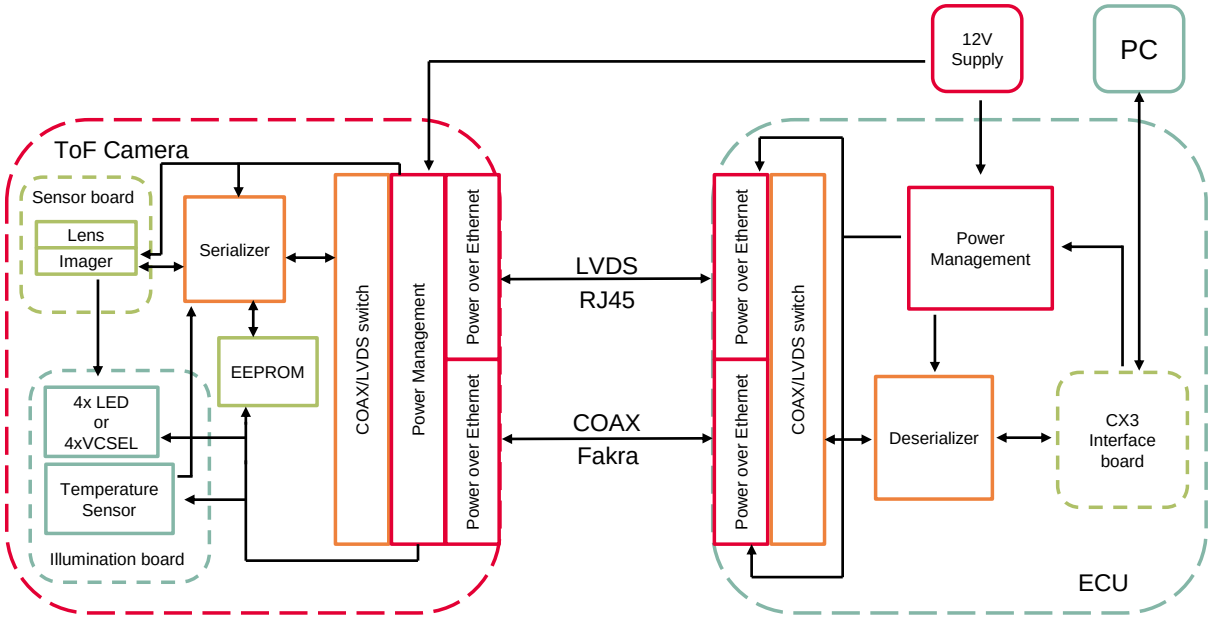

Figure 4.3: Required ToF setup block diagram

On the ToF camera is a socket, to mount the already existing and tested *Infineon sensor board*. This board includes the $IRS1125A$ and a lens with 100° degree field of view. For an easy change between the different illumination types, there is a second socket, which connects the ToF camera to the illumination board. The sensor board delivers the modulation signal, over single-ended interface or LVDS, to the illumination board.
To deliver the image data over a $2m$ long COAX or LVDS cable, a serializer is needed. This converts the PIF or CSI-2 data from the imager to an automotive signal, capable to reach this length. The serializer also converts the control signals from the link to I^2C and GPIO signals. The I^2C is connected to the EEPROM, the temperature sensor, on the illumination board (needed for temperature calibration, explained in **Chapter 5.1**), and the imager. The GPIO is reserved for additional control signals like reset or different enables.
To supply all ICs and the illumination a sufficient power management is needed. The $12V$ supply, delivered over the LVDS- or COAX-cable, has to be converted to the needed voltage domains and distributed to all parts.

For the link a FAKRA-COAX-cable was chosen. This choice was made because of the already established and proven implementations of this cable, by many car manufacturers. Additional a simple RJ45 cable is implemented, to verify the LVDS behavior.

The ECU board ensures the compatibility from the link signals to the CX3 interface board, therefore a deserializer converts the link data to CSI-2 data and delivers them to the CX3 board, apart from that it converts the GPIO and I^2C signals from the CX3 and provides them to the ToF camera.
A power management system captures the voltages from the CX3 board and the external $12V$ supply to deliver the power to the deserializer and the link.

4.2 Key-Components

4.2.1 3D-Imager

The 3D-Imager is the main component from a 3D-ToF system. It is defined in the requirements as the *Infineon REAL3^{TM} IRS1125A*. This imager is packed in an automotive qualified **Ball Grid Array** (BGA), suitable in an ambient temperature range of $-40°C$ to $+105°C$. A high imager resolution of $100k$ pixel can be used for a wide FoV. The *IRS1125A* uses the μLens technology, which leads to a robust indoor and outdoor behavior at low power consumption.
Some main features for the demonstrator are [Inf16b, Page 1]:

- High resolution 352×288 pixel (approx. 100k)
- Supporting $850nm$ and $940nm$
- Full operation in darkness, bright sunlight and heavily changing light conditions
- Fast object tracking
- Control of modulation frequency and illumination time
- $12Bit$ parallel interface providing VSYNC and HSYNC signals, with up to $66MHz$ pixel clock frequency
- MIPI-CSI-2 interface with data rates up to $1.6Gbit/s$
- Imager configuration via standard I^2C interface
- Qualification according to AEC-Q100, grade 2

The *IRS1125A* is a **System on a chip** (SoC)-device, which includes all key-functional-blocks required for generating a depth image. **Figure 4.4** shows the block diagram of the imager.

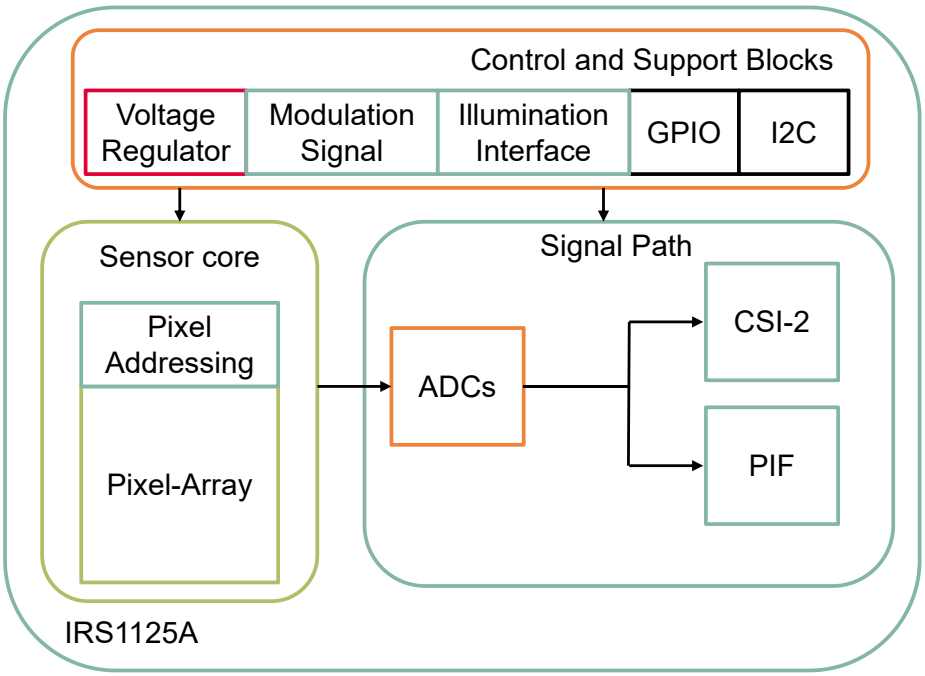

Figure 4.4: Block diagram of the IRS1125A

The Sensor Core consists of a PMD pixel array with the modulation driver and the addressing and read out of every pixel. The collected pixel-charges get digitized by several ADCs and provided by a CSI-2 and PIF interface to the host system. The control and

support blocks control this operation flow, provide the modulation signal to the Sensor core and the external illumination and can be configured over a I^2C interface. There are also additional GPIOs available.
The *IRS1125A* provides a wide field of possible use cases:

1. **Basic Four Phase Sequence**
   This is the simplest sequence for generating a 3D-ToF-image. The modulation frequency and the illumination time is constant and the phase is shifted by 0°, 90°, 180° and 270°. The z-image can be calculated by this four measurements, as explained in **Chapter 3.4**. At this sequence the unambiguity range is limited by $\lambda/2$ and the dynamic range is limited by the relation between the integration time, the illumination power, the pixel sensitivity and the pixel saturation.

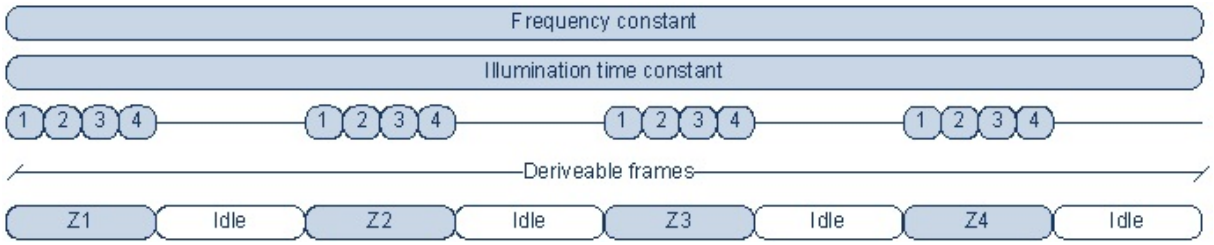

Figure 4.5: Basic Four Phase Sequence [Inf16b, Page 9]

2. **High Dynamic Range Sequence**
   The **High Dynamic Range Sequence** (HDRZ) improves the dynamic range by using different illumination times. Now one measurement block consists of two four-phase-sequences with constant modulation frequency but alternating illumination times. For close or high reflective targets a short illumination time can avoid saturation and for far or low reflective targets a long illumination time leads to a higher SNR.

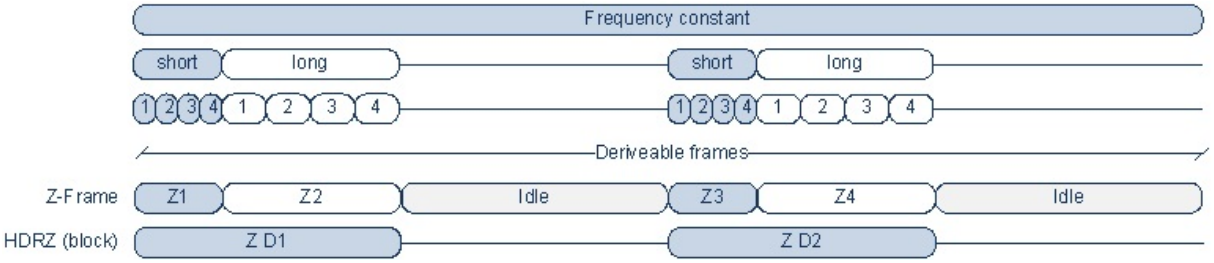

Figure 4.6: High Dynamic Range Sequence [Inf16b, Page 9]

3. **Extended Unambiguity Range Sequence**
   As explained in **Chapter 3.2** the unambiguous range can be increased by using different modulation frequencies. Therefore one measurement block consists, same as HDRZ, of two four-phase-measurement blocks, but now the illumination time is constant and the modulation frequency is alternating. The maximum distance increases from $\lambda/2$ to $c/(2gcd(f_{mod,1}, f_{mod,2}))$.

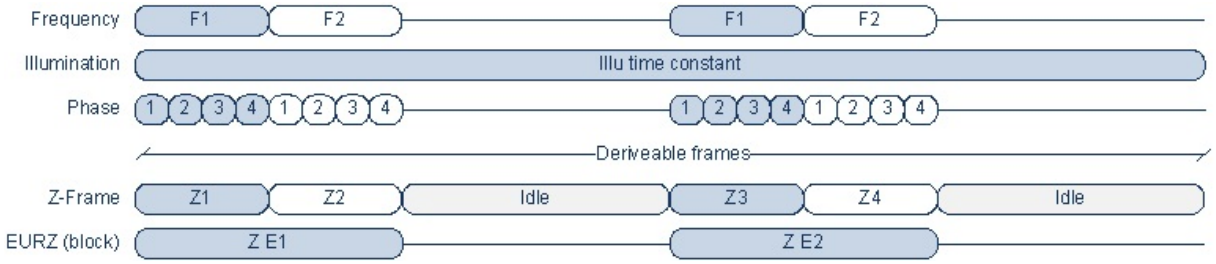

Figure 4.7: Extended Unambiguity Range Sequence [Inf16b, Page 10]

4. **Grey-Scale Image Measurement**
   With the *IRS1125A* also standard 2D grey scale images are also possible. Therefore a single frame measurement, instead of the four phase sequence, is used. This image can provide additional information of the scene. This information can be used to correct light-amplitude related errors.

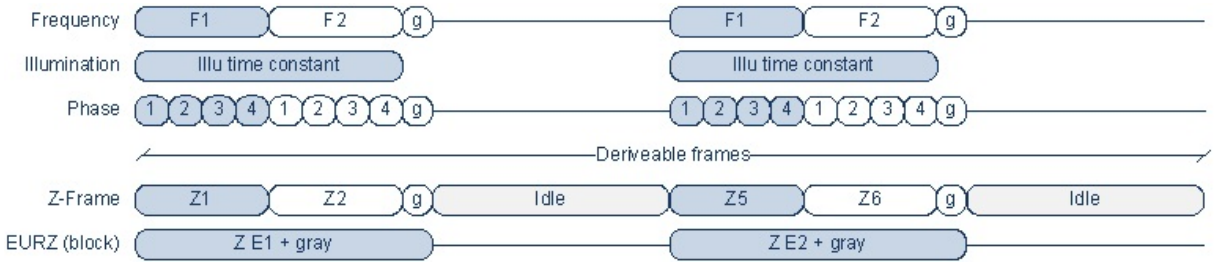

Figure 4.8: Grey-Scale Image Measurement [Inf16b, Page 10]

[Inf16b]

4.2.2 Serializer and Deserializer

For the choice of the **Serializer and Deserializer** (SERDES) some key features are required to operate with the *IRS1125A* and the Infineon software kits.
This features are:

- MIPI-CSI-2 with data rates up to $1.6 Gbit/s$ of the deserializer
- MIPI-CSI-2 with data rates up to $1.6 Gbit/s$ of the serializer
- Alternatively $12 bit$ PIF, HSYNC, VSYNC and a pixel clock frequency up to $66 MHz$ of the serializer
- I^2C control channel
- LVDS connection
- COAX connection with **Power over COAX** (PoC) possibility
- At least $2m$ supported cable length
- Automotive Grade

There are two main companies providing automotive camera SERDES systems *Texas Instruments (FPD-Link)* and *Maxim (GMSL)*.
Based on the needed key features **Table 4.1** is made up by the appropriate SERDES (stand of august 2017):

Serializer										
	Input	Output	12bit support	Pixel Clock [MHz]	Coax	Max. Data Rate [Mbps]	Bidirectional I2C	GPIO		Note
DS90UB913A	LVCMOS	FPD-LINK 3	YES	25-100 / 75@12bit	YES	1400	400kHz	4		low frequency mode for f25-50MHz
DS90UB913Q	LVCMOS	FPD-LINK 3	YES	10-100 / 75@12bit	NO	1400	400kHz	4		
DS90UB933	LVCMOS	FPD-LINK 3	YES	37.5-100 / 100@12bit	YES	1870	400kHz	4		Recommended for new design
DS90UB953	MIPI CSI-2	FPD-LINK 3			YES	3320				Not available now
MAX9257A	LVCMOS	LVDS	YES	5-70	NO	840	95kHz-4.25MHz	up to 10		not fully comaptible to the MAX9288
Deserializer										
	Input	Output	12bit support	Pixel Clock [MHz]	Coax	Max. Data Rate [Mbps]	Bidirectional I2C	GPIO	inputs	Note
DS90UB914A	FPD-LINK 3	LVCMOS	YES	25-100 / 75@12bit	YES	1400	400kHz	4	1	
DS90UB914Q	FPD-LINK 3	LVCMOS	YES	10-100 / 75@12bit	NO	1400	400kHz	4	1	
DS90UB934	FPD-LINK 3	LVCMOS	YES	25-133	YES	1600	400kHz	4	1	
DS90UB954	FPD-LINK 3	MIPI CSI-2	YES	25-100	YES	1866	up to 1Mbps	7	2	Not available now
DS90UB960	FPD-LINK 3	MIPI CSI-2	YES	25-100	YES	4000	up to 1Mbps		4	no eval board available
DS90UB964	FPD-LINK 3	MIPI CSI-2	YES	25-100	YES	1866	up to 1Mbps	8	4	
MAX9286	CML	CSI-2	YES			1500				nda required
MAX9288	CML	CSI-2	YES	6,25-104	YES	3120	up to 1Mbps	2	1	
MAX9290	CML	CSI-2	YES	6,25-104	YES	3120	up to 1Mbps	2	1	MAX9288 but with HDCP

Table 4.1: SERDES compare

As best fitting pair the *Texas Instruments DS90UB933* serializer and the *DS90UB964 deserializer* are chosen for evaluation.
There specifications are:

Texas Instruments serializer *DS90UB933* [Tex16a, Page 1]:

- 10bit or 12bit PIF with HSYNC and VSYNC
- 37.5MHz to 100MHz Pixel Clock
- Robust PoC Operation
- Bidirectional Control Interface Channel with I^2C Support at 400kHz
- Capable of Driving up to 15m Coax or **Shielded Twisted-Pair** (STP) cables
- 4 flexible **General Purpose Input/Output** (GPIO)
- 1.8V, 2.8V or 3.3V compatible Parallel Inputs
- Single Power Supply at 1.8V
- Automotive Grade

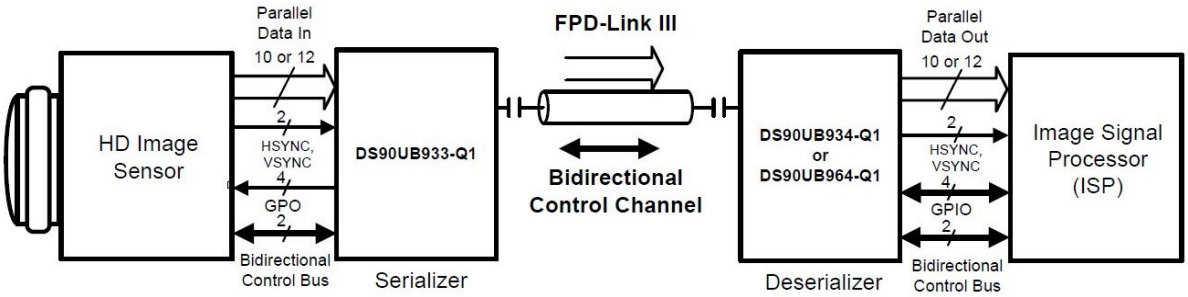

Figure 4.9: Application example for the DS90UB933 [Tex16a, Page 1]

Texas Instruments deserializer *DS90UB964* [Tex16c, Page 1]:

- Aggregates data from up to 4 Cameras over FPD-Link III interface
- Two CSI-2 Outputs with 1,2,3 or 4 Data Lanes per port
- CSI-2 Data Rate scalable for 400Mbps/800Mbps/1.5Gbps/1.6Gbps each Data Lane
- Robust PoC Operation
- I^2C with Fast-Mode Plus up to 1Mbps
- Supports Single-Ended Coaxial or Shielded Twisted-Pair (STP) cables
- 8 flexible GPIOs
- Compatible with *DS90UB913AQ/913Q/933Q* serializers
- Automotive Grade

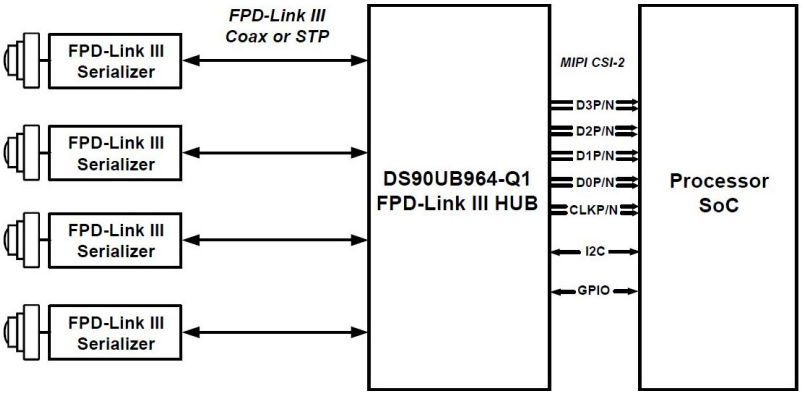

Figure 4.10: Application example for the DS90UB964 [Tex16c, Page 1]

During the thesis time, also a second possible SERDES-pair was released. The *Texas Instruments DS90UB935* and *Texas Instruments DS90UB936* fits perfect the requirements for the imager CSI-2 interface. So a second system also was built for evaluation.

Texas Instruments deserializer *DS90UB935* [Tex18a, Page 1]:

- Aggregates data from up to 2 Cameras over FPD-Link III interface
- CSI-2 Output with 1,2,3 or 4 Data Lanes
- Up to 2.528Gbps CSI-2 Bandwidth
- Robust PoC Operation
- I^2C with Fast-Mode Plus up to 1Mbps
- Supports Single-Ended Coaxial or Shielded Twisted-Pair (STP) cables
- 4 flexible GPIOs
- Compatible with *DS90UB936-Q1/954-Q1/960-Q1/934-Q1/914-Q1* Deserializers
- Automotive Grade

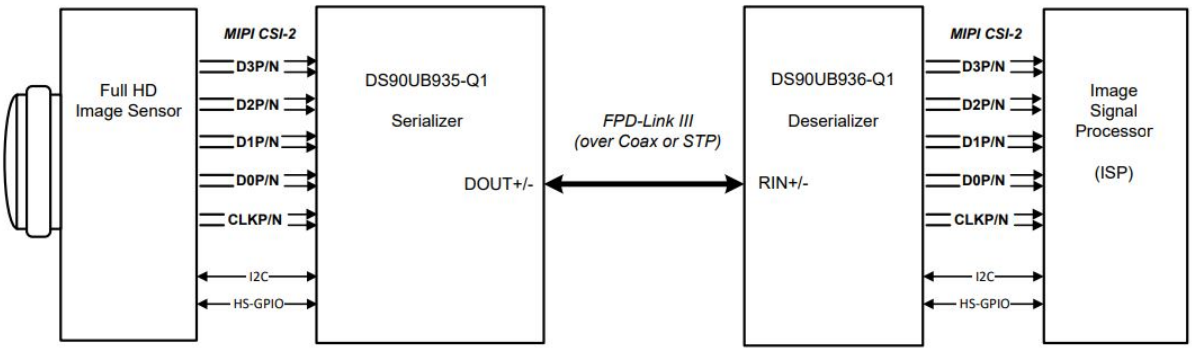

Figure 4.11: Application example for the DS90UB935 [Tex18a, Page 1]

Texas Instruments deserializer *DS90UB936* [Tex18b, Page 1]:

- CSI-2 Output with 1,2,3 or 4 Data Lanes
- CSI-2 Data Rate scalable for 400Mbps/800Mbps/1.5Gbps/1.6Gbps each Data Lane
- Robust PoC Operation
- I^2C with Fast-Mode Plus up to 1Mbps
- Supports Single-Ended Coaxial or Shielded Twisted-Pair (STP) cables
- 7 flexible GPIOs
- Compatible with *DS90UB935-Q1/933-Q1/913A-Q1* Serializers
- Automotive Grade

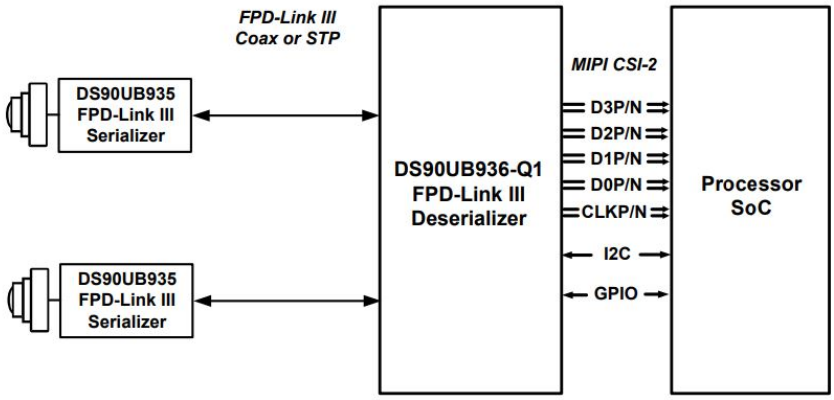

Figure 4.12: Application example for the DS90UB936 [Tex18b, Page 1]

Instead of the *DS90UB935-DS90UB936* pair, the more expensive *DS90UB953-DS90UB954* can be used also. They have the same footprint and register settings, the only difference is a higher data rate, which is not needed for this application.

4.2.3 CX3 Interface Board

The *CX3 Interface Board* serves as MIPI CSI-2 to USB 3.0 bridge controller, providing connectivity and control for the *REAL3*^{TM} 3D cameras.
The Key features are [Inf16a, Page 7]:

- Selectable main supply source - USB or external adapter
- External supply with 5V/4A wall plug adapter, standard barrel plug
- Onboard tunable voltage supply rails
- Individual DUT power rail on/off control, both manual and from software
- Possibility to connect and use external power supply for each DUT rail
- Voltage and current measurement points
- MIPI CSI-2 test points
- Selectable onboard DUT clock sources
- SPI and I^2C capability
- Selectable SPI or I^2C boot memory
- LED indicators for the supply rail and the DUT reset
- GPIO headers
- Debug readout via **Universal Asynchronous Receiver Transmitter** (UART) cable
- Robust high reliability connector
- Compact form factor

This features are shown in the block diagram **Figure 4.13**.

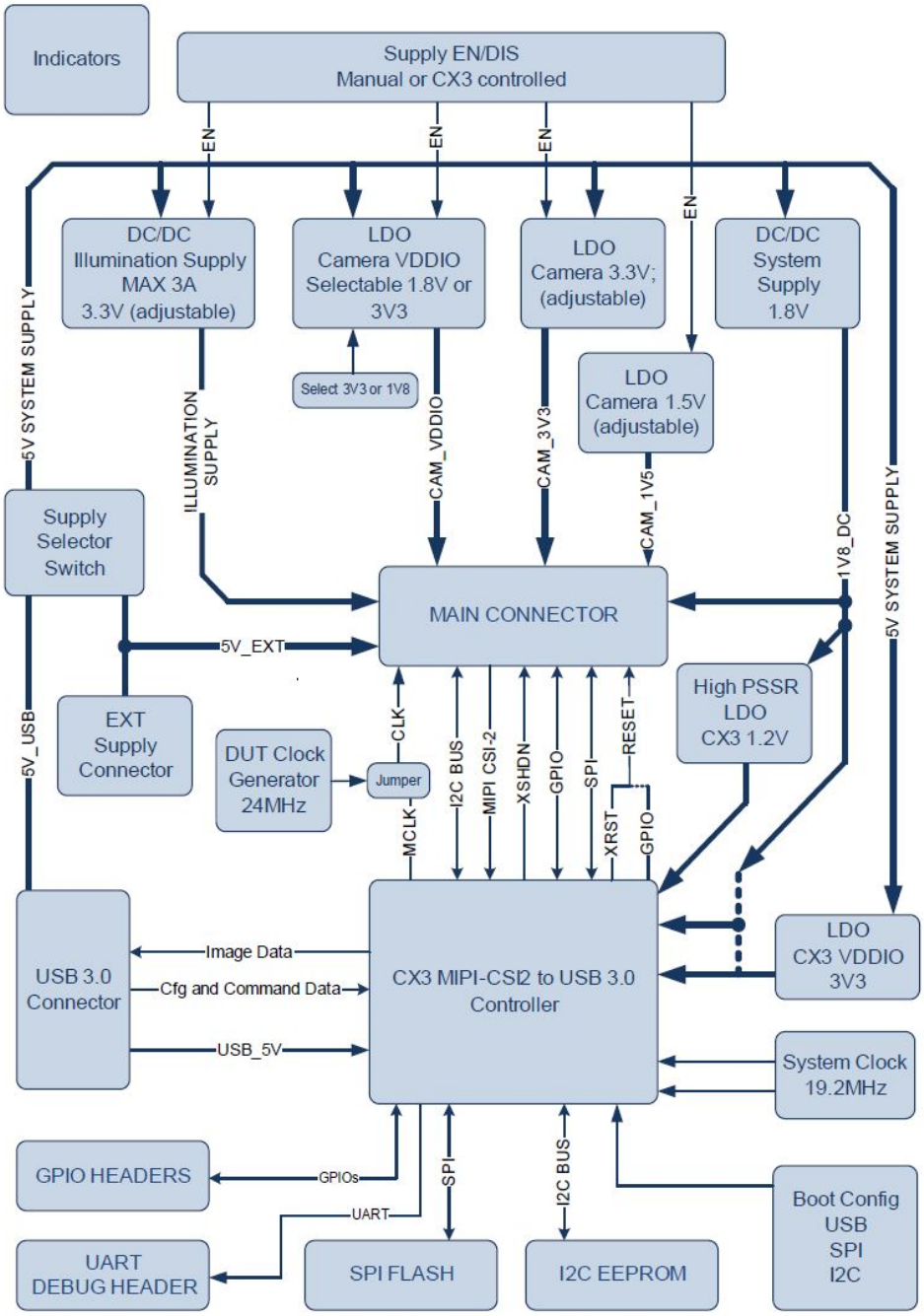

Figure 4.13: CX3 USB Interface Board block diagram [Inf16a, Page 9]

Figure 4.14 shows a picture of the *CX3 USB Interface Board* with all important control and connectivity options.

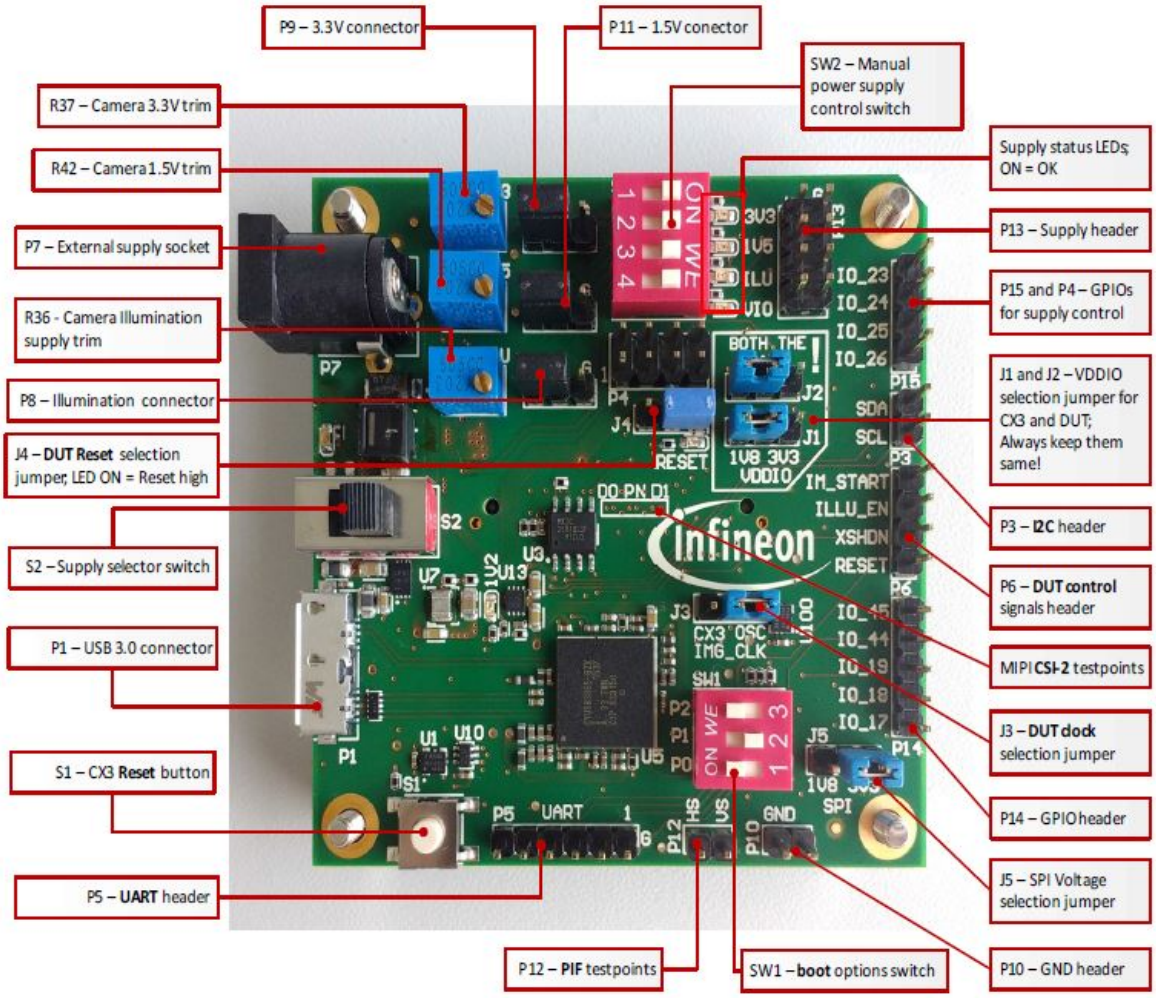

Figure 4.14: CX3 USB Interface Board picture [Inf16a, Page 10]

To use the interface-board, in the way mentioned in **Chapter 4.1**, some settings have to be made on the CX-3 board.

- Supply selector switch $S2$ on the left position to choose a supply over the USB connection
- Voltage at Potentiometer $R37$ to 3.3V
- Voltage at Potentiometer $R42$ to 1.5V
- Voltage at Potentiometer $R36$ to 3.3V
- Jumpers from $P9$, $P11$ and $P8$ on the left side to use the LDOs from the CX3 Interface Board
- All switches from $SW2$ on the right side to enable the power supply rails
- $J4$ on the right side to conncet the Reset with GPIO22
- $J1$ and $J2$ on the right side to choose 3.3V for the VDDIO
- $J3$ on the right side to use the 24MHz clock
- For the correct boot option $SW1$ set to: 3:left, 2:right, 1:left

In this mode the CX3-board serves as interface between the PC and the deserializer and supplies the deserializer with the required voltages.

4.3 Interface Option 1: PIF

At the beginning of the masterthesis there were no evalutaion kits for the CSI-2 SERDES available. So the first step was to verify the behavior with the PIF-SERDES evaluation kits and some developed adapter boards.

4.3.1 Evaluation-Kit

For a complete working evaluation environment six hardware parts are needed:

- **Sensor board**
  The sensor board (see **Figure 4.15**) is an easy to assemble and changeable PCB. Consisting of the 3D-Imager *IRS1125A* (see **Chapter 4.2.1**), the lens, bulk- and decoupling capacitors and pads on the bottom for the electrical connection to the Camera PCB.

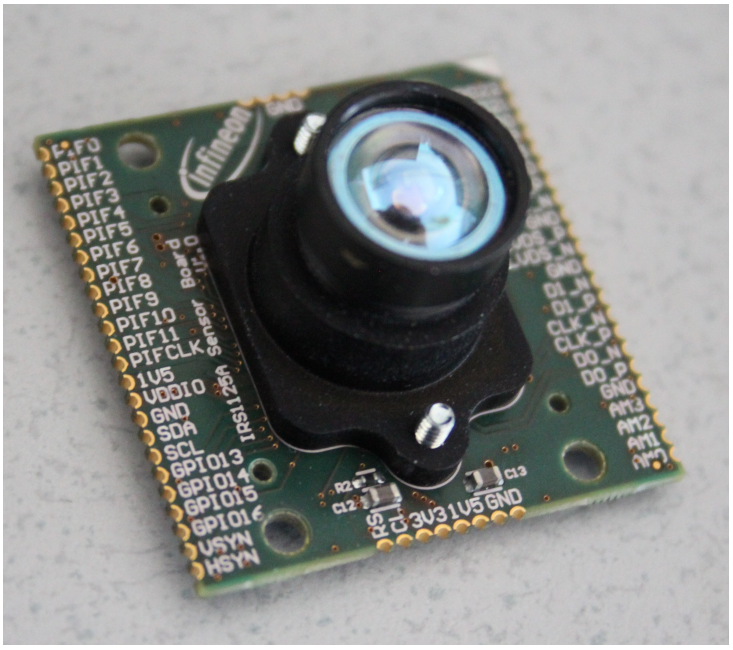

Figure 4.15: Infineon IRS1125A sensor board

- **CX3 Interface Board**
  The CX3 interface board is already described, see **Chapter 4.2.3**.

- **Serializer DS90UB933 Evaluation Kit**[Tex16b]
  The *Texas Instruments DS90UB933 Evaluation Module* provides an easy way to evaluate the operation and performance of the *DS90UB933*-serializer. The serializer board converts the data from the imager-PIF and delivers them over the FPD-III link.
  To run this board, a $3.3V$ and $5V$ power supply has to be connected to the connectors $J3$ and $J2$, as shown in **Figure 4.16**.
  The mode select Resistor $R19$ (yellow marked in **Figure 4.16**) is default set to $4.7k\Omega$ for external oscillator mode. Replace this Resistor with $100k\Omega$ for PCLK from imager mode.
  Connect the deserializer board over a *FAKRA COAX*-cable and the sensor board, over the serializer-evaluation kit adapter, to the connector $J1$.

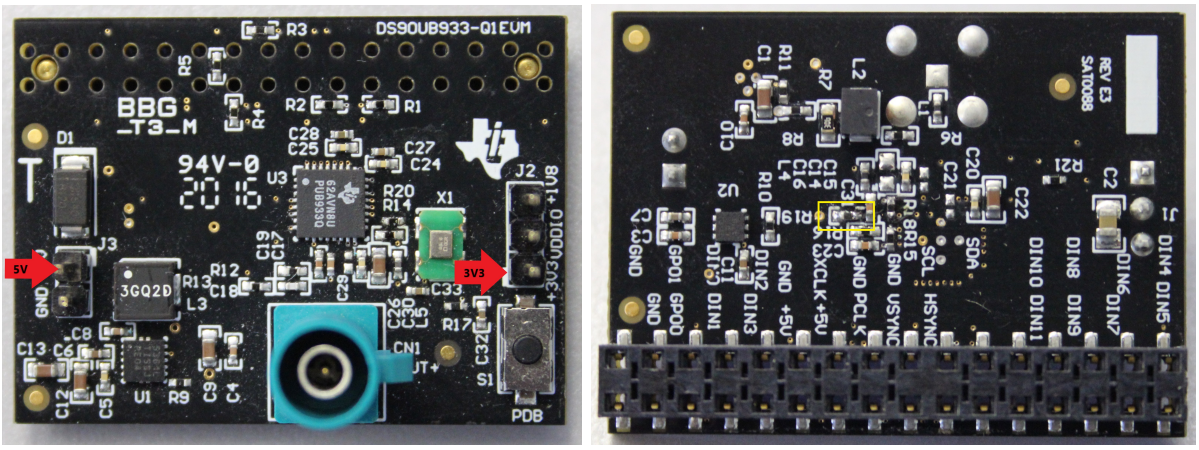

(a) Top view (b) Bottom view

Figure 4.16: DS90UB933 evaluation kit

- **Serializer-evaluation kit adapter**
  To connect the sensor board with the serializer-evaluation kit, an adapter is needed. This adapter routes the signals from the sensor board-connectors (two big connectors left side of **Figure 4.17**) to the connector, needed for the serializer evaluation kit (32-pinheader right side of **Figure 4.17**).
  Additional there are two LDOs to convert the $5V$-supply , from the serializer evaluation kit, to $1.5V$ and $3.3V$ for the imager, these voltages can be also delivered over the connectors $P5$ ($3.3V$) and $P6$ ($1.5V$). If not supplied external these connectors have to be shorted with jumpers.

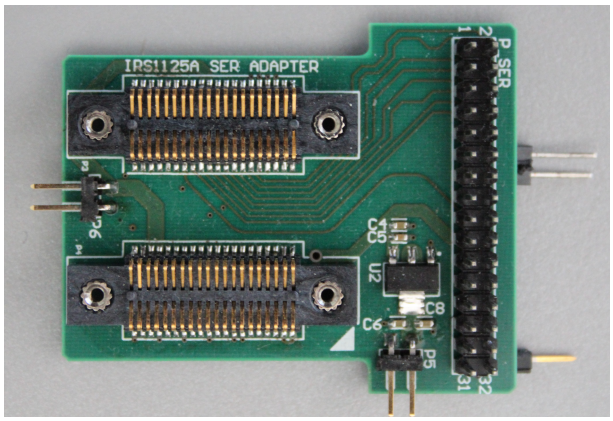

Figure 4.17: Serializer-evalkit adapter

- **Deserializer DS90UB964 Evaluation Kit**[Tex16d]
  The counterpart of the serializer evaluation kit is the *Texas Instruments DS90UB964 Evaluation Module*. This evaluation kit converts the data from the FPD III-link to CSI-2 and provides them to the deserializer-evaluation kit adapter.
  The evaluation module has to be supplied with $12V$ over the connector $J24$ (see **Figure 4.18**). Connect one of the four FAKRA-connectors, $CN1-CN4$, to the COAX-cable from the serializer and connect $J6$ or $J7$ with the deserializer-evaluation kit adapter.
  The serializer and deserializer have to be configured over the USB-connector $J36$, with the *Texas Instruments Analog Launch Pad (ALP)*-software.

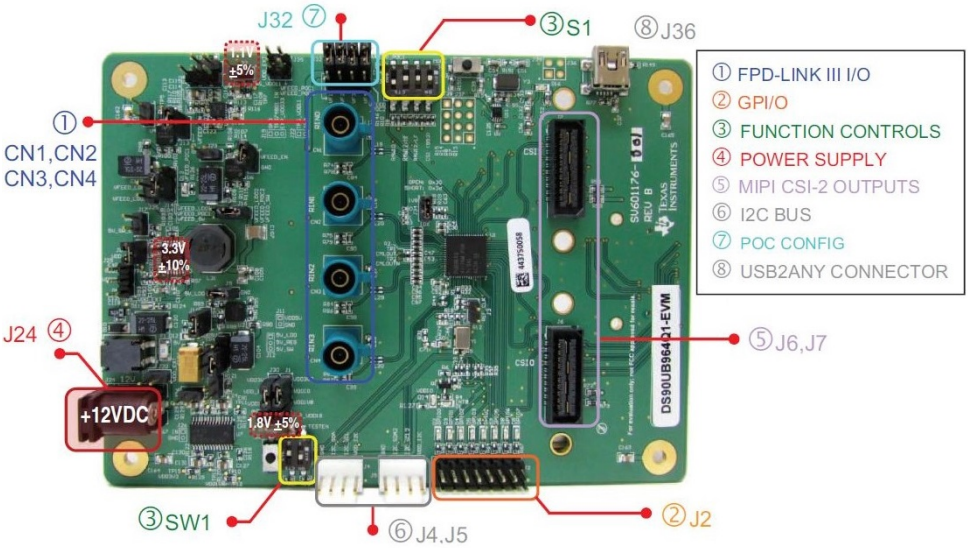

Figure 4.18: DS90UB964 evaluation kit [Tex16d, Page 9]

- **Deserializer-evaluation kit adapter**
  This adapter board, connects the signals from the deserializer evaluation kit to the connector needed for the CX3 board. Left all resistors $R1 - R11$ open (see **Figure 4.18**). If its necessary to connect the reset-signal from the CX3-board to the imager, solder a 0Ω-resistor at $R10$.

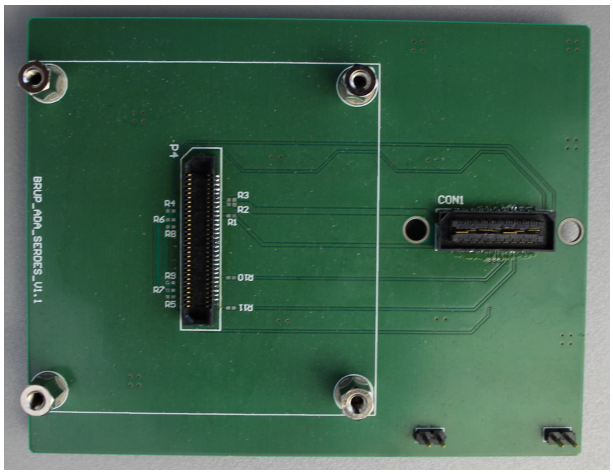

Figure 4.19: Deserializer-evaluation kit adapter

.

- **Evaluation kit setup**
  Figure 4.20 shows the complete setup, of the parts mentioned above.

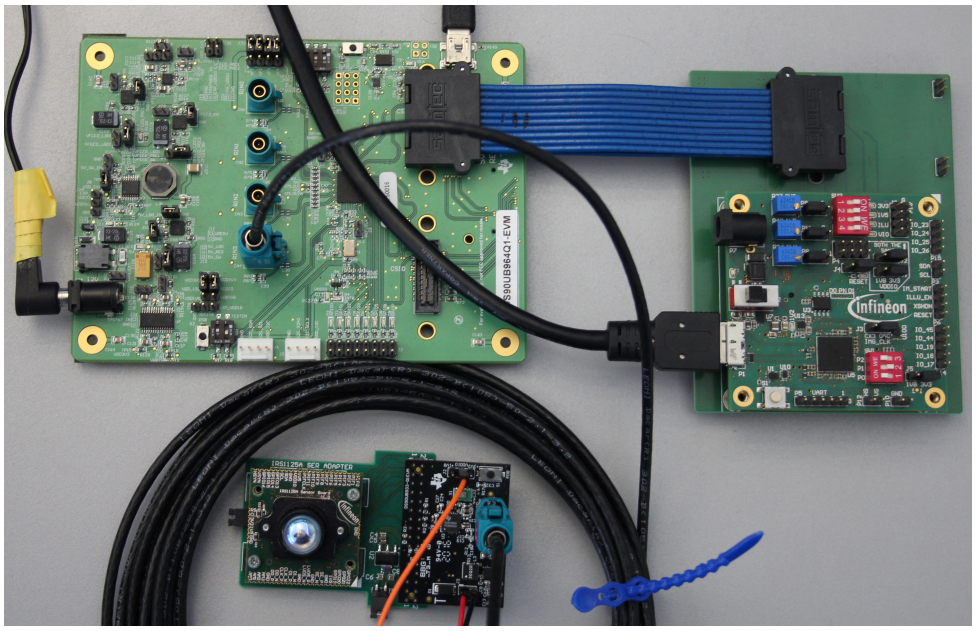

Figure 4.20: Evaluation kit setup

The sensor board is connected over the serializer-evaluation kit adapter to the serializer evaluation kit. The kit has to be supplied with $3.3V$ and $5V$ and is connected over a $5m$ long FAKRA COAX cable to the deserializer evaluation kit. This is supplied by $12V$ and delivers the image data, over the SAMTEC cable and the deserializer-evaluation kit adapter, to the CX3 board. Two USB cables connect a PC to the CX3 board and the deserializer evaluation kit. **Figure 4.21** shows the block diagram of this setup.

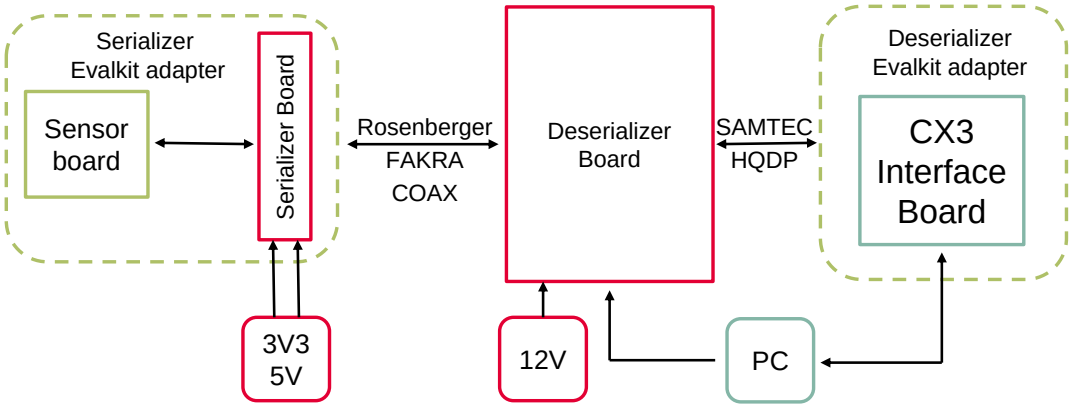

Figure 4.21: Evaluation kit block diagram

Together with the hardware there are some additional register settings needed to run the SERDES with the *Infineon animator* software. These settings are described in **Chapter 4.3.5**.
For a functional testing is no illumination needed. A picture from the ambient light scene together with the pseudo data from the imager are enough for a working assessment. It turned out, that the evaluation kit works completely transparent, in data perspective, this means the established software from Infineon/PMD can be used without any limitations for the demonstrator. The proof of concept is certified herewith.

4.3.2 Prototyp

After the proof of concept with the evaluation kit, a first prototype can be developed. This prototype should replace the evaluation kit, together with the adapter boards and manages the power supply for the sensor board and illumination board (the illumination boards are described later in **Chapter 4.5**). For the first version of the PIF-SERDES demonstrator, the priority is the valuation of the system and not to make it as small as possible. Therefore a lot of pin headers were added, for easy access with the measurement equipment, but this decreases the power- and signal integrity and increases the needed space. This tradeoff will be changed in the next version (see **Chapter 4.5**).

- **Serializer board:**
  The serializer board (see **Figure 4.22**) replaces the serializer evaluation kit and the serializer-evaluation kit adapter. Additional it should also provide all needed voltages. The power supply should run over a single $12V$-supply, delivered over the COAX-cable or the LVDS-cable. The $12V$-barrel connector, yellow marked on the upper right side from the board, is planned only for the case, that the power over coax or LVDS is not working as expected.
  At PoC the signal and the power is delivered over the same cable. This needs a sufficient coupling-decoupling network to separate them without decreasing the power and signal integrity. To decouple the signal from the power path, a impedance, at least 20 times higher then the conductor impedance, over the frequency range from $1MHz$ to $700MHz$ is needed [Tex14b, Page 2]. For this two ferrit beads, for high frequency image data and two inductors, for the low frequency backchannel (including I^2C and GPIO) are used. The $12V$-supply is decoupled over a DC-block capacitor located at the serializer input.
  To evaluate also the LVDS signal, a simple Ethernet connector is used. One pair carries the *FPD-Link III*-signal, the other pairs deliver the power. Caused by the separated pairs , there is no additional decoupling needed.
  To choose one of the supply options jumper connector $P18$ for PoC, $P19$ for Ethernet-supply or $P20$ for the barrel plug.
  To switch between the COAX and Ethernet connection, two resistors have to be changed at the serializer output (green marking under the Ethernet connector). For LVDS mode solder the resistor $R19$ and $R20$, for SE-COAX mode solder $R18$ and $R21$.
  There are two separated DCDCs on the board, one to set the illumination voltage (red marking at the left bottom) and one for the serializer board supplies. The output voltages can be controlled over the two potentiometers $R37$ and $R33$, located on the bottom of the board. Trim the output voltage, from the logic DCDC to $3.6V$, the illumination output voltage depends on the used LEDs or VCSELs and the required output power. On both DCDC outputs are pinheaders, $P8$ and $P9$, they give the possibility to measure the output current. Shorten them, if this is not needed.
  On the right upper middle (yellow marked) are three LDOs. These convert the $3.6V$, from the logic DCDC, down to the needed $1.5V$, $1.8V$ and $3.3V$. Same as at the DCDCs, there is also a current measurement option at the connectors $P10$, $P11$ and $P12$. The required IO voltages for the imager, the serializer and the illumination, can be chosen over the connectors $P13$, $P14$ and $P16$. Take care, that the same

voltage is selected for all of them.
The serializer is connected over $P30$ and $P31$ to the sensor board. This includes the PIF, the GPIO and the I^2C.
The I^2C is also connected to the EEPROM (red marked left from $P30$) and the illumination board over the connector $P40$ (marked green at the top side-bottom). The I^2C-address of the serializer can be changed over the voltage devider $R4$-$R5$ (green marking right of the serializer).
The GPIOs are combined with the different possibilities for the clock modes from the imager and the serializer. The imager clock can be delivered by the oscillator $U1$, then the resistor $R10$ has to be soldered and $R15$ must be open (green and yellow markings on the bottom side), but also the serializer can deliver the clock for the imager, therefore $R10$ must be open and $R15$ shorted. For the serializer clock there are also two options, the pixel clock from the parallel interface can be used (imager must be supplied over the oscillator $U1$), or an external oscillator $U2$ can deliver the clock. For the pixel clock solder $R51$, otherwise $R52$ (yellow marking right of the serializer) and the resistor $R13$.
To make all GPIOs usable, as IOs, supply the imager over $R10$ with the oscillator clock and use for the serializer the pixel clock option. When soldering $R14$, $GPIO2$ can be used as reset signal for the imager (green marking bottom side). The other three GPIOs can be used as illumination-enable, led1-enable and led2-enable. These three can be controlled over the serializer, the imager or can be left open and tied over a pullup/down to ground or illu-vddio. For default pullup solder the resistors $R58$, $R60$ and $R62$, otherwise $R59$, $R61$ and $R63$. For a connection to the rest of the board short $R48$, $R49$ and $R50$ (yellow marking left bottom). To connect them to the serializer, solder $R12$, $R55$ and $R56$ otherwise $R53$, $R54$ and $R57$ (red marking left upper top side and green marking bottom side).

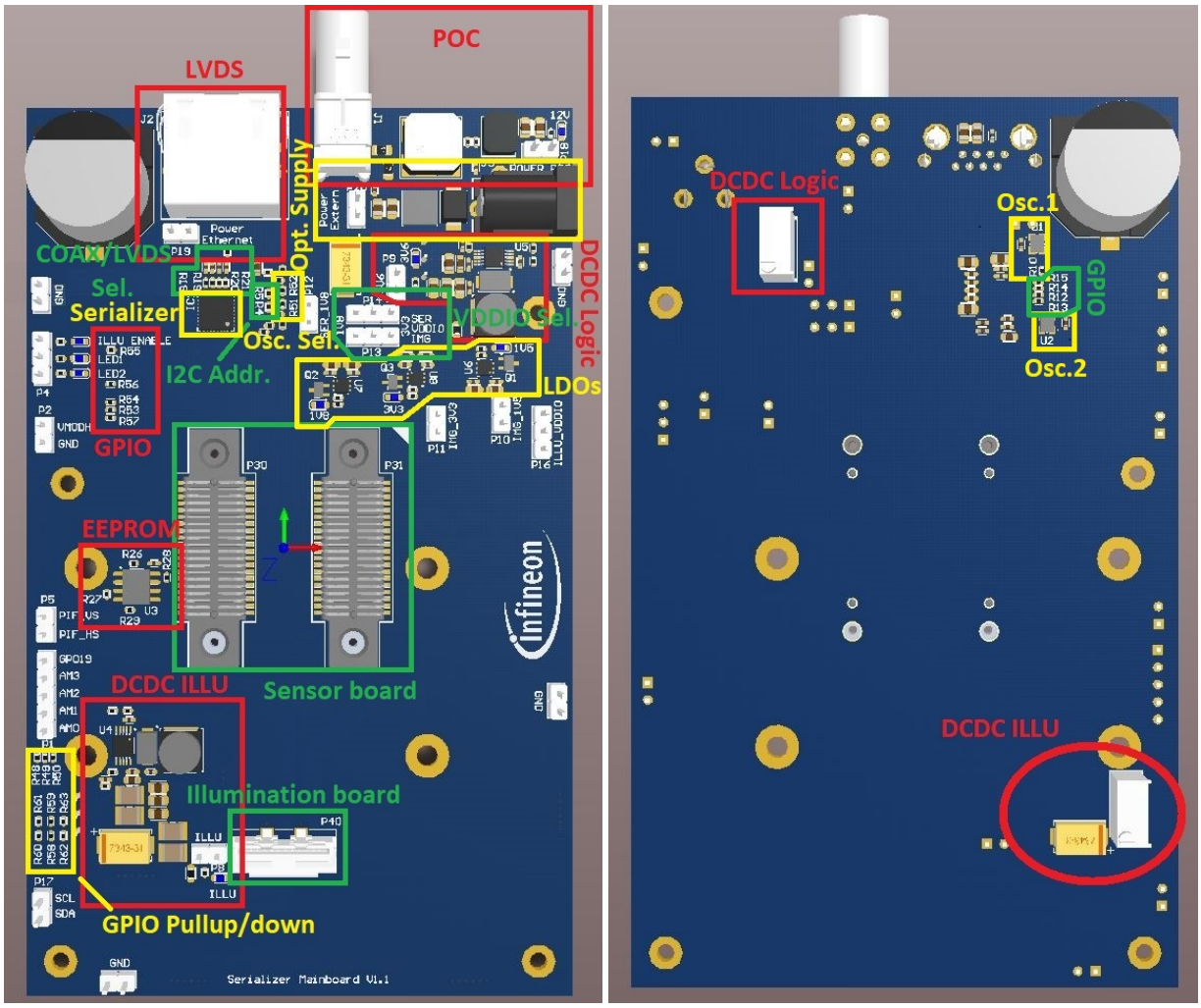

(a) Top view (b) Bottom view

Figure 4.22: Prototype of the PIF-serializer board

There are also additional testpoints, easy accessible, to measure different system parameters:

- $P4$ gives access to the three illumination enable GPIOs. The LEDs next to it indicates their logic state.
- $P2$ gives the possibility to monitor the $VMODH$-supply from the imager.
- $P5$ indicates the PIF-vertical sync and horizontal sync.
- $P1$ is connected to a fourth GPIO and 4 analog multiplexers.
- $P17$ gives access to the I^2C-bus of the serializer board.

- **Deserializer board:**
  The deserializer board (see **Figure 4.23**) replaces the deserializer evaluation kit and the deserializer-evaluation kit adapter and it provides the $12V$ supply voltage to the serializer board.
  The power from the $12V$ barrel plug (yellow marking on right upper corner) is fed, over a coupling-decoupling network, as mentioned above, to the COAX-connection (marked red in the upper left corner) or fed directly to the Ethernet-cable (yellow marking bellow). Connector $P9$ (PoC) or $P10$ (Ethernet) has to be shorten to

provide power to the cables. This connectors can be also used for current measurement.
The deserializer is fed by the CX3 interface board with an additional LDO (red marking right middle) for the $1V1$ supply.
To switch between the STP and the COAX option, place a 0Ω resistor on $R16$ and $R18$ for COAX, or $R15$ and $R17$ for STP. Furthermore the switch $SW1$ (marked green upper middle) has to be set in the correct way. Option 1 and 2 are for COAX-operation, 3 and 4 for STP. Set HF-mode, for PCLK frequencies between $37,5MHz - 100MHz$ and LF, for $25MHz - 50MHz$.
Connector $P4$ (green marked on bottom half of the board) connects the deserializer to the CX3 interface board, including CSI2, I^2C, GPIOs and supply voltages. The I^2C-address, from the deserializer, can be changed over the voltage divider $R10-R11$ (green marking in the deserializer area).

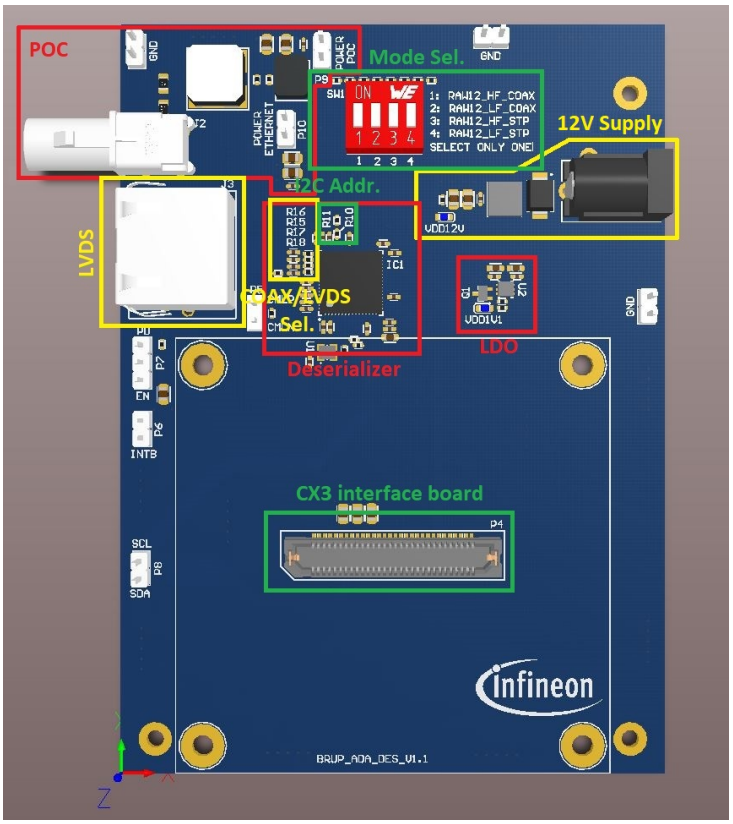

Figure 4.23: Prototype of the PIF-deserializer board

The four connectors, on the lower left side of the board and right of the Ethernet connector, $P7$, $P6$, $P8$ and $P5$, give control and monitoring possibility to the deserializer board.

- $P7$ has to be set to EN to enable the deserializer, PD switches to power down mode.
- $P6$ shows the status of the internal deserializer interrupt register.
- $P8$ gives access to the I^2C-bus of the deserializer board.
- $P5$ gives the possibility to measure the serializer-deserializer connection quality via an eye pattern measurement.

4.3.3 Lessons learned - Serializer-Deserializer

Measurements on the prototype board (see **Attachment B**) lead to some insights:

- The coupling-decoupling network, needed for PoC operation, adds additional resistance in the range of a few Ohms, which limits the maximum current and makes a big capacitor in the mH-range necessary. A second big capacitor does not lead to significant improvement.
- The big amount of jumpers lead to a significant decrease in power integrity.
- The measurement point for the $VMODH$-supply catches some noise from the environment to the very sensitive supply.
- Layout for the DCDCs should be made as carefully as possible, otherwise this would decrease the supply quality.
- To much options for GPIOs and clock signal lead to an unnecessary error sources. So simplify this circuit and remain on the external oscillator, for the imager and pixelclock, for the serializer.
- Also two $VDDIO$-options makes no sense. Take the $3.3V$-option, due to illumination board compatibility, this simplifies and improves also the supply-rails.
- For the power over Ethernet-option, much less capacity is needed. Also without the electrolyte capacitors the voltage drop is smaller then at the PoC option.
- From data perspective STP or COAX does not matter. Both options work fine with $5m$ long cables.
- The optional barrel plug on the serializer board is not needed, the other supply options work as expected.
- The for debugging most efficient measurement points are the current measurement for the illumination board and the I^2C connector on the serializer board. Therefore try to implement them on all future designs also.
- The prototype together with the illumination boards (described in **Chapter 4.5**) is capable to fulfill the required setup, illustrated in **Figure 4.3** for the PIF-option.

4.3.4 Optimized Board

The second version was developed, taking account of the lessons learned, mentioned above.

- **Serializer board:**
  The optimized serializer board (**Figure 4.24**) is simplified due to GPIO-options and $VDDIO$-power supply possibilities.
  The GPIOs are connected fix to the imager and can be connected to the serializer, over the resistors $R3$, $R6$, $R9$ for the illumination enable signals and $R38$ for the imager reset signal (red serializer marking at the bottom side). For the illumination enable signals pullup- and pulldown-resisitors are available (green marking on bottom side).
  The imager clock is connected directly to the external oscillator and the serializer runs over the imager pixel clock.
  The $VDDIOs$ are connected to $3.3V$ and the additional barrel plug is removed.
  The DCDC layout is made in a more carefully way. One electrolyte capacitor is removed.
  Some measurement points are removed and the power supplies are connected directly without pinheaders between them.
  The board size is reduced from $80mm \times 130mm$ to $75mm \times 85mm$.

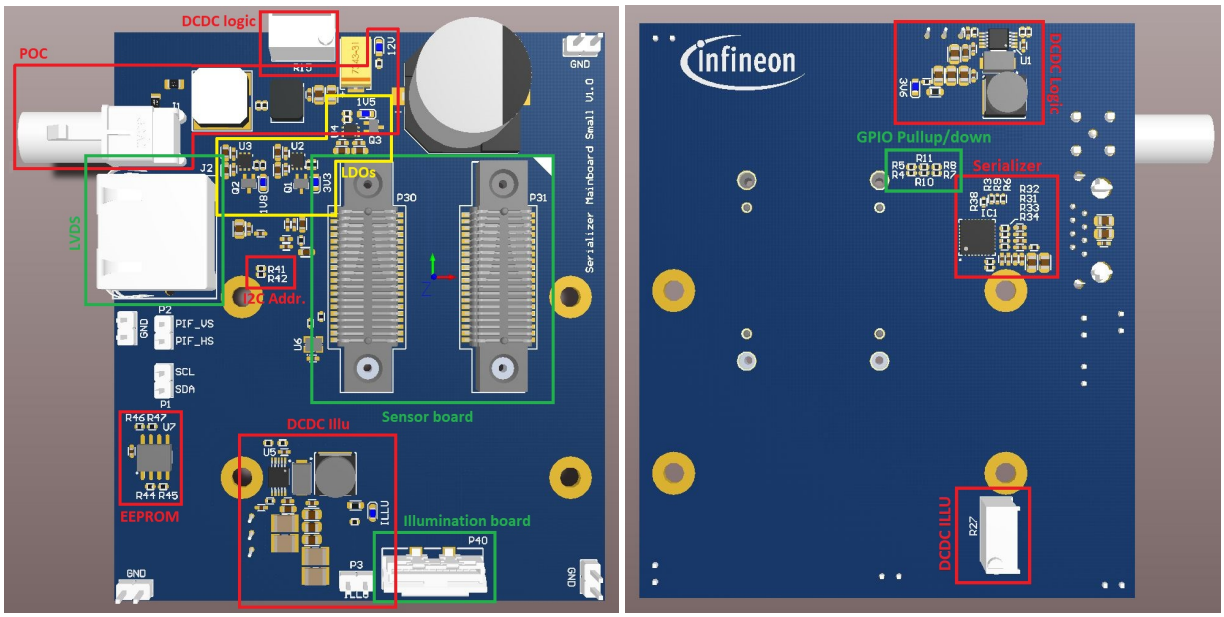

(a) Top view (b) Bottom view

Figure 4.24: Optimized PIF-serializer board

- **Deserializer board:**
  The deserializer board (see **Figure 4.25**) stays nearly the same. There are only some layout improvements and the components are placed more dense. This leads to a size reduction from $80mm \times 110mm$ to $80mm \times 90mm$.

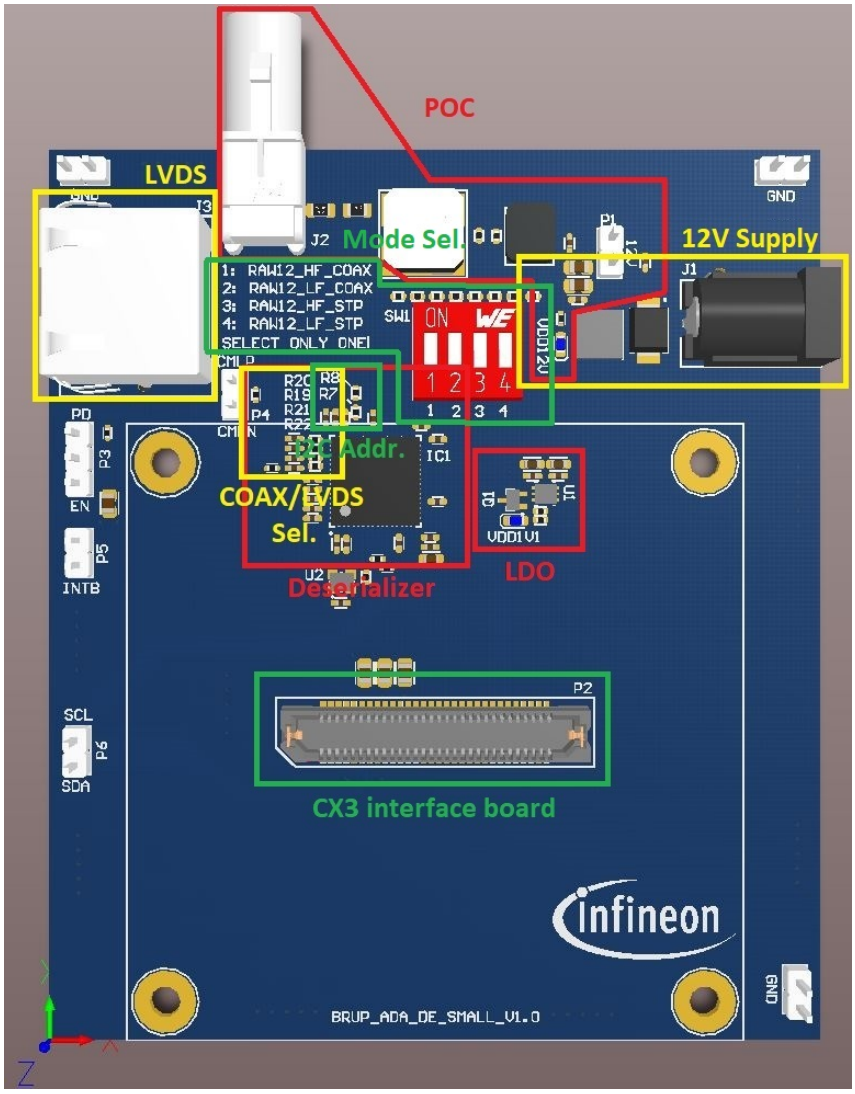

Figure 4.25: Optimized PIF-deserializer board

- **PIF interface system:**
  Figure 4.26 shows a picture, of the complete PIF interface setup. On the serializer board, the mounted illumination board can be seen. The two boards are connected over a kind of flat band cable. This cable also includes a reference plane for controlled impedance connections, needed for the LVDS-modulation signal. The illumination board will be described more in detail in **Chapter 4.5**.

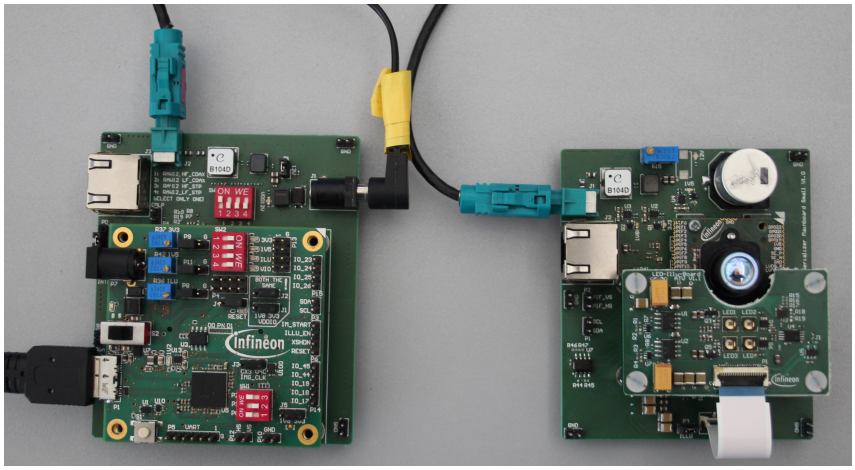

Figure 4.26: PIF interface system

4.3.5 Register Settings

To run the imager over the serializer and deserializer, it is necessary to set some registers. These are described below.
At first it is necessay to configure the CX-3 interface board.

```
#set CX3-board
import animator.animator as A

cx3ib = A.Mani()
cx3ib.referenceClockFrequency = 2400000
cx3ib.error_break = True
cx3ib.setSuperframeSeparationSize(352, 288, 0, 1)
status=cx3ib.open()
print(status)
cx3ib.setGpio(A.Pin_IM_RESET, A.Gpio_High)
```

Then configure the I^2C parameters from the deserializer, enable the backchannel and the I^2C pass through, for all I^2C-addresses. For better failure detection enable the CRC-Generator.

```
#Deserializer
des = A.I2CDevice()
des.address = 0x30
des.clock_frequency = 400000
des.register_address_width = 8
des.data_value_width = 8

#Deserializer config
```

```
#Selecting Port 0
cx3ib.i2CWrite(des, 0x4C, 0x01)
#I2C pass Through All enabled, Backchannel allways enabled
#Back Channel CRC Generator Enabled
cx3ib.i2CWrite(des, 0x58, 0x58)
```

Enable the deserializer CSI-2 and configure it to two data lanes, from CSI-2 Port 0 to RX-Port 0. Set the minimum Frame Valid time for stable operation.

```
#Set CSI-2
#CSI Port 0 Write Enbled
cx3ib.i2CWrite(des, 0x32, 0x01)
#Set CSI-2 to 2 Lanes
#Enable CSI-2 Output
cx3ib.i2CWrite(des, 0x33, 0x21)
#Forwarding RX-Port0 enabled
#Map CSI-2 Port0 to RX-Port0
cx3ib.i2CWrite(des, 0x20, 0xE0)
#Set minimum Frame Valid time
cx3ib.i2CWrite(des, 0xBC, 0x05)
```

The *DS90UB964* can communicate with up to four cameras. If this cameras or devices on the camera-boards have the same I^{2}C-address, it is possible to give them a different, virtual I^{2}C-address on deserializer side. The mapping of these virtual- to real I^{2}C-addresses is made over deserializer register settings. Take care that the address is programmed with a 0_b at the end, so the address has to be shifted by one bit left.

```
#Setting physical and virtual Serializer ID
cx3ib.i2CWrite(des, 0x5B, 0xB0)
cx3ib.i2CWrite(des, 0x5C, 0xB0)

#set address of the imager(Slave0)
cx3ib.i2CWrite(des, 0x5D, 0x7A)
cx3ib.i2CWrite(des, 0x65, 0x7A)

#set address of the tempsensor(Slave1)
cx3ib.i2CWrite(des, 0x5E, 0x30)
cx3ib.i2CWrite(des, 0x66, 0x30)

#set address of the EEPROM(Slave2)
cx3ib.i2CWrite(des, 0x5F, 0xA8)
cx3ib.i2CWrite(des, 0x67, 0xA8)
```

Set the serializer I^{2}C-parameters and route the reset-signal from the deserializer GPIO5-pin to the serializer GPIO0-pin.

```
#Serializer
ser = A.I2CDevice()
ser.address = 0x58
ser.clock_frequency = 400000
ser.register_address_width = 8
ser.data_value_width = 8
```

```
#route imager_reset from cx3board to imager
#Enable all GPIO inputs of the deserializer
cx3ib.i2CWrite(des, 0x0F, 0xFF)
#Set Back Channel BC_GPIO3_SEL the physical GPIO5 Pin from the Deserializer
cx3ib.i2CWrite(des, 0x6F, 0x50)
#Set GPIO3 Pin from the Serializer enable
#Enable GPIO control from remote Deserializer
#Disable GPIO2
cx3ib.i2CWrite(ser, 0x0E, 0x50)
#Disable GPIO 0 and 1
cx3ib.i2CWrite(ser, 0x0D, 0x00)
```

4.4 Interface Option 2: MIPI CSI-2

After the finishing of the PIF-demonstrator, there is now also a fitting CSI-2 serializer-deserializer pair available. To evaluate also this option, the optimized PIF-boards (see **Chapter 4.3.4**) are adapted for the work with the *Texas Instruments DS90UB935/36*.

4.4.1 Serializer-Deserializer

- **Serializer board:**
  The biggest difference is a layout change from the PIF to the CSI-2 interface. The power management and connections stay the same.
  Only one adaption has to be made, in perspective of control circuits. The $DS90UB935$ (red marking on the left side from **Figure 4.27**) does not support a $3.3V$-$VDDIO$. Therefore a level shifter from $1.8V$ to $3.3V$ is needed between the serializer and the imager and illumination. This levelshifter is shown in **Figure 4.27**. If the GPIO connections to the serializer are not needed, it is possible to disconnect them, one by one, over the resistors $R48 - R55$. The I^2C-bus is not effected due to its open drain output stage.
  It was possible to reduce the board dimensions to $76mm \times 68mm$.

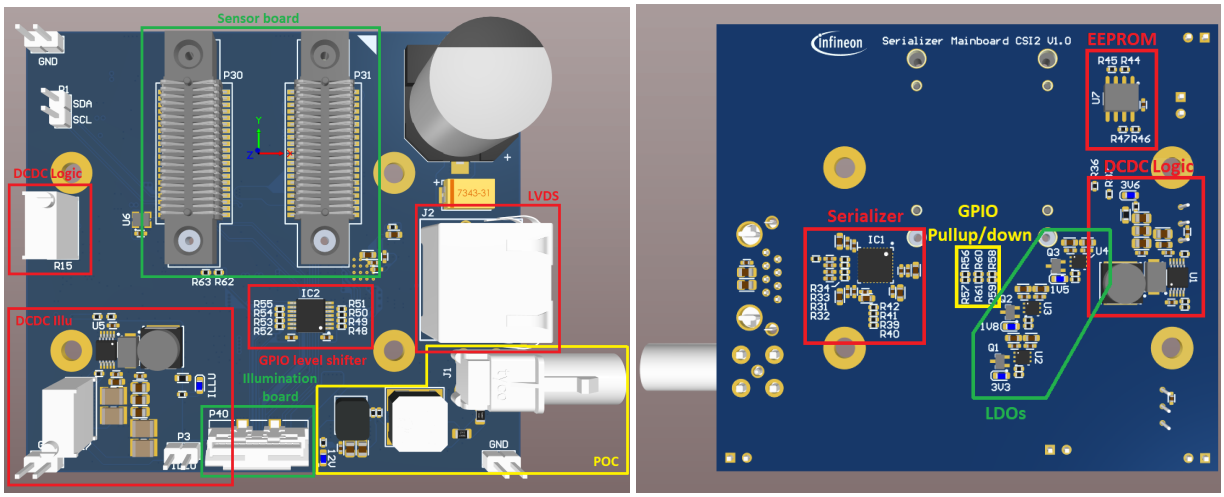

(a) Top view (b) Bottom view

Figure 4.27: CSI-2 serializer board

- **Deserializer board:**
  Due to the change from the *DS90UB964* to the *DS90UB936*, the derializer board can be a little bit simplified. Both versions work with the CSI-2 interface, so there are no changes needed.
  The *DS90UB964* is designed to work with up to four cameras, the *DS90UB936* can only work with two cameras, therefore the IC is smaller and less complex. The additional $1.1V$ is now not needed any more and so removed from the board. All other circuits stay the same (see **Figure 4.28**).
  Also the deserializer-board is reduced in size to $73mm \times 80mm$.

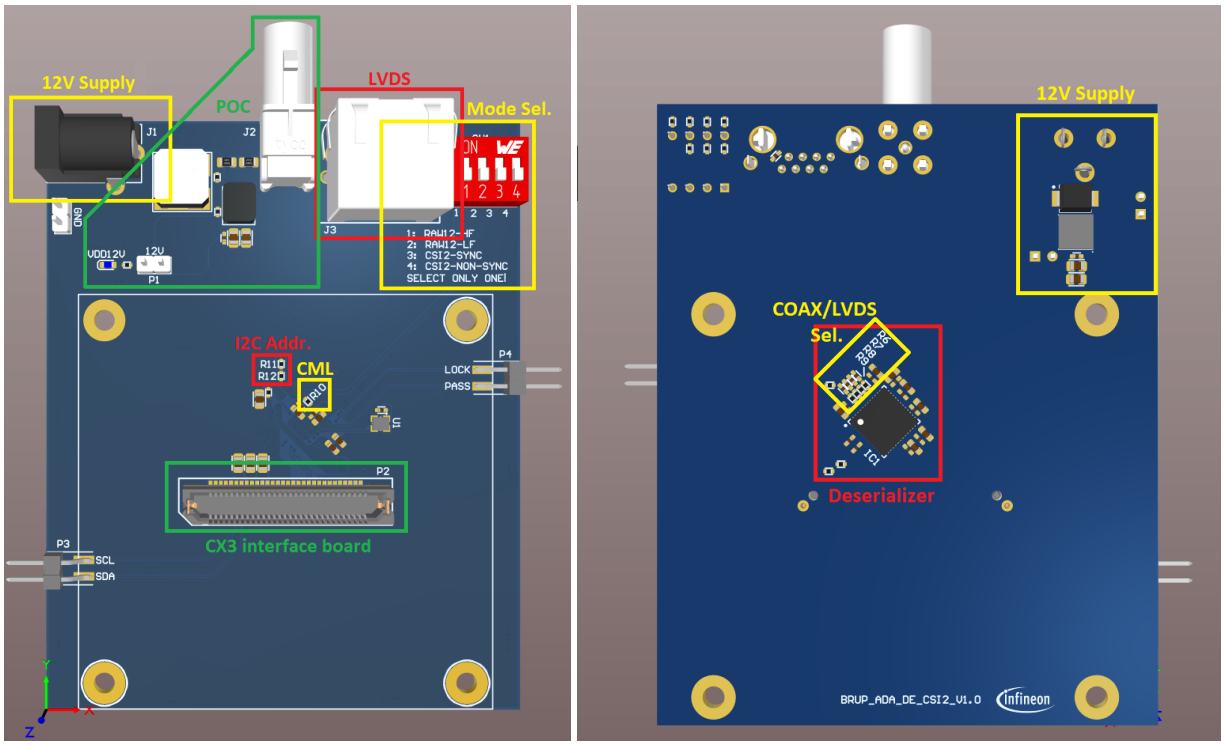

(a) Top view (b) Bottom view

Figure 4.28: CSI-2 deserializer board

- **CSI-2 interface system:**
  Figure 4.29 shows the CSI-2 setup. The frame rate can be higher compared to the PIF-version, due to the higher bandwidth of the CSI-2 interface. But both versions can exceed the required $45 fps$.

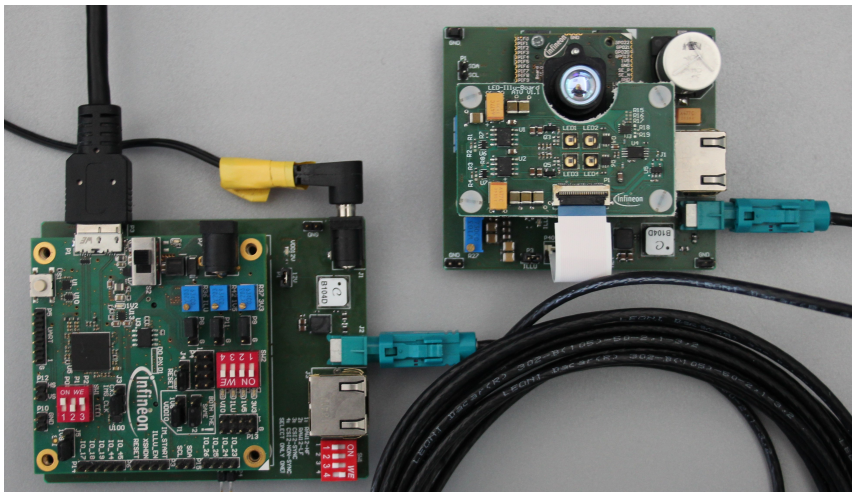

Figure 4.29: CSI-2 interface system

The *DS90UB935/36* can be run in the same way as the PIF-version, only some different registers have to be configured.

4.4.2 Register Settings

This chapter lists the register settings for the CSI-2 version.
At first configure the CX3 interface board.

```
#set CX3
import animator.animator as A

cx3ib = A.Mani()
cx3ib.referenceClockFrequency = 2400000
cx3ib.error_break = True
cx3ib.setSuperframeSeparationSize(352, 288, 0, 1)
status=cx3ib.open()
print(status)
cx3ib.setGpio(A.Pin_IM_RESET, A.Gpio_High)
```

If the interface board is working, set the deserializer I^2C parameters.

```
#Deserializer
des = A.I2CDevice()
des.address = 0x30
des.clock_frequency = 400000
des.register_address_width = 8
des.data_value_width = 8
```

Configure the MIPI CSI-2 interface for two data-lanes and $800 Mbps$ datarate.

```
#CSI settings
#CSI speed control = 800Mbps
status = cx3ib.i2CWrite(des, 0x1f, 0x02)
#CSI enable, 2 lanes
status = cx3ib.i2CWrite(des, 0x33, 0x21)
```

Set Port0 as receiving port and enable write-permission for the back-channel on this port.

```
#FPD-PORT_Control
#video stream forwarding enabled for Port0
status = cx3ib.i2CWrite(des, 0x20, 0x20)
#Write enable Port0
status = cx3ib.i2CWrite(des, 0x4c, 0x01) #receive port changed to 0
```

Configure the back-channel to 10Mbps (recommended for CSI-2 non-synchronous). Enable the I^2C pass-through for configured I^2C addresses and set the serializer I^2C address. Take care that the I^2C address is programmed with a 0_b at the end, so the address has to be shifted by one bit left. For better failure detection enable the CRC generator.

```
#Back channel Config
#BCC data-rate 10Mbps(=recommended for CSI-2 non synchronous)
#CRC Generator enabled
#Back Channel enabled
#I2C Pass-Through to Serializer if decode matches
status = cx3ib.i2CWrite(des, 0x58, 0x5a)
```

```
#I2C device config
status = cx3ib.i2CWrite(des, 0x5c, 0x32) #serializer physical address 0x19
```

Also the *DS90UB936* can communicate with more than one camera. If this cameras or devices on the camera-boards have the same I^2C address, it is possible to give them a different, virtual I^2C address on deserializer side, the mapping of these virtual- to the real I2C address is made over deserializer register settings.

```
status = cx3ib.i2CWrite(des, 0x5d, 0x7a) #imager physical address 0x3D
status = cx3ib.i2CWrite(des, 0x65, 0x7a) #imager virtual address 0x3D

#status = cx3ib.i2CWrite(des, 0x5e, 0x30) #temp sensor physical address 0x18
status = cx3ib.i2CWrite(des, 0x5e, 0x92) #temp sensor physical address 0x49

#status = cx3ib.i2CWrite(des, 0x66, 0x30) #temp sensor virtual address 0x18
status = cx3ib.i2CWrite(des, 0x66, 0x92) #temp sensor virtual address 0x49

status = cx3ib.i2CWrite(des, 0x5f, 0xA8) #EEPROM physical address 0x54
status = cx3ib.i2CWrite(des, 0x67, 0xA8) #EEPROM virtual address 0x54
```

Then set the serializer I^2C parameters.

```
#Serializer
ser = A.I2CDevice()
ser.address = 0x19 #address changed to 0x19
ser.clock_frequency = 400000
ser.register_address_width = 8
ser.data_value_width = 8
print("configure serializer")
```

Set the CSI-2 interface to two data-lanes, configure the I^2C-interface for 3.3V and set I2C-clock high- and low- times. For better failure detection enable the Transmitter-CRC generator

```
#General Config
#CSI-2 continuous clock on
#CSI-2 2 data lanes
#Transmitter CRC generator enabled
#I2C voltage is 3.3V
status = cx3ib.i2CWrite(ser, 0x02, 0x52)
#I2C-SCL High Time
status = cx3ib.i2CWrite(ser, 0x0B, 0x13)
#I2C-SCL Low Time
status = cx3ib.i2CWrite(ser, 0x0C, 0x26)
```

To connect the reset-signal from the CX3 interface board to the imager, you have to configure the back channel remote GPIO on the serializer and deserializer.

```
#route imager_reset from cx3board to imager
#Enable all GPIO inputs of the deserializer
cx3ib.i2CWrite(des, 0x0F, 0x7F)
```

```
#Set Back Channel BC_GPIO3_SEL the physical GPIO5 Pin from the Deserializer
cx3ib.i2CWrite(des, 0x6F, 0x50)
#Set GPIO3 Pin from the Serializer enable and enable GPIO control from remote
    Deserializer
#disable all other GPIO
cx3ib.i2CWrite(ser, 0x0D, 0x80)
cx3ib.i2CWrite(ser, 0x0E, 0x80)
```

4.5 Illumination board

As mentioned above, a full ToF camera system needs also an illumination to emit the modulated light for the distance measurement. Three different illumination-options have to be evaluated:

- 2×2 850nm LEDs
- 2×2 940nm LEDs
- 4 850nm VCSEL

The 850nm- and 940nm-LEDs have the same footprint, therefore the same PCB can be used for this two options. All three illumination-options have the same board outlines, so only one head sink design is necessary, if needed.

4.5.1 LED Illumination

Figure 4.30 shows the block diagram, of the LED-illumination board.

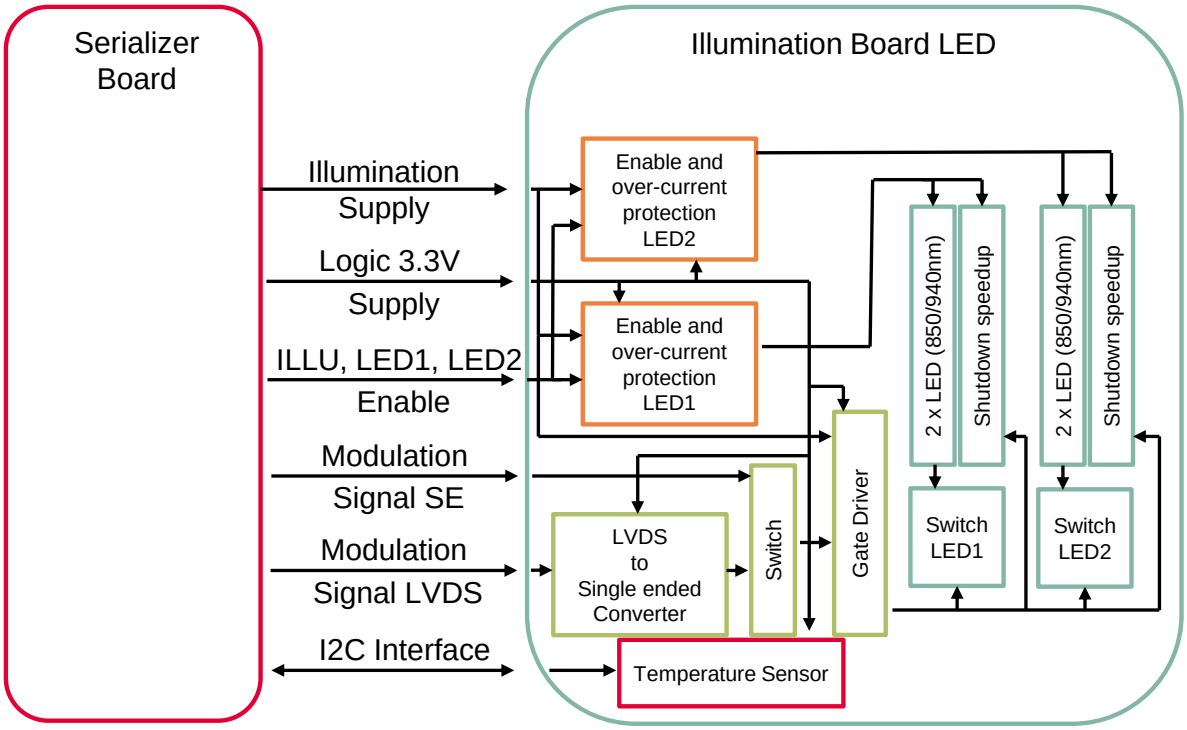

Figure 4.30: Block diagram Illumination board LED

The illumination board consists of eight main parts:

- **Enable and over-current protection:**
  Enables the two illumination paths, depending on the LED1- and LED2-enable signal. Also includes a adjustable over-current protection, the limit can be set over the resistor $R7$ and $R8$ (see **Figure 4.31** orange marking).

- **LED:**
  The LEDs emit a CW-light signal for the indirect ToF measurement. They are assembled in two versions, 850nm and 940nm wavelength.

- **Shutdown speedup:**
  LEDs have a very slow turn off behavior. For higher modulation frequencies, up to $30MHz$, an additional speedup circuit is required. With the assistance of this circuit, a similar turn-on and turn-off time can be achieved.

- **Illumination switch:**
  The illumination switch controls the emitted light depending on the modulation signal.

- **Gate driver:**
  The illumination switch needs a high power control signal, a dedicated Gate driver delivers this signal.

- **LVDS/SE switch:**
  There are two modulation signals available, a LVDS and a SE. Short the switch $J1$ (green marking **Figure 4.31**) to choose one of them.

- **LVDS to Single ended converter:**
  On the gate driver is no differential input available, so a LVDS to SE converter is necessary.

- **Temperature Sensor:**
  The temperature sensor measures the LED temperature and delivers it, over the I^2C-interface, to the PC. The PC needs this data to correct the temperature failure, from the z-image (described in **Chapter 5.1**).

Figure 4.31 shows the implementation of the block diagram **Figure 4.30**. The board is designed to mount it as near as possible to the lens. The dimensions of the board are $57mm \times 35mm$

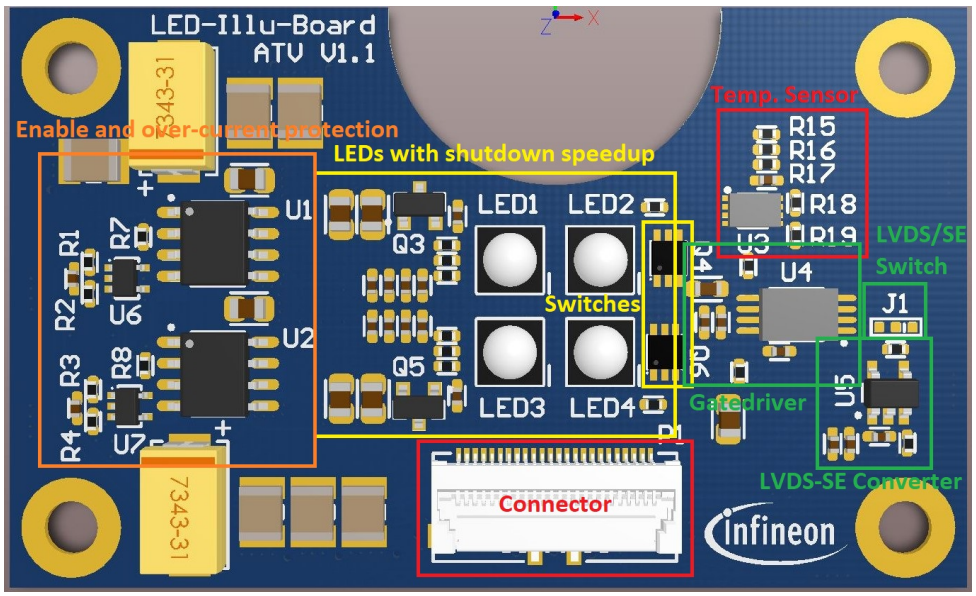

Figure 4.31: Illumination board LED

4.5.2 VCSEL Illumination

The VCSEL-board uses VCSELs, instead of LEDs, for illumination. This leads to some changes shown in **Figure 4.32**.

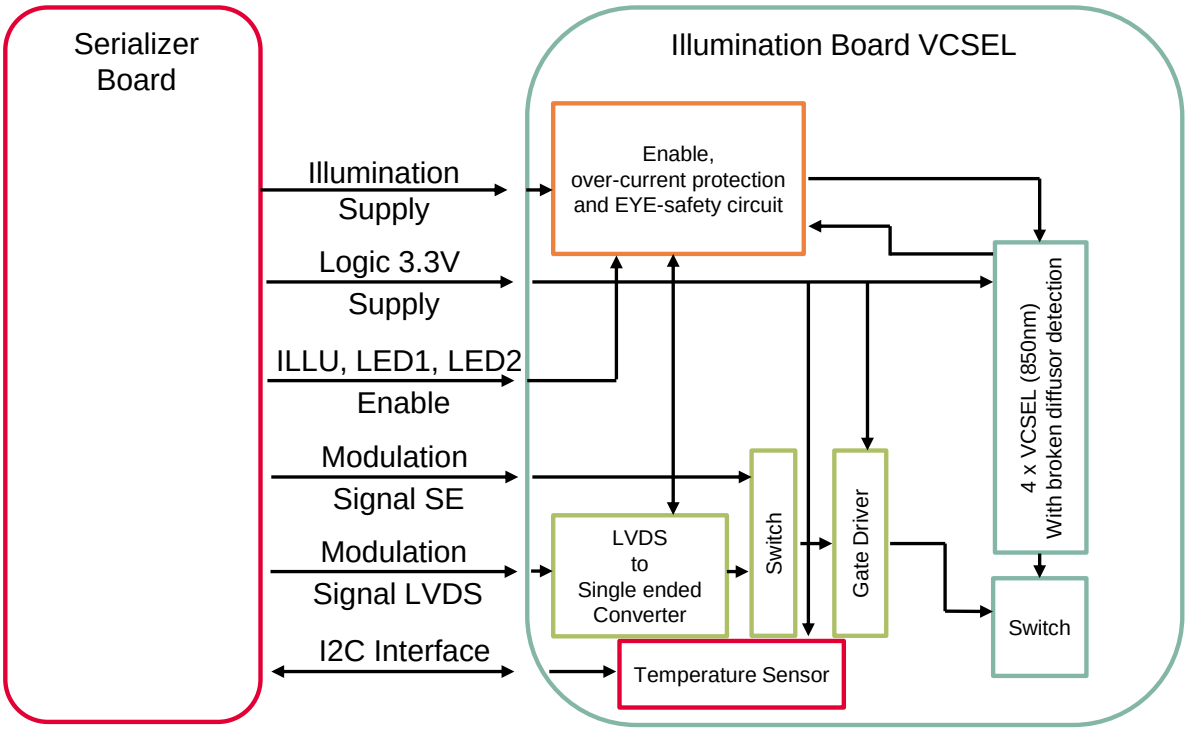

Figure 4.32: Block diagram Illumination board VCSEL

The four VCSELs are arranged in serial, so only one path is needed. The VCSEL does not need an additional turn-off circuit, due to there very good switching behavior. The gate driver circuit has to be changed, because the driver from the illumination board does not reach the possible high switching frequencies.
Working with Lasers can lead to damage to human eyes and skin. Therefore a safety circuit has to be integrated (see **Figure 4.33** orange marking). The safety concept includes a peak power detection, an average power detection and a broken diffuser detection. The function of the circuit was tested and proven, but the illumination power limits were not calculated and implemented, this would exceed the boundaries of this masterthesis. So laser-safety goggles are necessary, when operating the demonstrator with VCSEL-illumination.

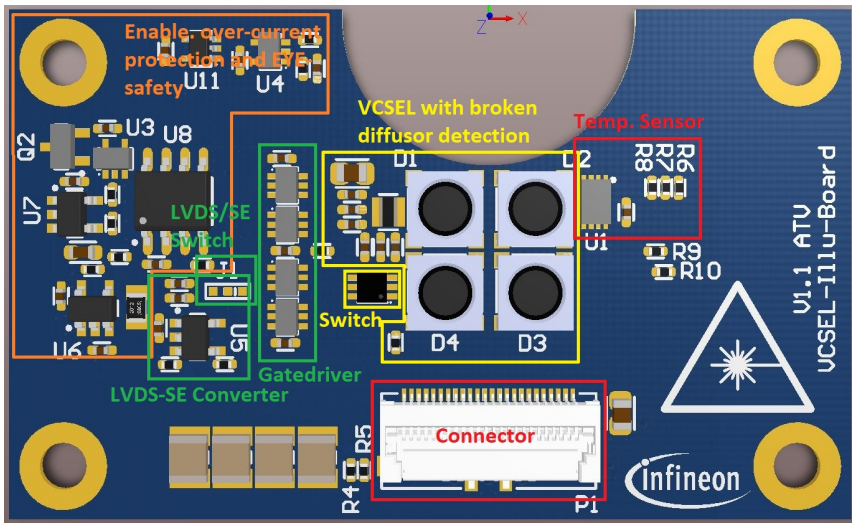

Figure 4.33: Illumination board VCSEL

4.5.3 Lessons learned - Illumination

Measurements on the illumination boards (see **Attachment B**) lead to some insights:

- The four LEDs or VCSELs are operated in a very inefficient region. The limiting factor for the LEDs is the maximum current from approx. $1.5A$, average during illumination. The VCSELs would need a higher voltage, but more then $10V$ are not possible, due to the voltage drop, over the coupling-decoupling network and the minimum voltage difference, between the output and input of the DCDC. Its better to use only two LEDs and VCSELs with a DCDC, which is capable to deliver higher currents.
- The LVDS to SE converter needs a pull-down resistor on the positive input and a pull-up on the negative. Otherwise it can cause a permanent turn-on of the VCSELs, when the LVDS-modulation output is not enabled.
- The illumination shape of the VCSELs is much more uniform and illuminates nearly the whole FoV. In comparison the LEDs have a peak in the middle and decreasing very fast to borders.
- Due to the higher modulation frequency and as a consequence the faster rise- and fall-times, the VCSEL-system has a lower depth noise.
- Higher modulation frequencies correspond with lower output power. A tradeoff between power and signal shape must be found.
- The LED-turnoff-speedup improves heavily the turn turnoff behavior, but increases also strongly the current consumption. Here must be also found a tradeoff between power loss and signal shape.
- For higher modulation frequencies or longer distances between imager and gate driver the LVDS-option should be used.
- A carefully routed low impedance layout, especially between the VCSEL- or LED-bulk capacitors and the illumination switch and at the gate-signal, heavily effects the optical signal shape.
- A proper heat-sink is necessary to get rid of the temperature, caused by the power losses.
- The impedance controlled cable is very stiff, a normal flat-band cable should be also sufficient.

4.6 Finalized demonstrator

For the finalized demonstrator (see **Figure 4.35** and **Figure 4.36**), the boards should be as small as possible, all parts must have an automotive qualification. Considering the lessons learned, the COAX connector is removed and a special automotive two pair *FAKRA*-STP-connector is used. One pair connects the FPD-Link III, containing image data, GPIOs and I2C. The other pair delivers the power supply. The illumination connector is also replaced by a normal, dense flat-band connector. The two DCDCs are changed to smaller versions. The illumination-DCDC can now deliver currents up to $3A$.

4.6.1 Serializer-Deserializer

- **Serializer board:**
  Figure 4.34 shows the block diagram of the finalized serializer board: The imager delivers the picture data over a CSI-2 interface to the serializer. The serializer converts this data and sends them to the STP-cable. Furthermore the imager provides the modulation signal to the illumination board, using the LVDS-interface.
  An oscillator supplies the imager with a $26MHz$ clock signal. The serializer controls the imager reset signal in dependence of a deserializer GPIO remote connection. The reset signal has to be level shifted between the imager and the serializer. The serializer connects also the I^2C-bus with the FPD-Link. The I^2C-bus links the serializer, the imager, the EEPROM and the temperature sensor from the illumination board. The second STP-pair delivers the $12V$ power supply to the power management (red markings in **Figure 4.34** and **Figure 4.35**). The power management converts the $12V$ down to $7V$ for the illumination, capable to deliver $3A$. A second DCDC converts the $12V$ to $3.6V$, which is delivered to a $3.3V$ LDO and a $1.8V$ DCDC. The $1.8V$ gets down-converted once again to $1.5V$. The $3.3V$ supplies the illumination board, the imager, the oscillator, the EEPROM and the high-side of the level-shifter. The $1.8V$ are delivered to the serializer and the level-shifter low-side. Additional to the $3.3V$ the imager needs also a $1.5V$-supply, provided by the power management.

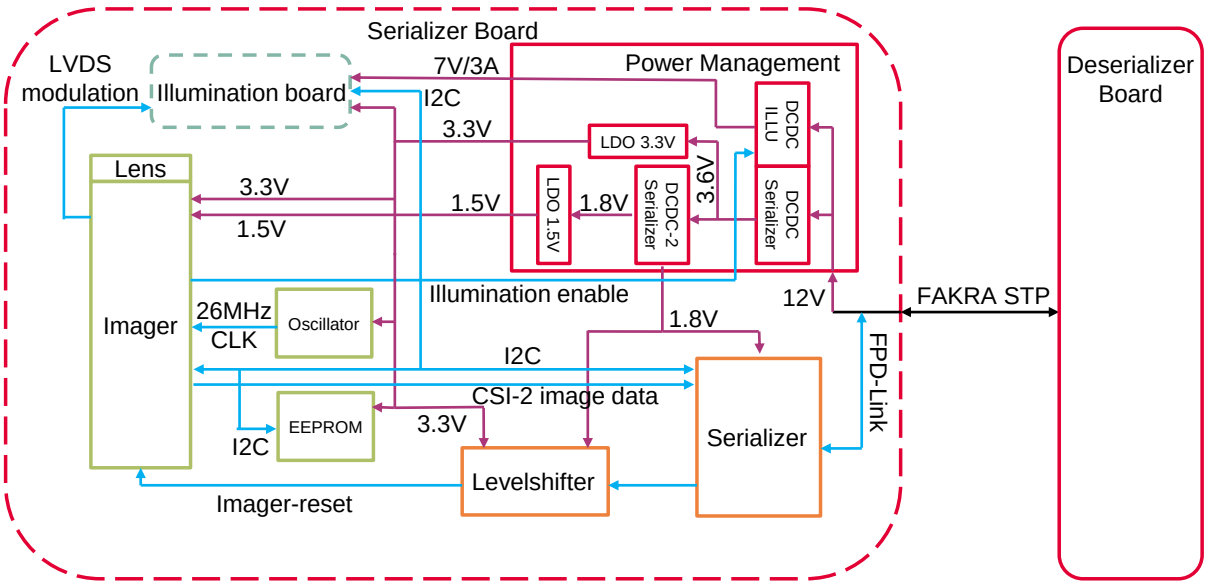

Figure 4.34: Blockdiagram demonstrator serializer board

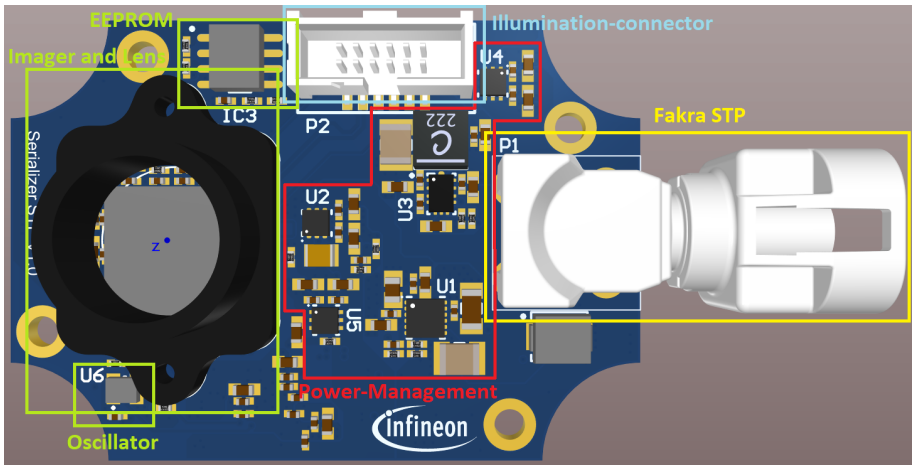

Figure 4.35: Demonstrator serializer board top view

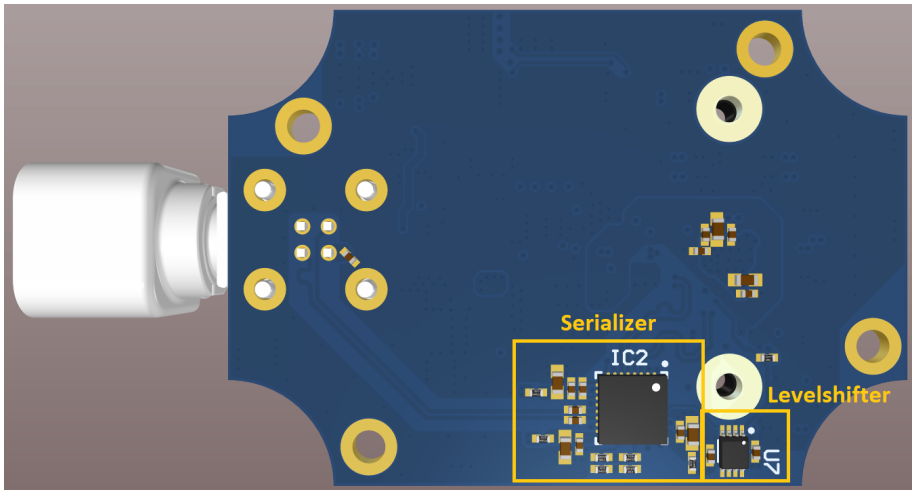

Figure 4.36: Demonstrator serializer board bottom view

- **Deserializer board:**
  At the deserializer board, the COAX- and the Ethernet-connector are replaced by the FAKRA-STP connector (see **Figure 4.38**), otherwise some layout optimizations are made.

  Figure 4.37 shows the block diagram of the deserializer board.
  An external power supply delivers the $12V$ to the FAKRA STP-cable. The deserializer and the oscillator are supplied from the $1.8V$- and $3.3V$-supply, coming from the CX3 interface board.
  An oscillator supplies the deserializer with the $26MHz$ clock. The different deserializer modes can be chosen over a switch (Mode Control **Figure 4.37** or yellow marking **Figure 4.38**).
  The image data, coming from the FPD-LINK, are converted, from the deserializer to a CSI-2 signal, delivered to the CX3 board and sent from this to the PC over a USB-cable.
  The control signals are delivered in the opposite direction from the PC to the CX3

interface board (USB cable), then to the deserializer (CSI-2) and then to the FAKRA STP-cable (FPD-Link). Only the I^2C is bidirectional and can go in both directions.

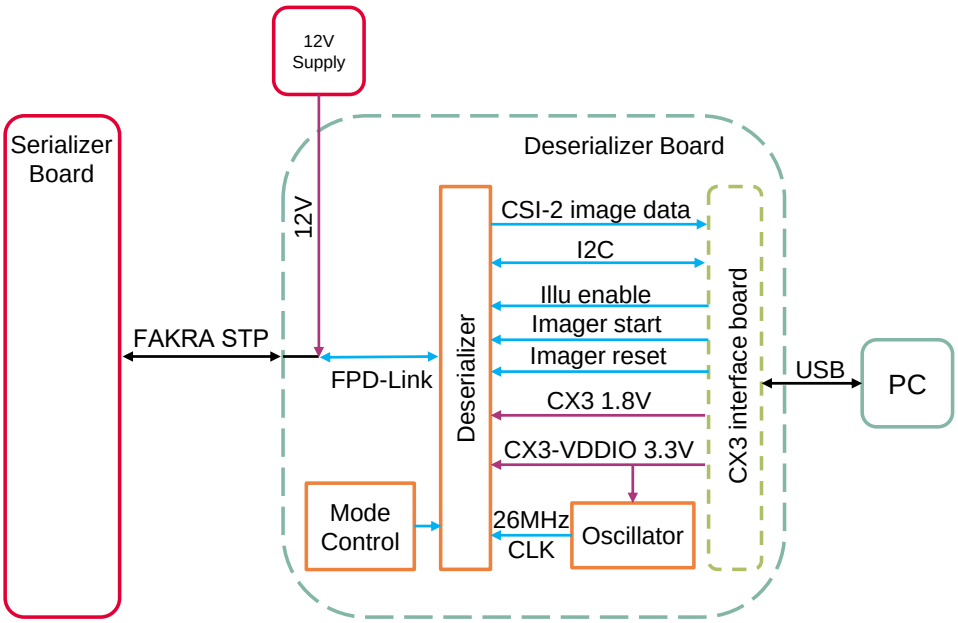

Figure 4.37: Blockdiagram demonstrator deserializer board

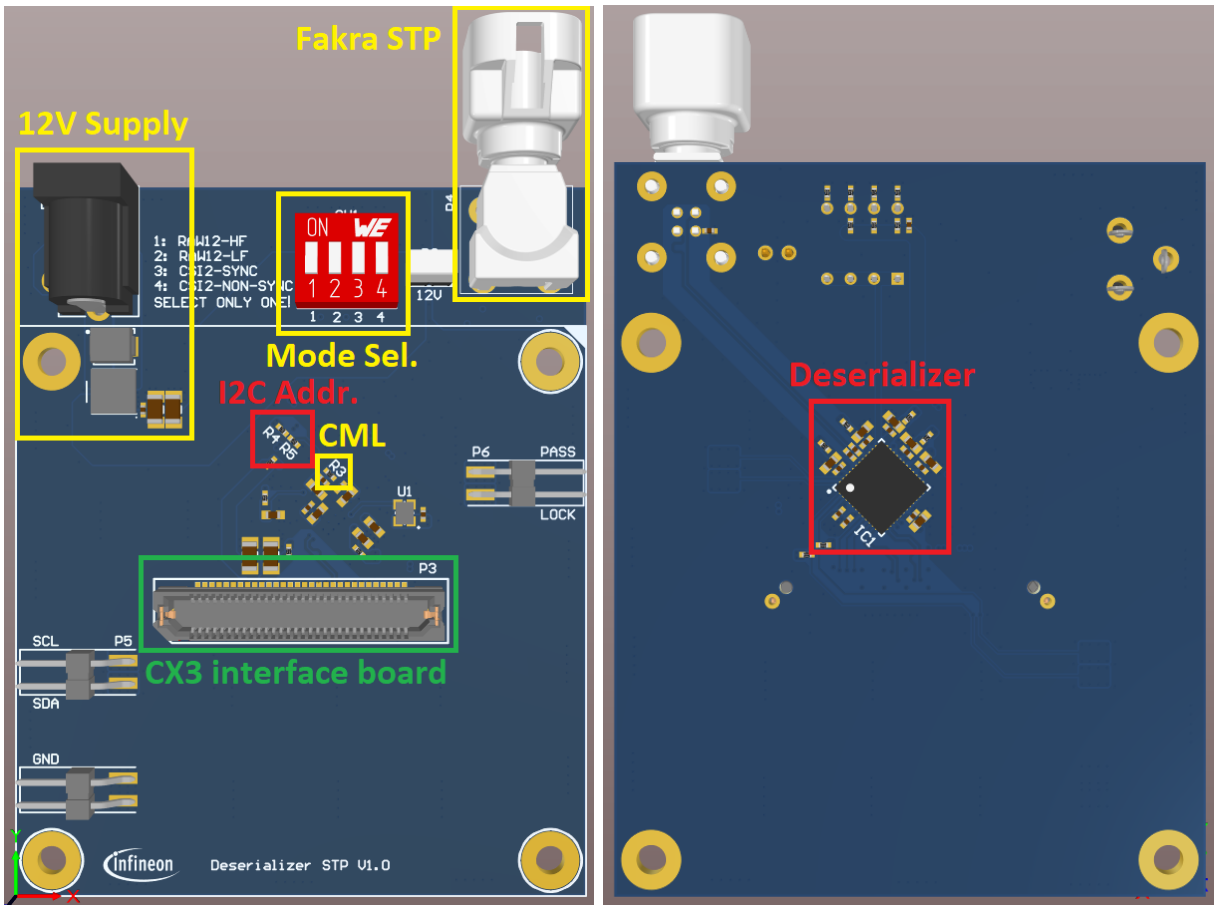

(a) Top view (b) Bottom view

Figure 4.38: Demonstrator Deserializer board

4.6.2 Illumination boards

Also at the illumination boards some changes were made. Reducing the amount of LEDs and VCSELs together with the better illumination DCDC, leads to a much more efficient operating region. Even the amount is half, the optical output is higher then at the old boards.
Due to the better properties the decision was to use VCSEL illumination for the demonstrator, a $850nm$- and a $940nm$-version was developed, but there is also an additional $850nm$-LED-board, caused by the missing Eye-safety certification.
The connection is changed to a normal flat-band, the single ended option and the over-current protection are removed and the enable signal is now connected to the DCDC.
The boards are designed in that way, they can be easily exchanged without any adoptions on the serializer board. All illumination boards are fitting in the demonstrator case and have as less as possible parts on the top side. This leads to a maximum surface thermal-coupled to the box, acting as head-sink.

- **Illumination Board LED:**
  Figure 4.39 shows the block diagram from the LED-illumination board shown in **Figure 4.40**.

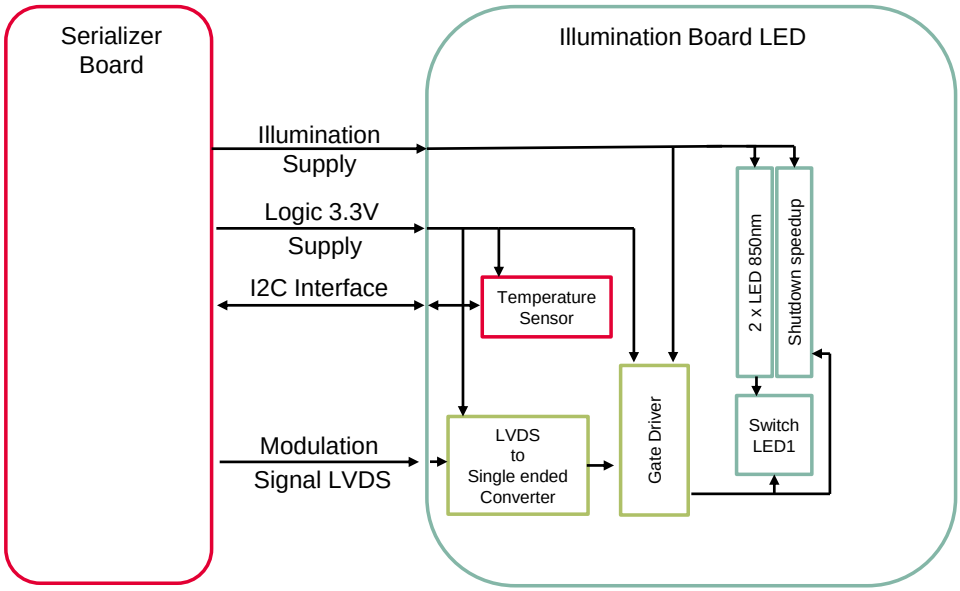

Figure 4.39: Blockdiagram demonstrator illumination LED

The illumination board is adopted, the two LEDs, in serial, are directly supplied over the connector. The modulation signal is coming from the LVDS interface. This is converted to SE and delivered to the gate-driver. The gate-driver controls the illumination switch. A shut-down-speedup circuit decreases the LED turn-off times. A sensor measures the approximated LED temperature and delivers it to the I^2C-bus.
The LVDS-SE converter, the gate-driver and the temperature sensor are supplied with $3.3V$, coming from the serializer board.

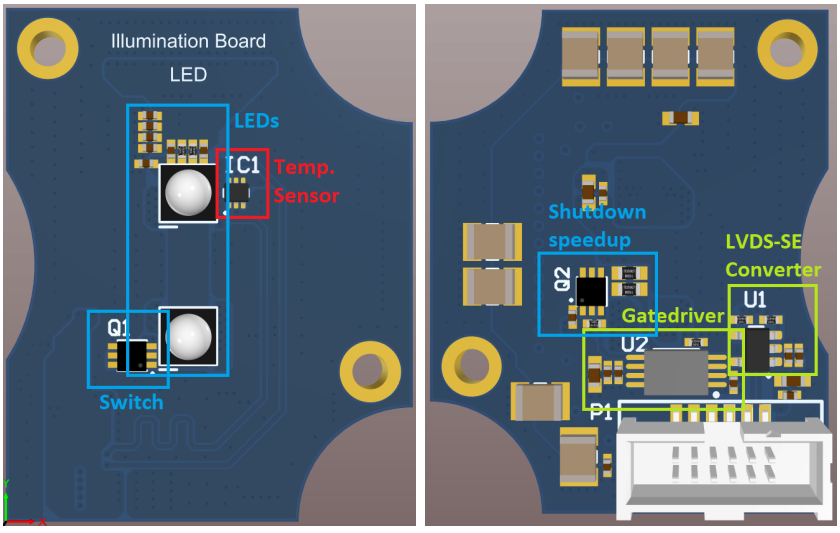

(a) Top view (b) Bottom view

Figure 4.40: Demonstrator illumination board LED

- **Illumination Board VCSEL:**
  Figure 4.41 shows the block diagram from the VCSEL-illumination boards shown in **Figure 4.42** and **Figure 4.43**. The structure from the $850nm$- and the $940nm$-version is the same, only the footprints from the VCSELs are different, therefore two versions had to be developed.

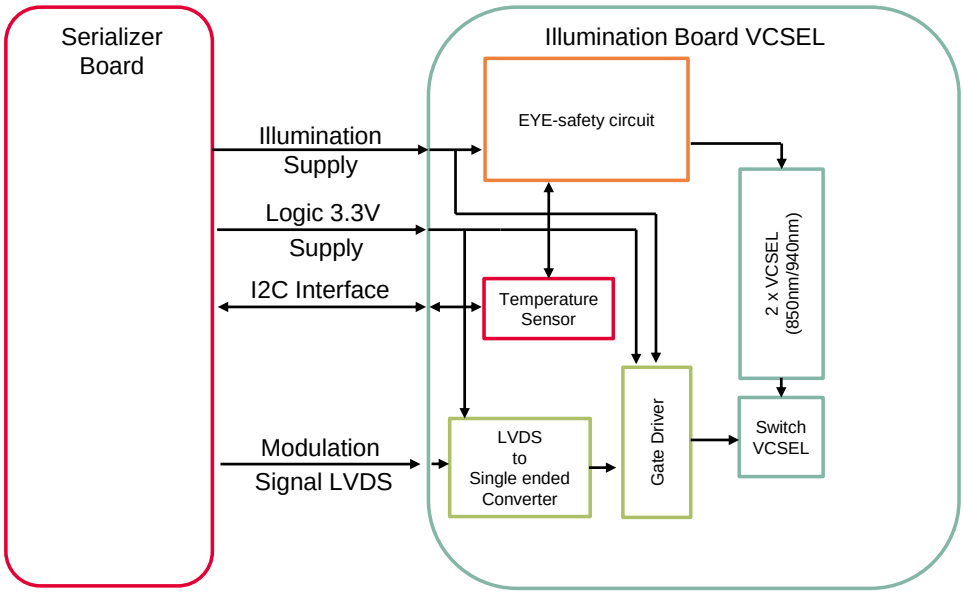

Figure 4.41: Blockdiagram demonstrator illumination VCSEL

The VCSEL-boards differ in three parts from the LED-board:

- At the VCSEL board is no turn-off speedup circuit needed.
- The gate driver is a different, faster one. There is also a change compared to the first VCSEL-board, the driver ICs are reduced and changed to a smaller version.
- There is an additional eye-safety circuit on the board (necessary for Laser-illuminations). Also the eye-safety circuit is adopted. There is no broken-diffuser-detection any more, is not necessary if the optical power is limited in the safe-region, and there is now one IC, instead of two, for average- and peak-current monitoring. This IC also turns of the power in case of a limit-violation. Take care that also at this board the safety circuit is not trimmed as mentioned above the correct settings are topic of further research and are not part of this master thesis.

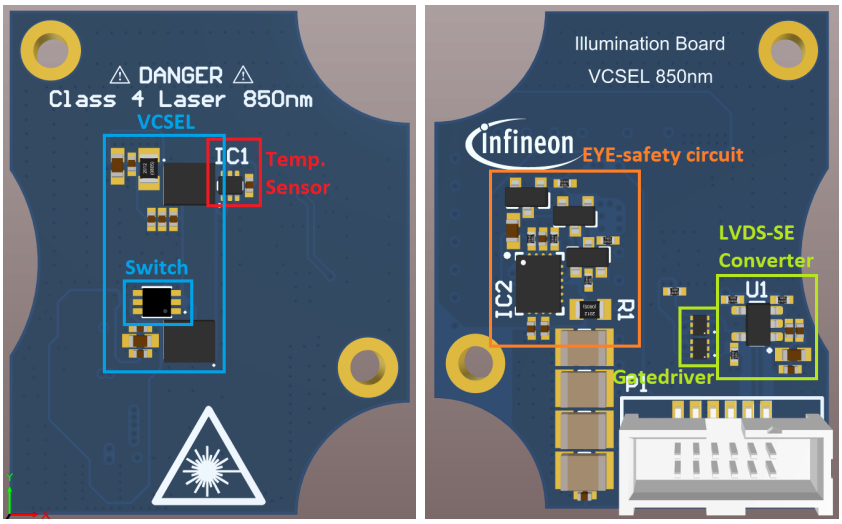

(a) Top view (b) Bottom view

Figure 4.42: Demonstrator illumination board VCSEL 850nm

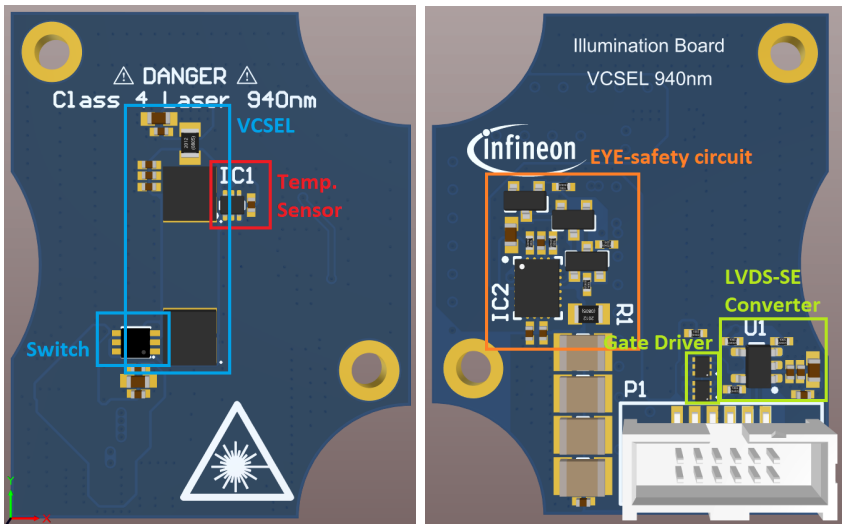

(a) Top view (b) Bottom view

Figure 4.43: Demonstrator illumination board VCSEL 940nm

4.6.3 Assembled Demonstrator

This chapter describes the mechanical design considerations and shows afterward some pictures of the assembled demonstrator.

- **Lens:**
  The lens, shown in **Figure 4.44**, has 100° FoV and focuses the incoming light on the imagers active region. This results in a FoV of $100° \times 85°$. For better ambient light performance an optical filter is mounted in the lens holder. For the different wavelengths are different filters needed. One for $850nm$ and one for $940nm$ both have a bandwidth from approximately $30nm$.

Figure 4.44: Demonstrator Lens

- **Demonstrator - Box:**
  Figure 4.46 and **Figure 4.47** show the demonstrator box- body and lid. The box has a big contact area to the board to transport the heat away from the board. The serializer board has as less parts as possible on the bottom side, only the serializer and some decoupling-capacitors for the imager are attached. This is made due to some electrical design- and board space-considerations, but under all power management devices (LDOs and DCDCs) the board has direct contact to the box.
  The illumination board, especially the LED-board (due to the switching losses of the turn-off speedup circuit), has even a higher thermal generation then the serializer board. Therefore the thermal layout has to be made very carefully. Only the parts which directly affect the optical signal shape mounted on the top side. Also the FoV from the illumination has to be considered in the design.
  The box has an optical separation between the illumination- and receiving-path (lens) (see **Figure 4.47**). Without this separation light travels between optical window and the PCB surfaces and can reach in this way the imager. This leads to a corruption of the z-image. Also a separation of the two windows is necessary. If only one big window is used for illumination, receiving light can pass through the window to the lens. This issues are illustrated in **Figure 4.45**

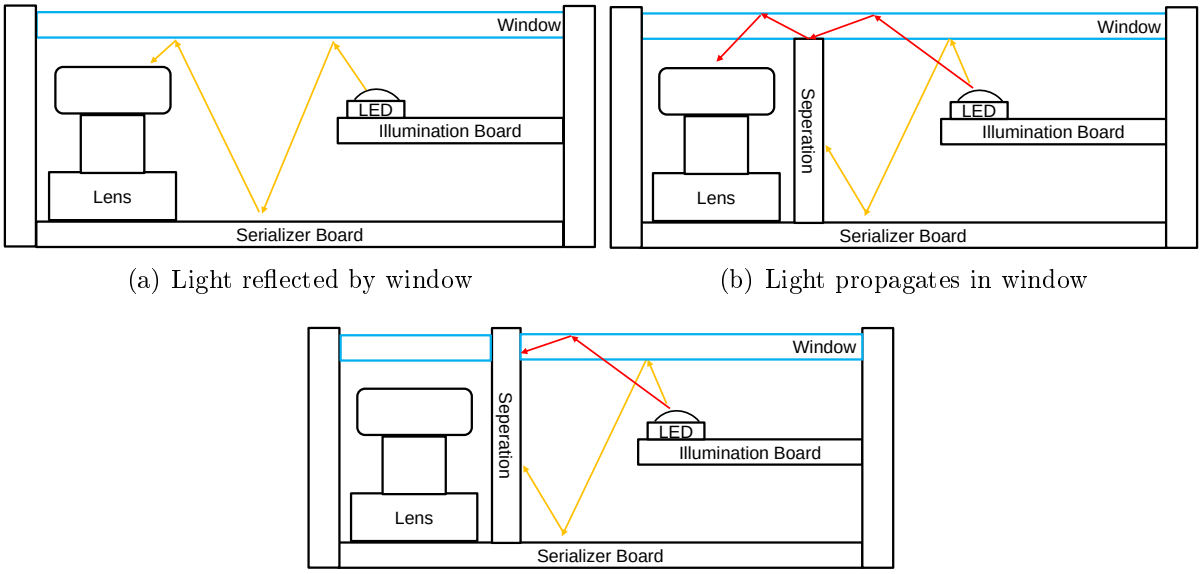

(a) Light reflected by window

(b) Light propagates in window

(c) Solution to solve this issue

Figure 4.45: Possible light paths

To protect the windows from scratches, they are embedded in the box surface. Due to its mechanical stability, the good machine-ability and the low thermal resistance aluminum was chosen as box-material. The box is manufactured by a 3D-printing company, aluminum powder is melted with a laser, layer over layer, and so the box can be manufactured with low tolerances and also sharp angles can be made, not as at CNC machining.

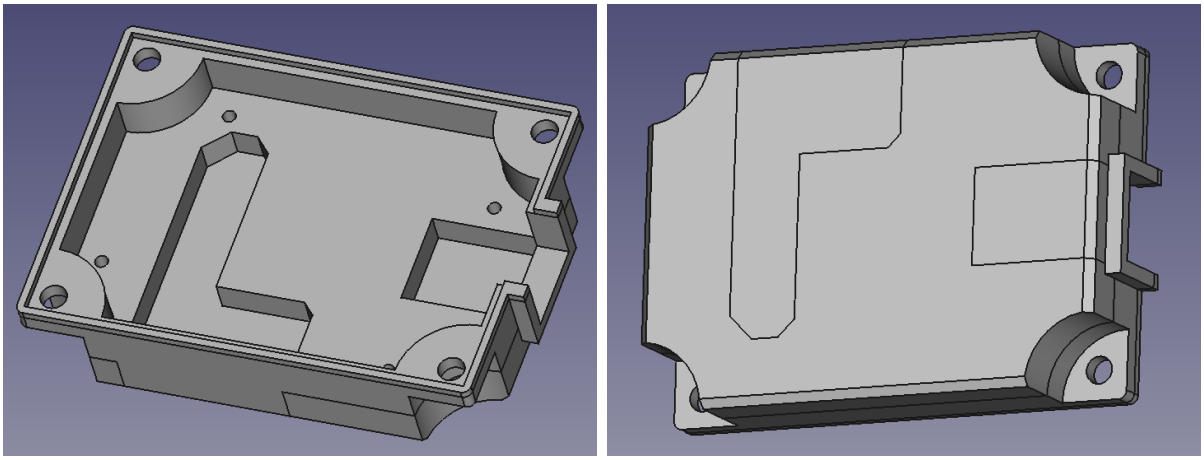

(a) Inside view

(b) Outside view

Figure 4.46: Demonstrator Serializer Box-Body

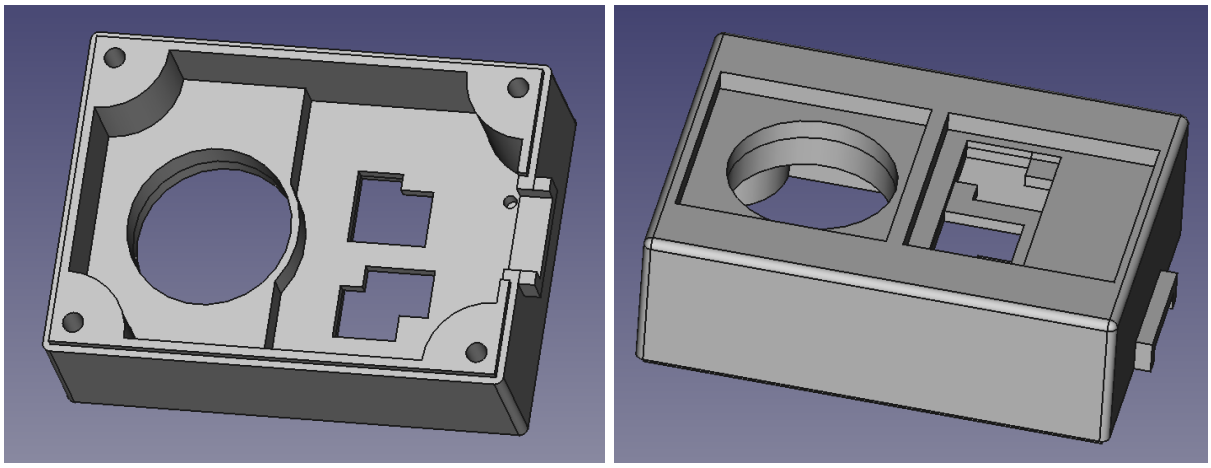

(a) Inside view (b) Outside view

Figure 4.47: Demonstrator Serializer Box-Lid

- **Demonstrator Box - Windows:**

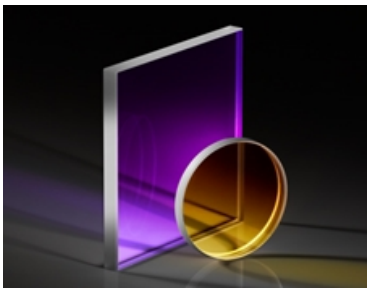

Figure 4.48: Demonstrator window [Opt19]

The windows (see **Figure 4.48**) have to fulfill special requirements. They must have high stability, a very good transmission profile, especially in the IR-region and they should have a good flatness, because surface irregularities can lead to distortions. It is also important that the windows have an anti-reflective coating, otherwise it will come to reflections between the window and the lens, as shown in **Figure 4.49**.

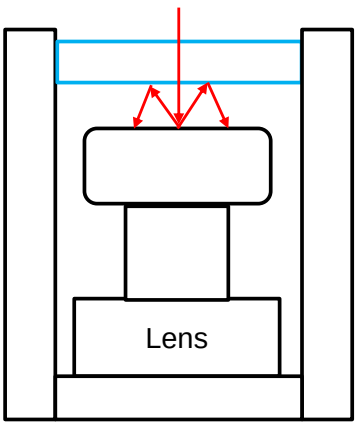

Figure 4.49: Demonstrator window: anti-reflective coating

- **Assembled demonstrator:**
  The next pages show some pictures of the finalized demonstrator. In the figures, **Figure 4.50**, **Figure 4.51** and **Figure 4.52**, the serializer board, the deserializer board and the illumination boards are shown in bottom and top view. **Figure 4.53** shows the serializer board connected with the illumination board. In **Figure 4.54** the boards are mounted in the open box. **Figure 4.55** displays the assembled ToF-3D-camera.
  Figure 4.56 shows the complete automotive grade ToF camera demonstrator. This setup is used to characterize the demonstrator in the next chapter, **Chapter 5**.

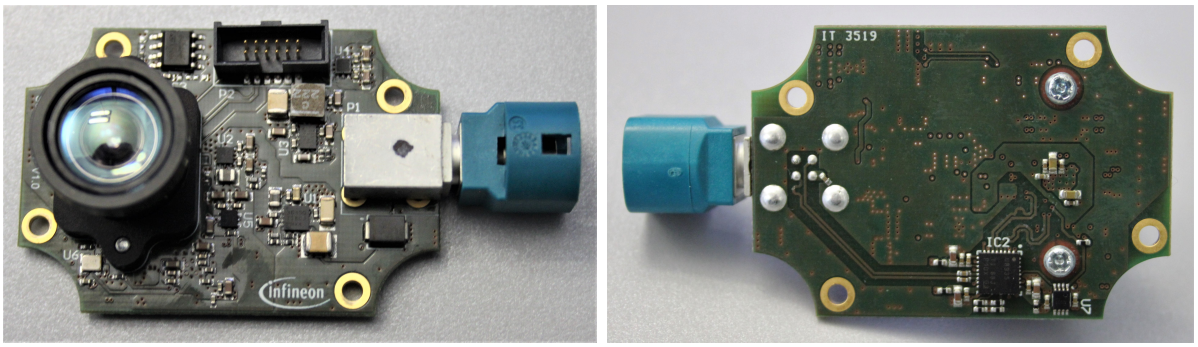

(a) Top view (b) Bottom view

Figure 4.50: Picture Serializer board

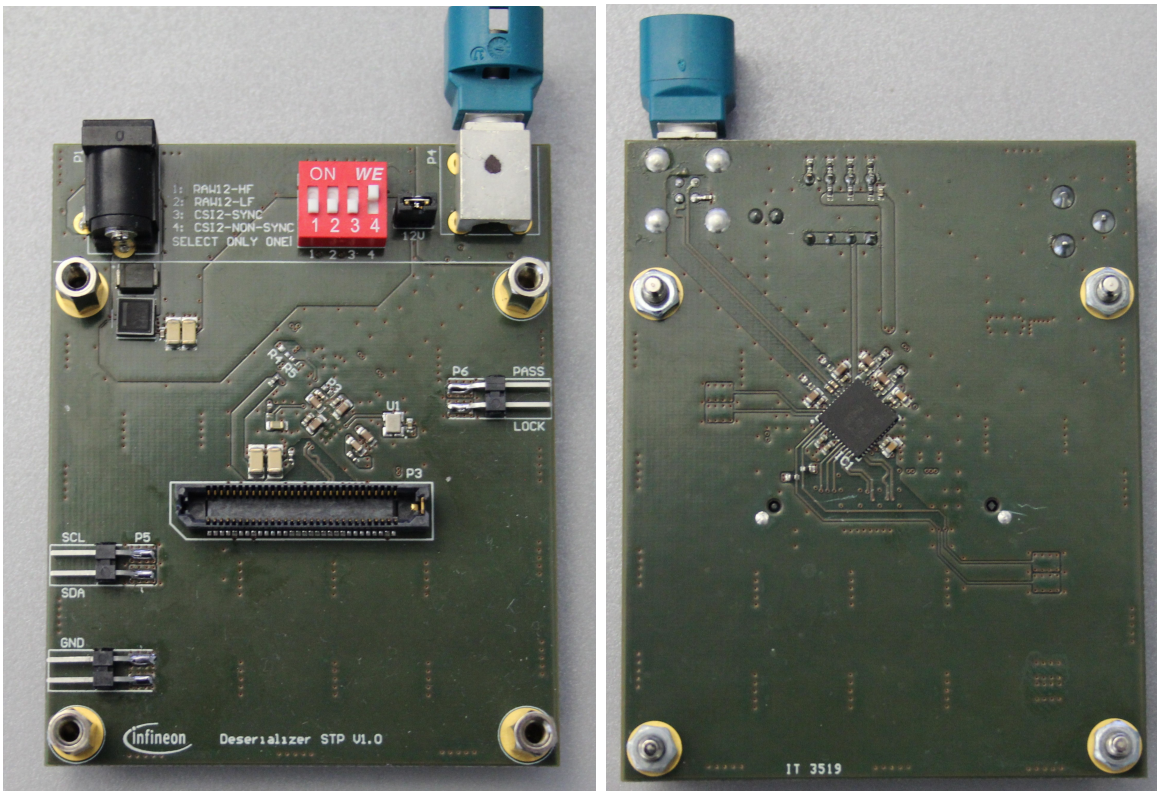

(a) Top view (b) Bottom view

Figure 4.51: Picture Deserializer board

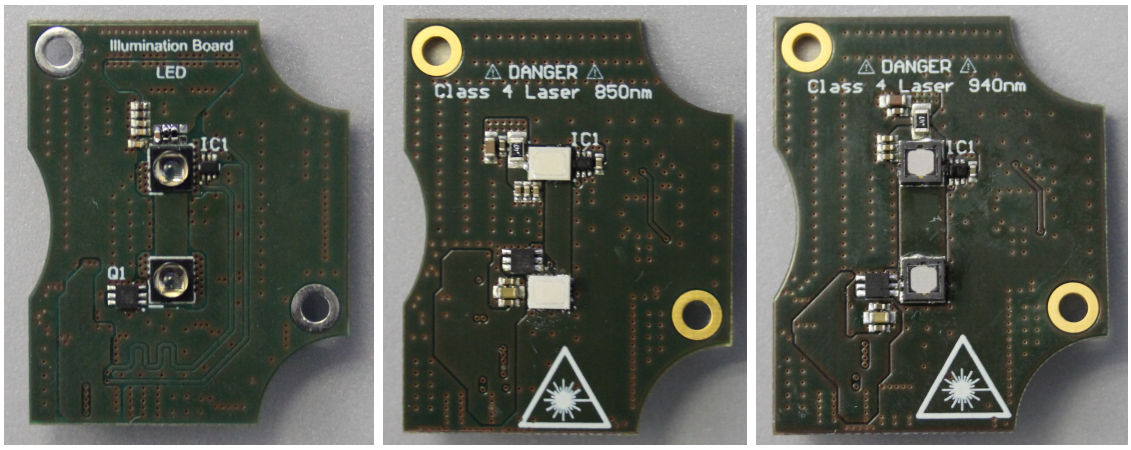

(a) LED-850nm-Top (b) VCSEL-850nm-Top (c) VCSEL-940nm-Top

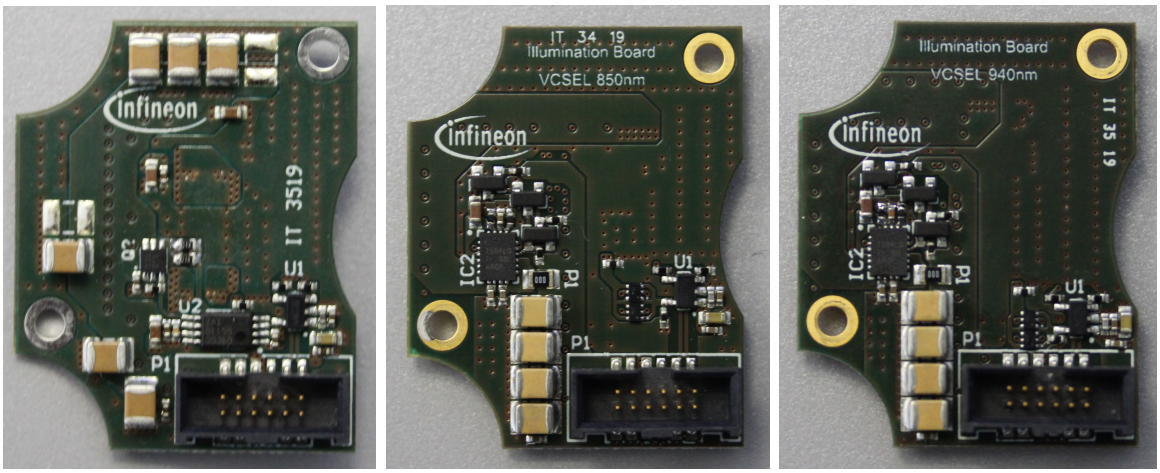

(d) LED-850nm-Bottom (e) VCSEL-850nm-Bottom (f) VCSEL-940nm-Bottom

Figure 4.52: Picture illumination boards

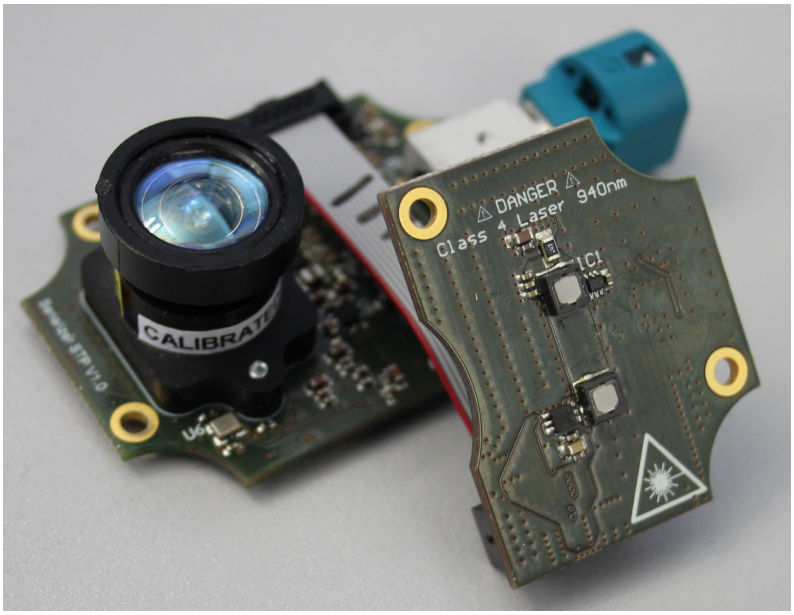

Figure 4.53: Demonstrator serializer board with illumination board

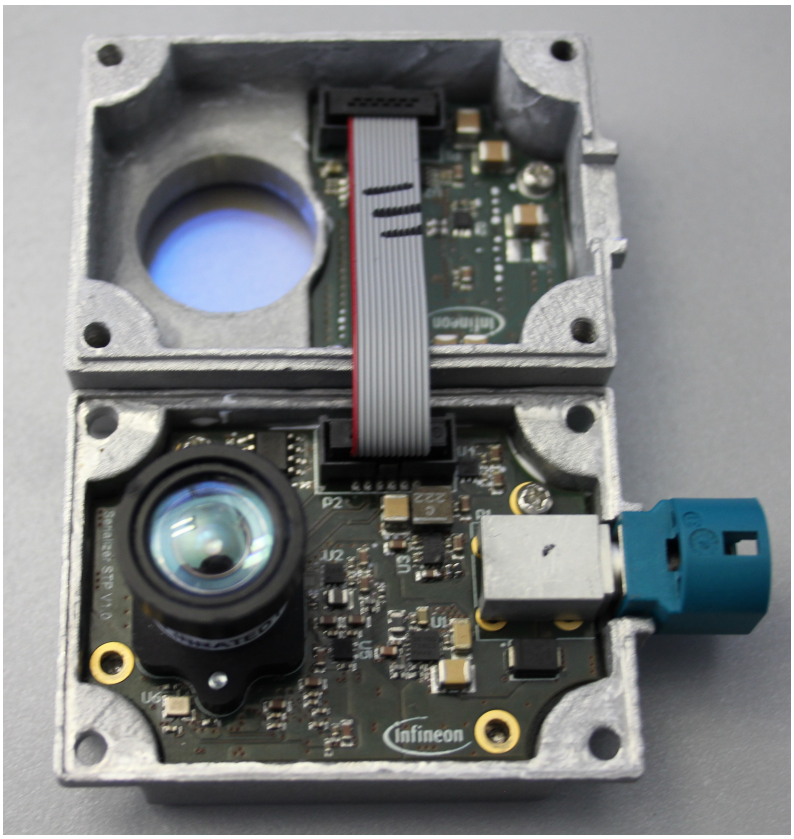

Figure 4.54: Assembled camera inside

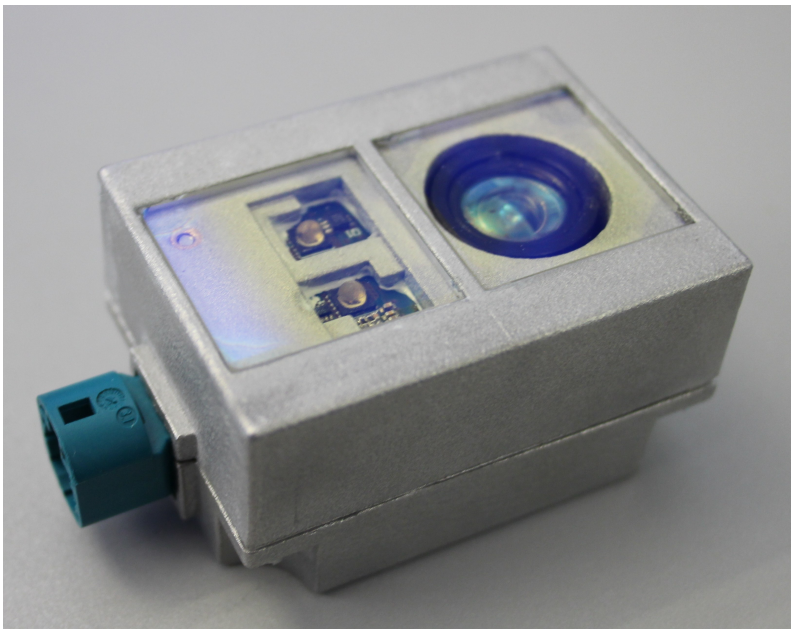

Figure 4.55: Assembled camera outside

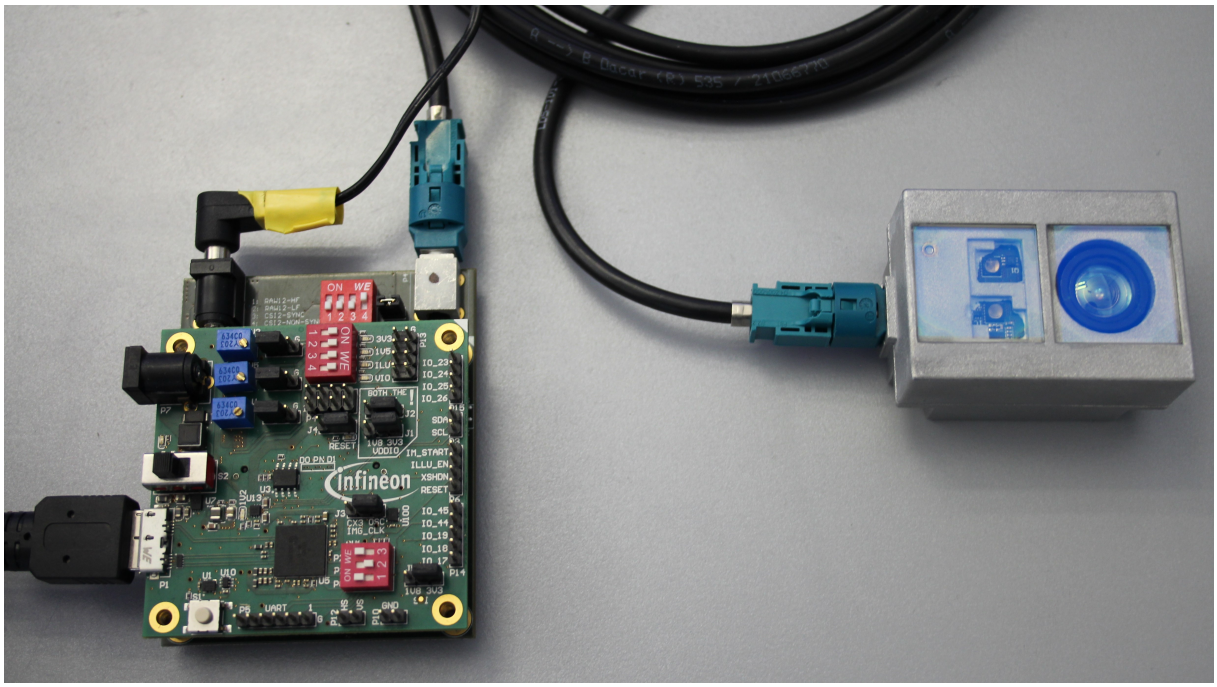

Figure 4.56: Demonstrator system

5 Time-of-Flight Camera characterization

In this chapter the characterization of the ToF camera demonstrator is shown. It is divided in three parts. Starting from the overall camera performance. Later going more in detail with the determination of the optical signal, later thermal images were made to evaluate the performance of the heat management. And at least the characterization of the whole power supply system is presented.

5.1 Linear translation stage measurements

To evaluate the 3D-depth performance a basic calibration is necessary. After this calibration, the system is measured with all three types of illumination, 850nm-LED, 850nm-VCSEL and 940nm-VCSEL.

5.1.1 Calibration

This chapter gives a short overview of the parameters which are necessary to calibrate. The effort was to adopt some already existing scripts. Therefore a detailed description of every parameter, especially for the lens calibration, is not given. This would exceed the range of the this master thesis.

- **Lens focus:**
  The Lens focus can be trimmed with a checked pattern. Point the camera to the checked pattern. A software calculates the peak contrast value from the image. Tune the lens as long this contrast value reaches its maximum.

- **Lens parameters:**
  Position the checked pattern mentioned above, in small sections whole over the region of interest and save at every move a picture from it. Make at least 50 pictures in total. A software can extract the lens parameters from this pictures, including focal length, position of the central pixel, camera matrix, distortion coefficients and r-vector and t-vector.

- **Global offset and frame pattern phase noise:**
  Cause of electrical delays between modulation signal on the imager and the optical signal, there is a constant offset in the depth measurement. With a picture, made from a flat uniform surface and known distance, this offset can be calibrated. A special offset failure is the **Frame pattern phase noise** (FPPN) the FPPN results from incontinuous in the modulation regulator (see **Figure 5.1**). This can be calibrated also with a flat surface picture. The offset errors are strongly depending on the modulation frequency. If a use case with a different modulation frequency is chosen, the calibration must be made again.

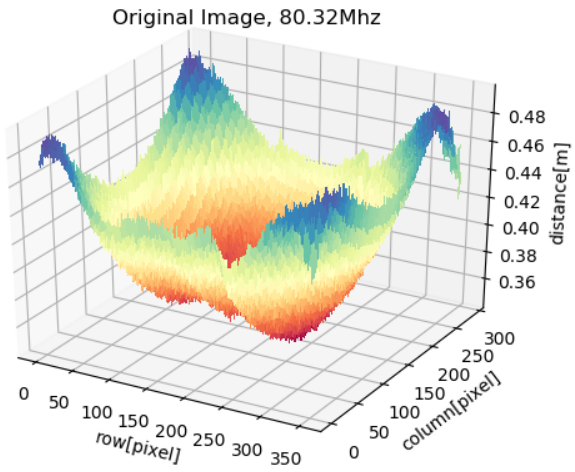

(a) Original Image

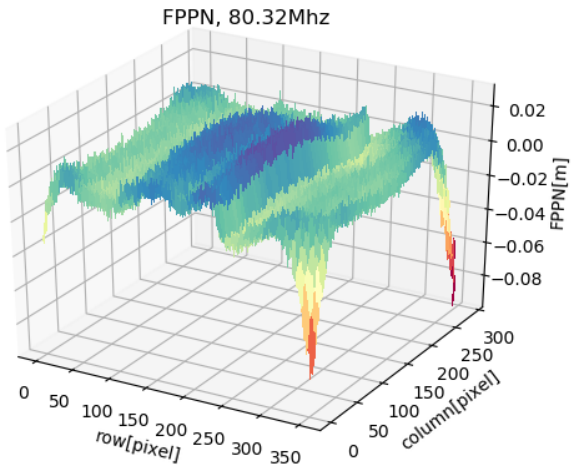

(b) Frame pattern phase noise

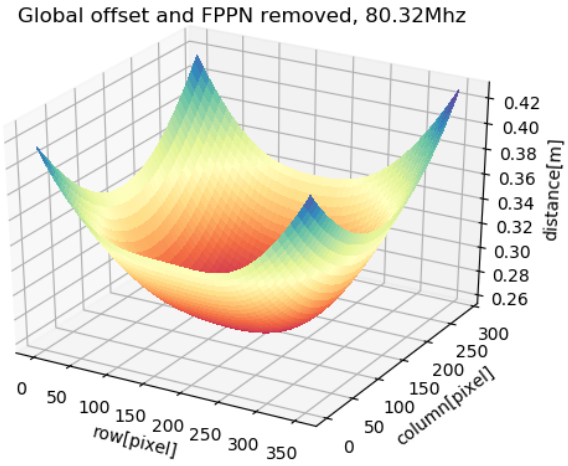

(c) FPPN and global offset removed

Figure 5.1: Global offset and frame pattern phase noise

- **Temperature slope:**
  With rising temperature the efficiency from VCSELs and LEDs are decreasing, this also effects the depth measurement. For this issue a temperature sensor is located near to the illumination. Over a long period of time a continuous depth measurement is performed. Due to the power losses temperatur is increasing and the effect on the depth data is monitored. Out of this data a linear approximation is extracted for calibration (see **Figure 5.2**).

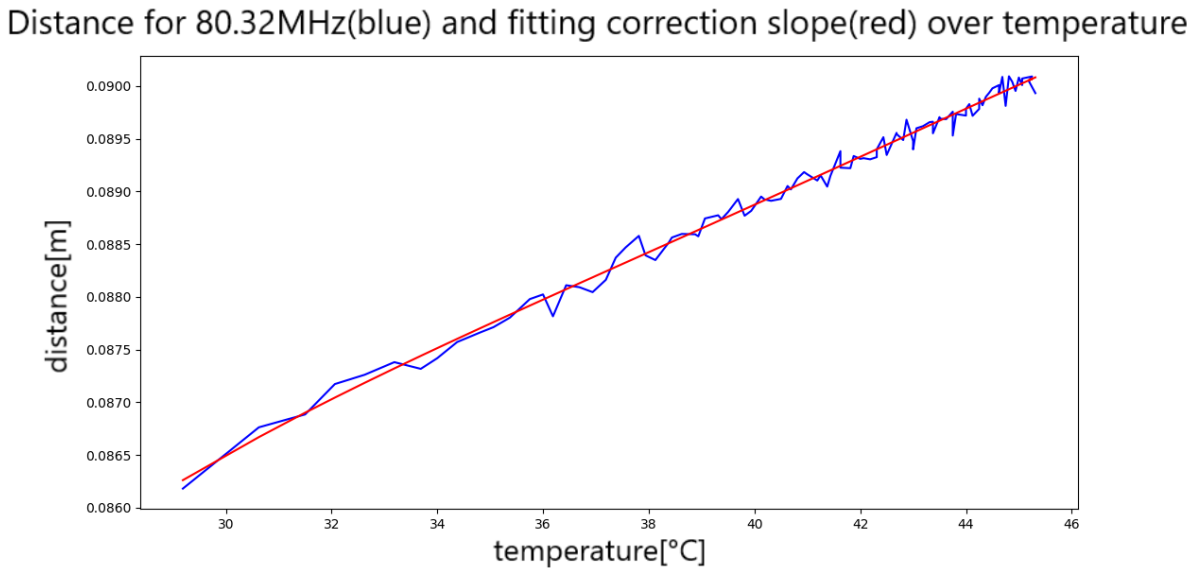

Figure 5.2: Temperature calibration slope

- **Wiggling:**
  The wiggling error compensation was not developed for the calibration routine, this was part of the work. Therefore this error calibration is described more in detail.
  The wiggling error originates from the fact that the cross-correlation function contains harmonics of higher order as the depth estimation algorithm assumes a plain sinusoidal signal. Its compensation is still diffcult though, because the exact shape of the correlation signal is not known. Therefore the error has to be calibrated over the whole distance range which necessitates extensive calibrationsetups. [Gru13, Page 7]
  To implement the wiggling error in the calibration routine, two correction methods were developed and compared. To extract the wiggling shape, it is necessary to make distance measurements over the whole distance range. The camera is mounted on a **linear translation stage** (LTS). The LTS is capable to position the camera very accurate in z-direction. A flat target is mounted in front of the LTS and the LTS gives the distance from the camera to the target.
  The LTS starts from low distance and drives in certain steps to the maximum distance, at every step the distance is measured with the camera and the LTS. The difference between this two values gives the wiggling failure (see **Figure 5.3**).

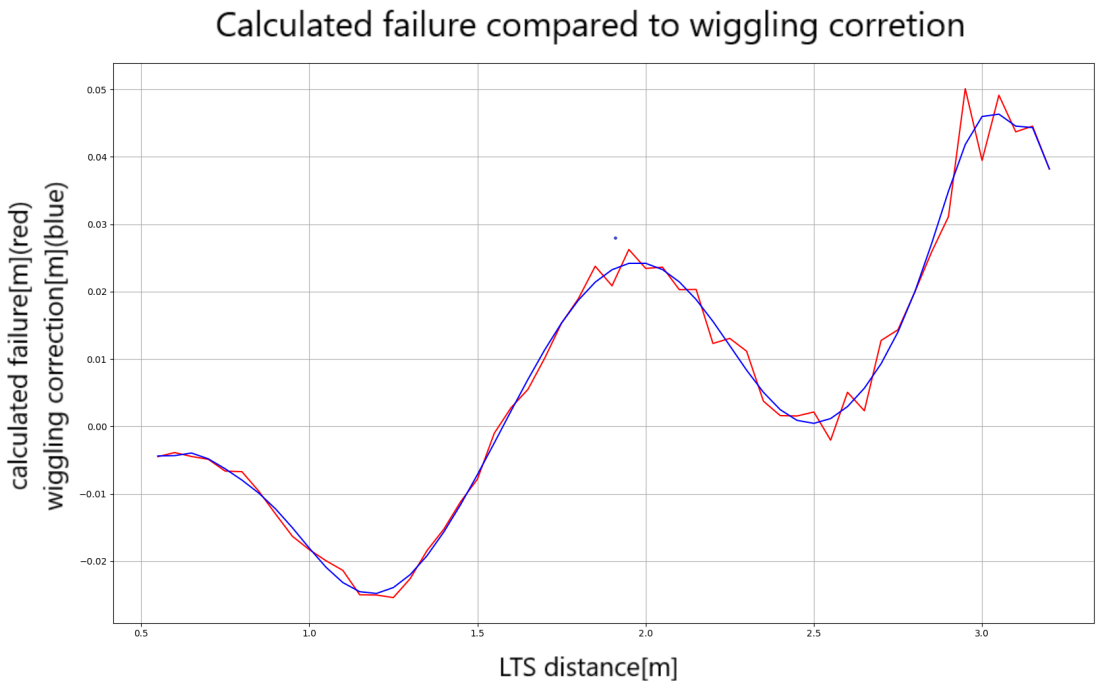

Figure 5.3: Wiggling error

There are now two possibilities too compensate this failure. One is to make a look-up table out of this data and match the measured distance to this table. The second is to extract a fitting polynomial or sinusoidal approximation out of the waveform and correct the measured distance with this approximation. The two methods are compared in **Figure 5.4**

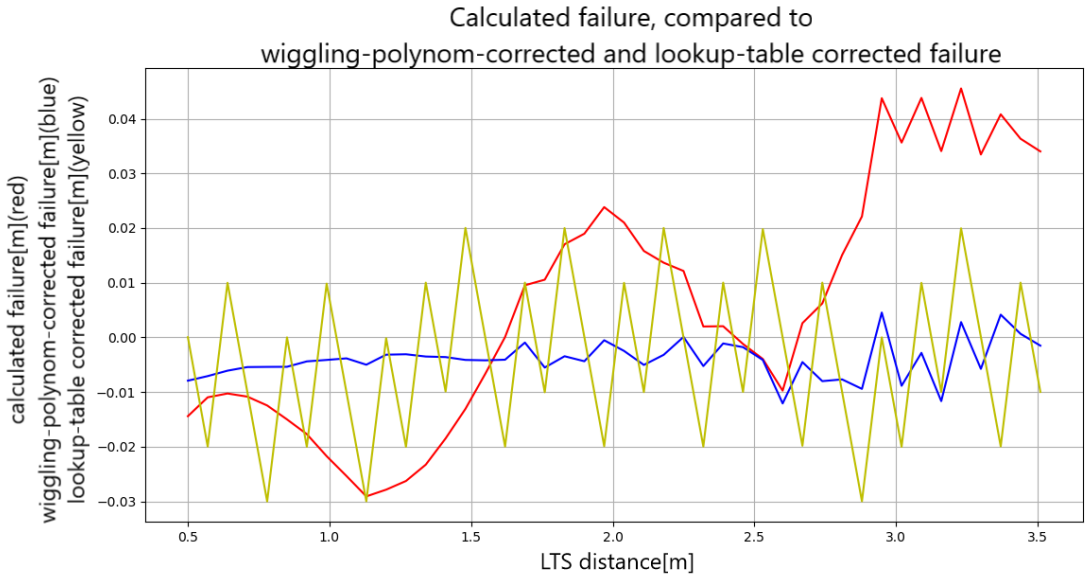

Figure 5.4: Wiggling correction

For a precise correction with the look-up table a lot of data are required. Its recommended to use the polynomial correction method, which is more precise with a lower amount of measurement points and needs much less amount of storage.

5.1.2 Camera performance measurements

After the calibration it is possible to evaluate the camera performance. The performance is evaluated with the LTS, described in chapter **Chapter 5.1.1**. The performance measurement is made with all illumination board-versions, LED850nm, VCSEL-850nm and VCSEL 940nm. Every board needs a dedicated calibration. To reach the best performance, as high as sufficient, modulation-frequencies are configured. To extend the unambiguity range to the required distance, the two frequency measurement (EURZ) are used. For the LED the frequencies are 22.125MHz and 29.5MHz, and for VCSEL 60.24MHz and 80.32MHz.
Figure 5.5 shows the three distance measurements compared to the real distance, given from the LTS.

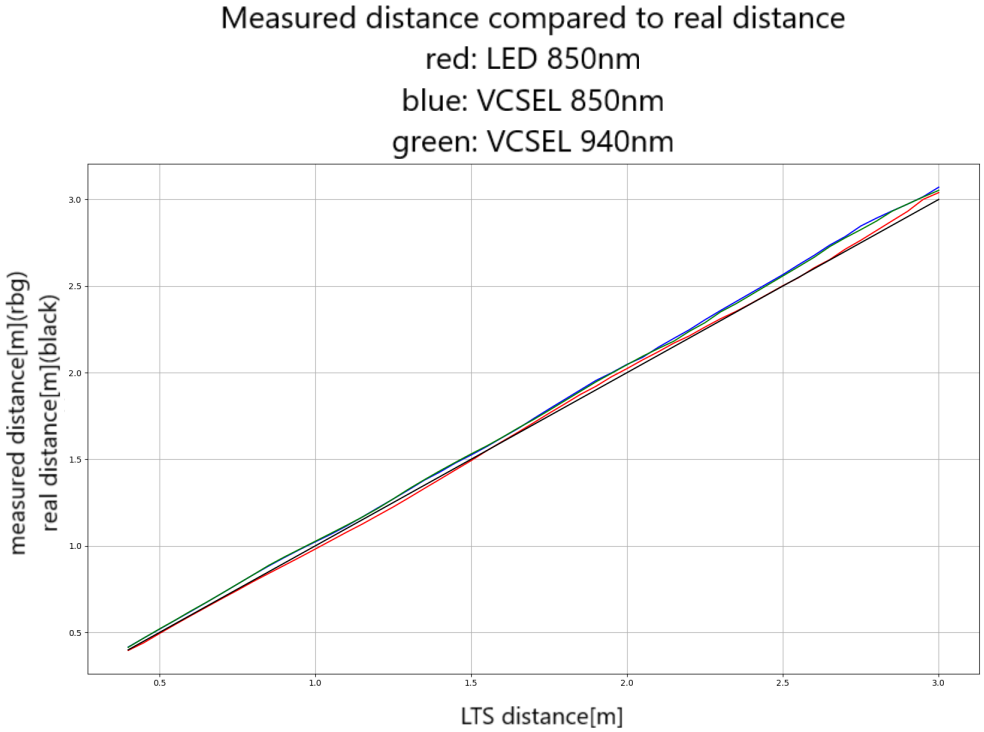

Figure 5.5: Comparison measured- to real-distance

To see the difference between real and measured distance better, the depth failure is printed in the next figure, **Figure 5.6**.

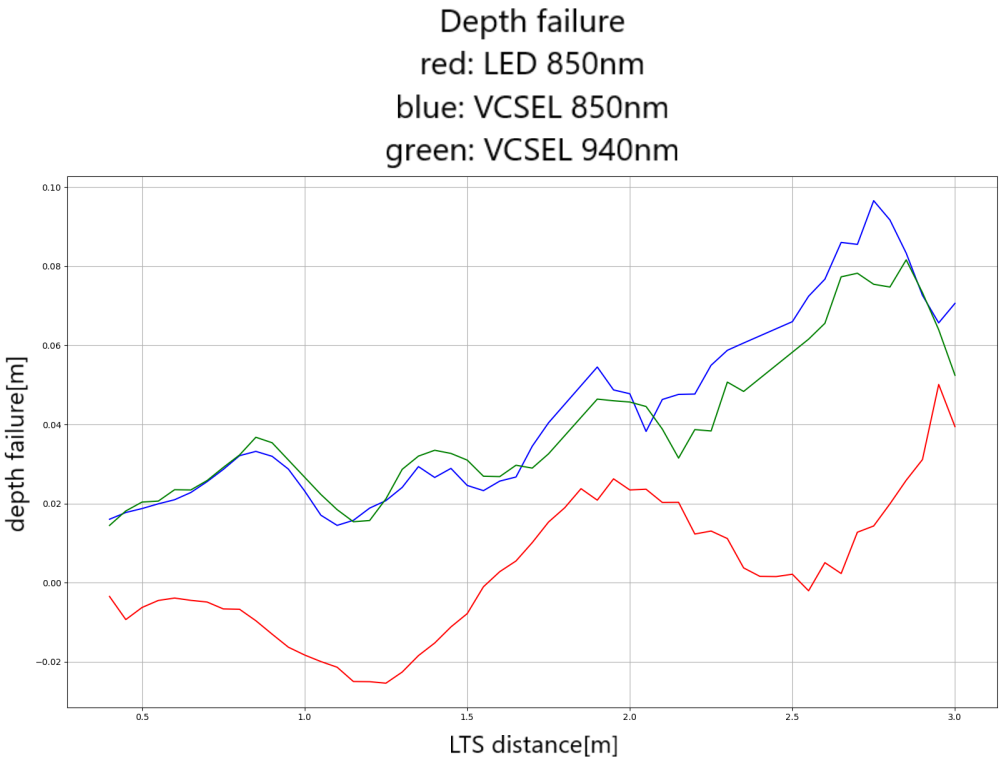

Figure 5.6: Measured depth failure

The depth failure, shown in **Figure 5.6**, consists of three parts:

- **Constant failure:**
  The constant failure results from a small camera position difference, occurred during the changes of the different illumination boards. Most likely this is caused by a not complete parallel alignment of the camera to the target wall.

- **Linear failure:**
  The linear failure has the same root cause as the constant error. Due to the not parallel alignment failure is increasing with increasing distance.
  Another reason for this failure is the so called amplitude related error. The root cause for this error,is not fully understood yet. [Gru13, Page 8]

- **Sinusoidal failure:**
  This failure is caused by the wiggling error explained above.

Now also the wiggling compensation is performed (polynomial approximation), the wiggling error compensation includes also the constant and the linear failure. The results are shown in **Figure 5.7** and **Figure 5.8**.

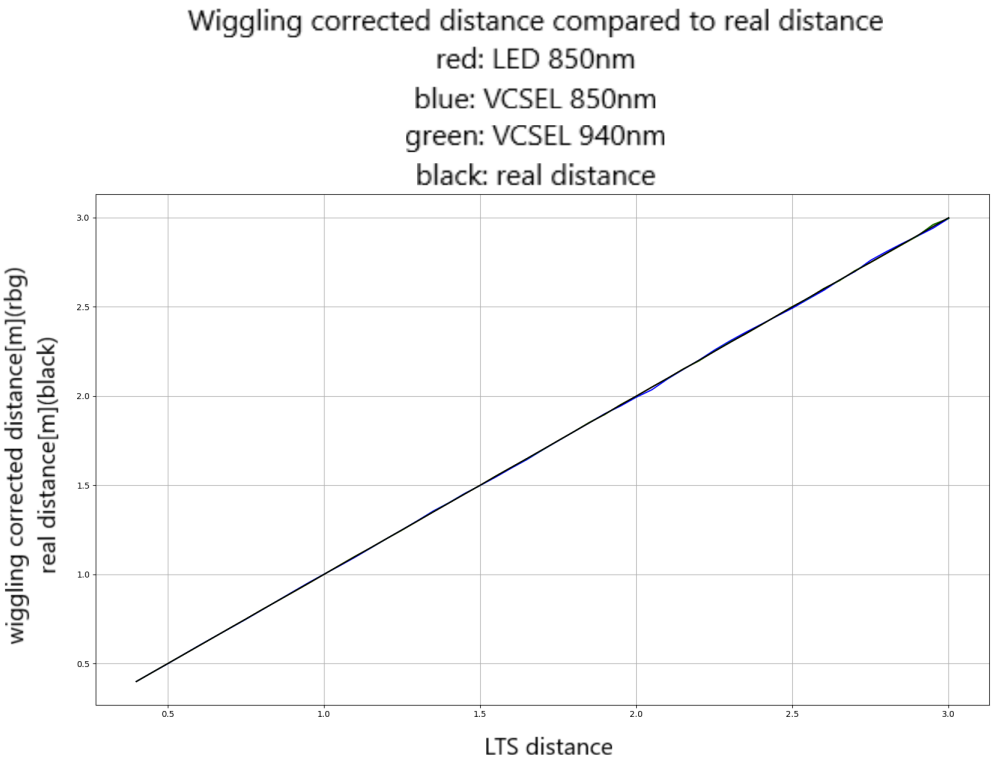

Figure 5.7: Comparison wiggling- corrected to real-distance

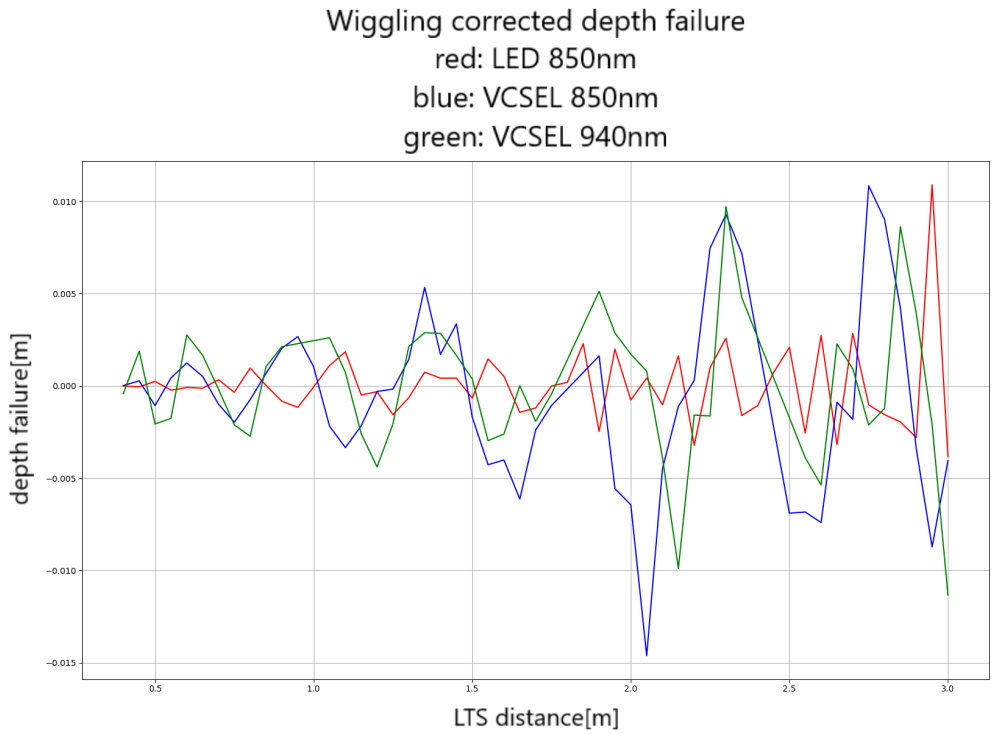

Figure 5.8: Wiggling corrected depth failure

The accuracy is now improved approximately by a factor of 10. The maximum relative-failure, of all illumination types, is 0.71% (VCSEL-850nm at 2.05m), see **Figure 5.9**.

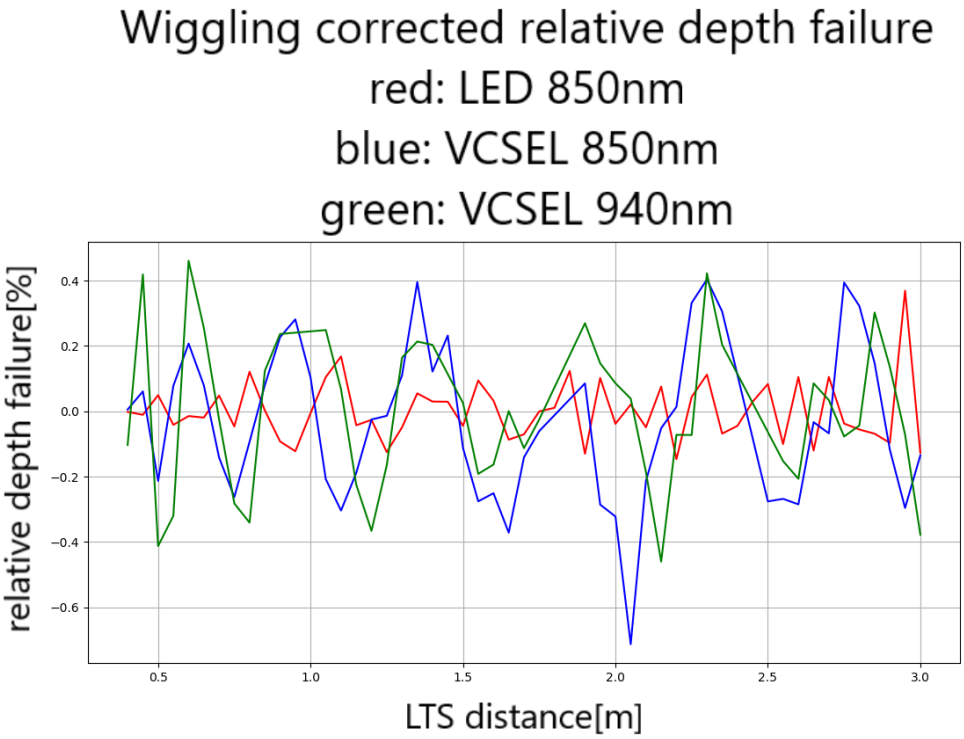

Figure 5.9: Wiggling corrected relative depth failure

In the required range of 2m the maximum relative failures are:

- LED-850nm: 0.168%
- VCSEL-850nm: 0.4%
- VCSEL-940nm: 0.46%

At least **Figure 5.10** shows the depth noise of the ToF-camera. Because of competition reasons the absolute values are not given, but for a recommendation, which illumination should be preferred, the comparison of the depth noises, is very important.

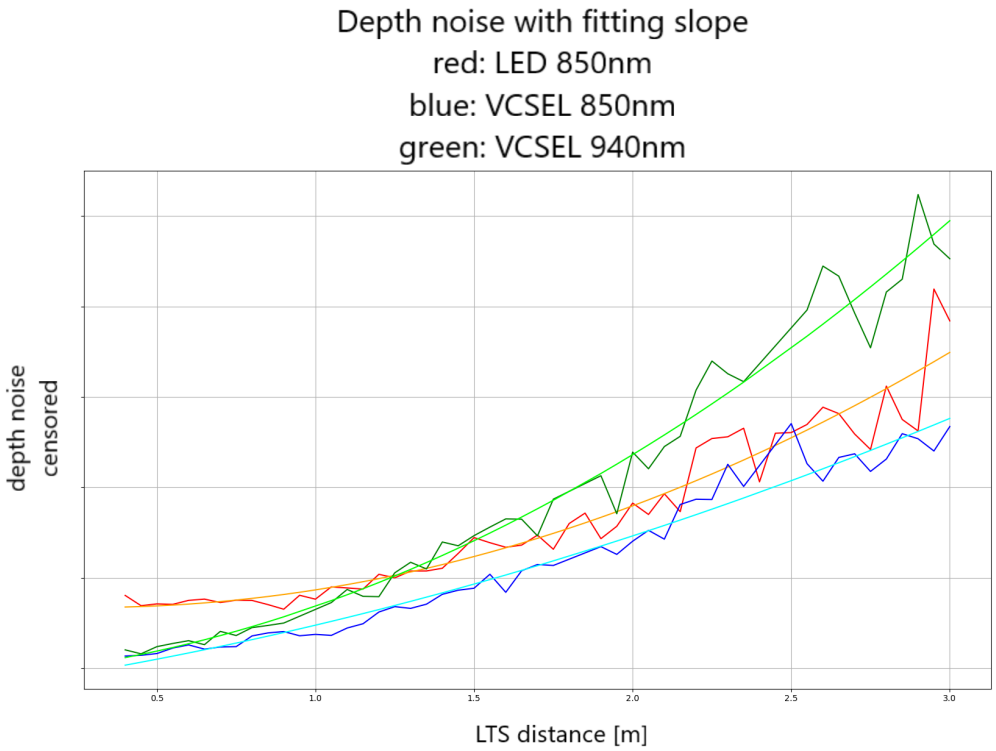

Figure 5.10: Depth noise

The 850nm-VCSEL has the best noise performance. Then the 850nm-LED has the second best, the slight week performance, whole over the distance range, is caused by the lower modulation frequency. The 940nm-VCSEL has the worst performance, this is due to the face that the pixel efficiency is approximately one third less, compared to 850nm. Therefore the depth noise rises much faster then the 850nm-versions.

5.2 Illumination characterization

Next to the sensor performance the illumination is the most affective part for the system performance. This chapter compares the behavior from the three illumination types.

5.2.1 Illumination shape

The first parameter to evaluate is the illumination shape. The illumination shape shows how much area of the imager is how intensive illuminated. Therefore the camera was pointed to flat target and an amplitude image was calculated from the raw data.

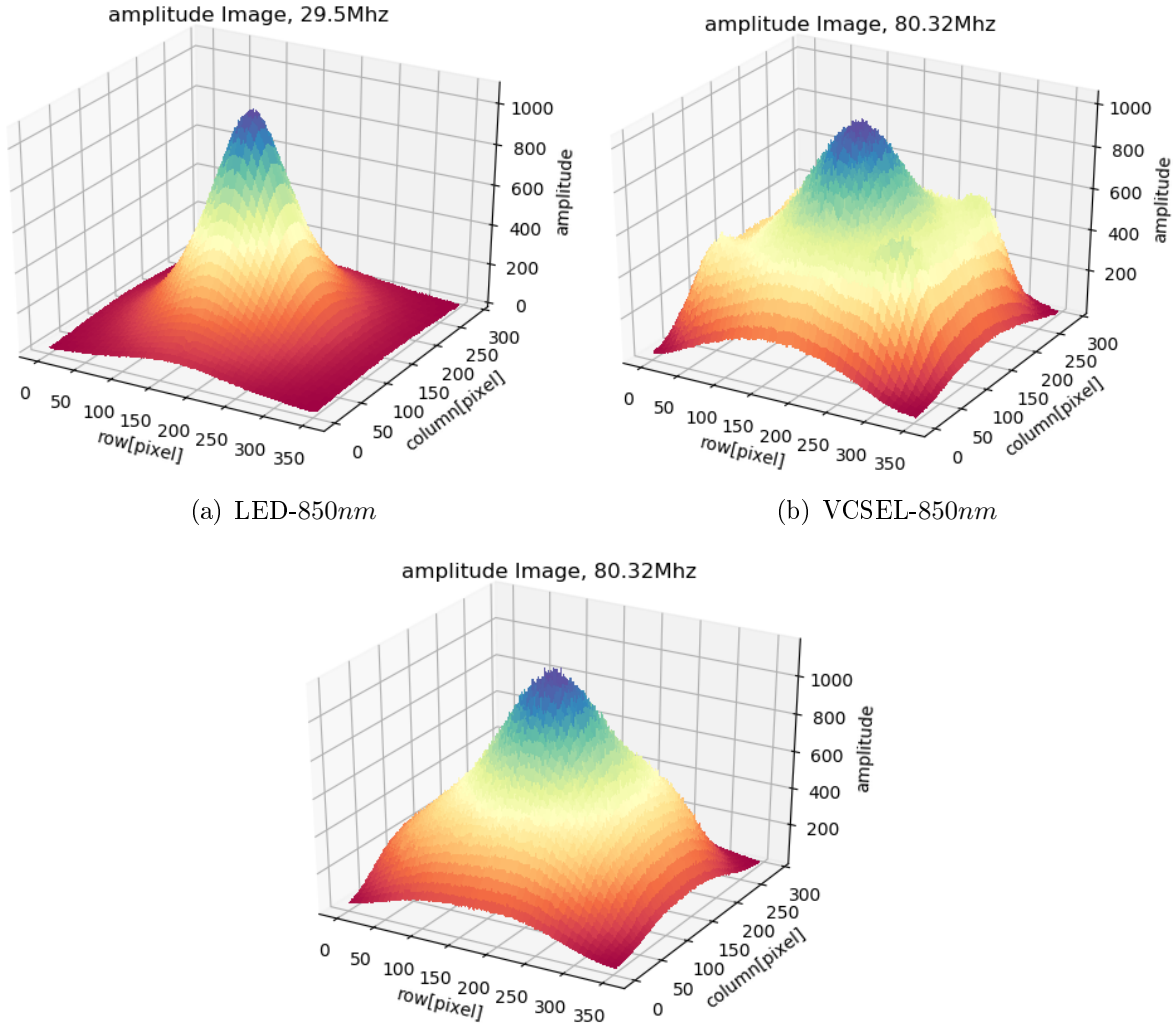

(a) LED-850nm

(b) VCSEL-850nm

(c) VCSEL-940nm

Figure 5.11: Different illumination shapes

Figure 5.11 shows the result of this measurement. The VCSELs, with the proper diffuser, illuminate a rectangular shape nearly all over the imager area. Both have a peak in the middle and the 850nm-VCSEL has also four peaks at the edges.
The illumination from the LED has a peak in the middle and the edges are nearly not illuminated.

5.2.2 Optical-waveform

Low rise- and fall-times from the CW illumination signal effects directly the depth noise of the system. So its important to get the best possible result.
To achieve this target special care must be taken in low impedance layout, sufficient bypass-capacitors and fast switching devises with proper drivers.
The next oscilloscope-plots show the optical-waveform measured with an optical probe. To show the maximum performance of the illumination boards and also to make them comparable, two measurements are performed. One to compare the three illumination types at the highest LED-modulation frequency of $29.5MHz$ (**Figure 5.12**), and one to show the performance of the VCSEL boards at $80.32MHz$ (**Figure 5.13**).

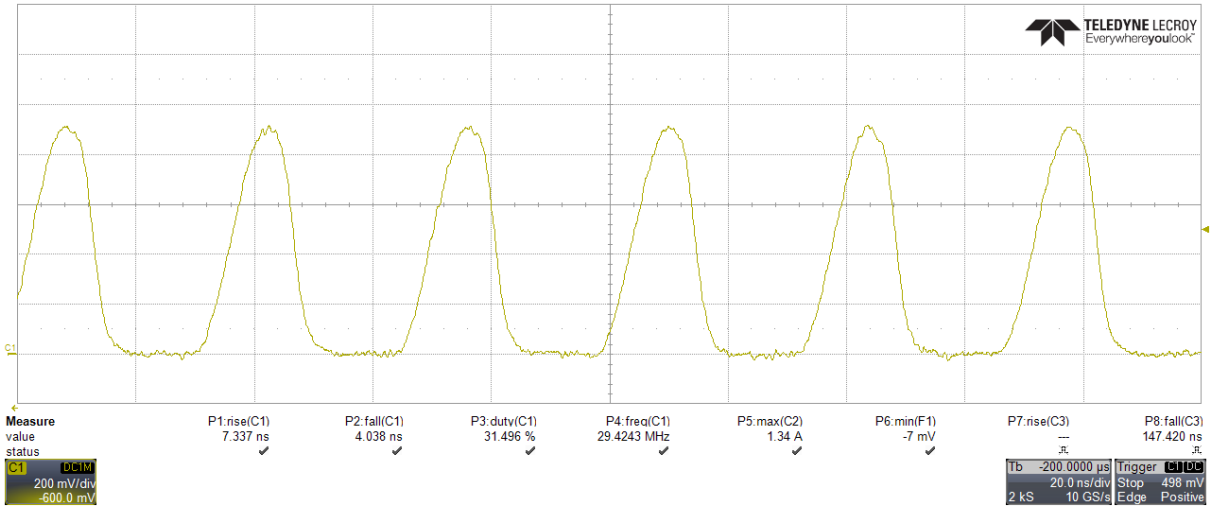

(a) LED-850nm

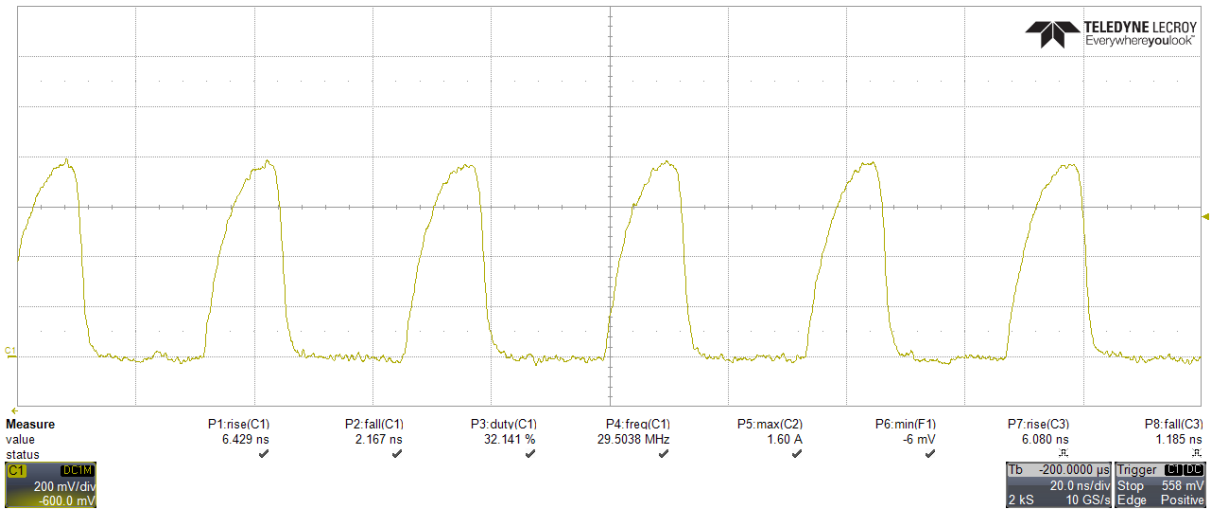

(b) VCSEL-850nm

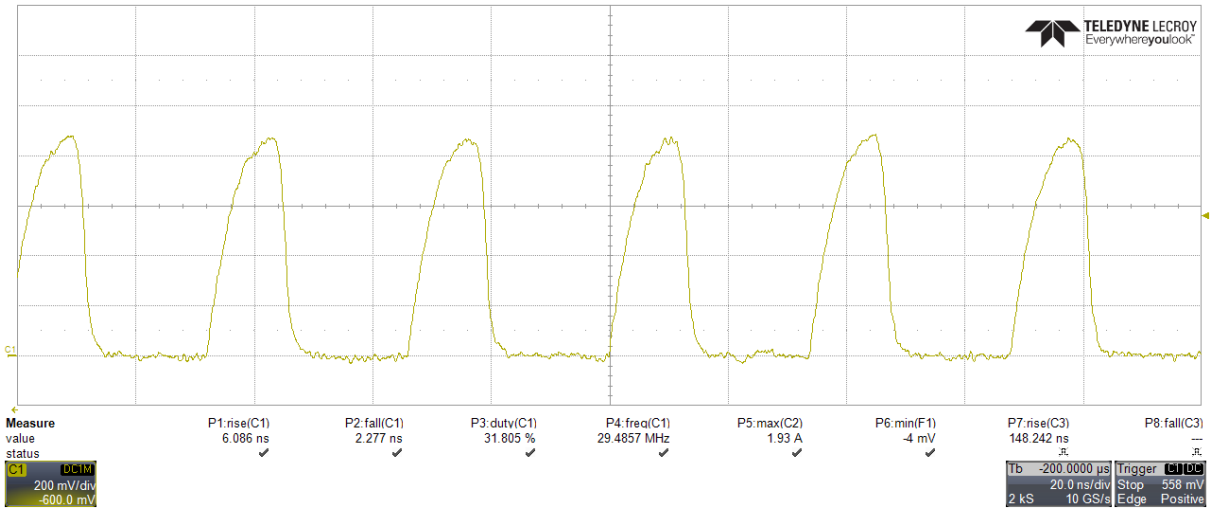

(c) VCSEL-940nm

Figure 5.12: Optical waveform from the different illumination types at 29.5MHz

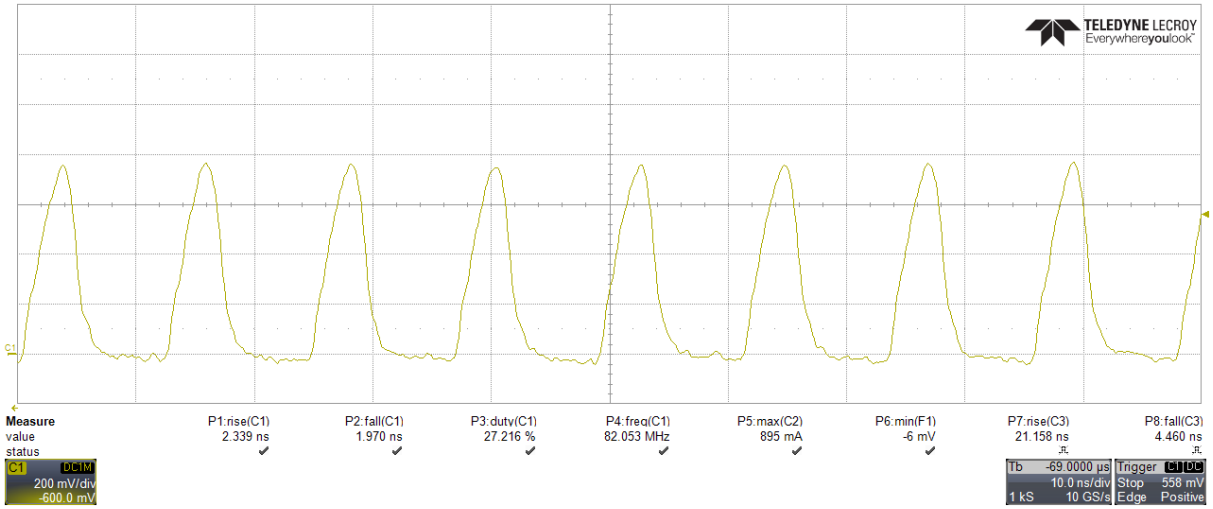

(a) VCSEL-850nm

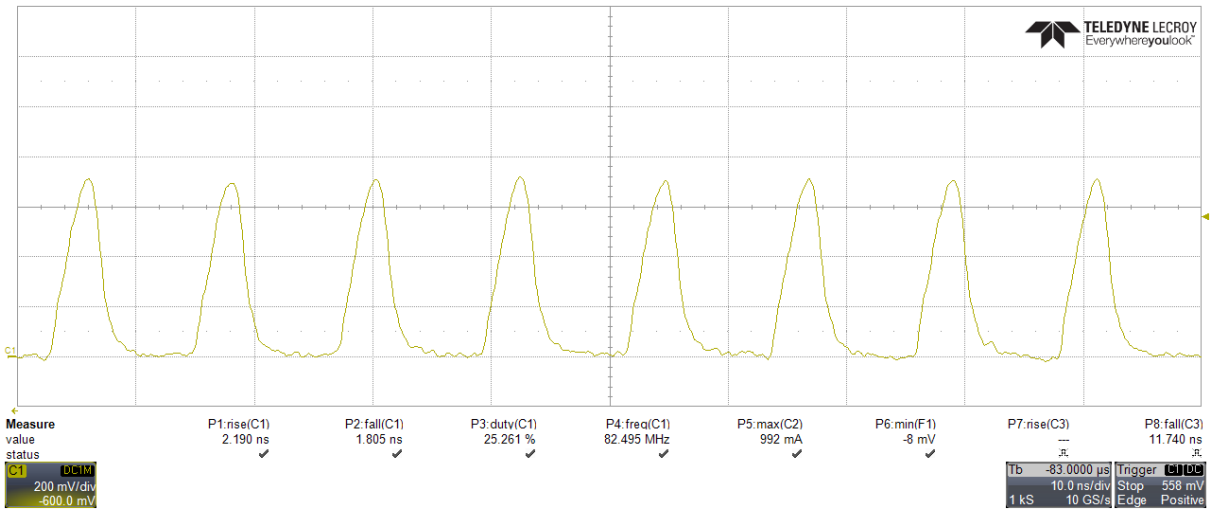

(b) VCSEL-940nm

Figure 5.13: Optical waveform from VCSELs at 80.32MHz

The LEDs can reach 7.3ns rise-time and 4.0ns fall-time. The fall time is only possible because of the additional turn-off speedup circuit. The VCSEL can achieve 2.3ns/2ns (VCSEL-850ns) and 2.2ns/1.8ns (VCSEL-940ns) rise/fall-time.
At 29.5MHz it can be seen that the LED has more a sinusoidal shape and the VCSEL has a sharp rising edge and flattens then until a very fast turn-off.
The duty-cycle is degrading with higher frequencies, this is caused by the limitations of the LVDS-SE converter. If a higher duty-cycle is needed, the imager LVDS signal has to be adjusted.

5.2.3 Optical power and efficiency

At least the optical power, the voltage at the LED/VCSEL-bypass-capacitors, and the current through the LEDs or VCSELs, during illumination, was measured. With this measurements and the values from the figures above, it is possible to calculate the optical peak power (**Equation 5.1**) and the illumination efficiency (**Equation 5.2**), see **Table 5.1**.

$$Power_{Peak} = \frac{Power_{Average}}{FrameRate \times ExposureTime \times DutyCycle} \tag{5.1}$$

$$Efficiency_{Illu} = \frac{\frac{Power_{Average}}{FrameRate \times ExposureTime}}{Voltage_{Illu} \times Current_{Illu}} \tag{5.2}$$

$Power_{Average}$ refers to the whole camera running period. $Voltage_{Illu}$ and $Current_{Illu}$ refer to one integration cycle (one sequence of the basic four sequence measurement). $Power_{Peak}$ is the maximum power over one switching cycle.

Optical-Power Measurement (37,5% Duty-Cycle)						
	850nm LED		850nm VCSEL		940nm VCSEL	
	20,5MHz	29,5MHz	29,5MHz	80,35MHz	29,5MHz	80,35MHz
Average power(mW)	160	110	250	50	280	50
Frame rate(fps)	210	217	217	230	217	230
Exposure Time(us)	725	510	510	180	510	180
Duty Cycle(%)	32	31,5	32,7	27,2	31,8	25,2
Peak Power(W)	3,28407225	3,155384017	6,908159338	4,44018187	7,956114075	4,792577256
Voltage(V)	6,77	6,82	6,72	6,77	6,7	6,8
Current(A)	1,1	1,38	1,6	0,8	1,9	0,9
Efficiency(%)	14,11176474	10,5608607	21,00974799	22,29928856	19,87466045	19,73414164

Table 5.1: Optical power and efficiency

The VCSELs can reach approx. 20% efficiency, this matches also the values from the data sheets.
The LEDs have only an efficiency of about 10%, this is caused by the turn-off circuit. With increasing switching frequency the power consumption from the turn-off circuit increases, this leads to the drop in the LED efficiency from $20.5MHz$ to $29.5MHz$.

5.2.4 Illumination type recommendation

Summarizing **Chapter 5.1.2**, **Chapter 5.2.1**, **Chapter 5.2.2** and **Chapter 5.2.3**, VCSEL-850nm is the recommended illumination type.
Reasons for this recommendation are:

- **Depth-failure:** It seems that the LED has a much better depth performance then the VCSEL-options, but this is only because the illumination beam is much more focused and only the center area is illuminated.
- **Depth-noise:** The VCSEL-850nm illumination has the best depth-noise performance. This is the main advantage compared to the VCSEL-940nm
- **Illumination-shape:** The VCSEL-850nm has the most uniform shape and has also a more intensive illumination at the edges, which leads to the best illumination over the whole FoV of the imager.
- **Optical-waveform:** The two VCSEL options have nearly the same waveform. The 940nm-VCSEL is a little bit faster. The LED is not able to match with the VCSEL-speed.
- **Optical Power:** The 940nm-VCSEL has the highest peak power. But if the reduced imager sensitivity of about one third at 940nm is also taken under account, the 850$nm-$VCSEL has the highest used power.
- **Illumination efficiency:** The efficiency is the highest for the 850nm-VCSEL, the LED is much worse, because of the turn-off speedup circuit.

A further increase of the VCSEL-power should be also possible, especially if they are used with 80MHz-modulation frequency. This needs only a change of the illumination-DCDC output-voltage. The adjustment was not done because of the better comparison between the LEDs and VCSELs and the unknown eye-safety. A increase of the LED-power is not recommended, because otherwise the turn-off speedup circuit gets too hot.

5.3 Thermal image

To evaluate the performance of the heatsink, the camera is running until it reaches its peak temperature, one time attached in the box and one time in free air. To get the maximum temperature, the LED board was attached and modulated with $29.5MHz$.

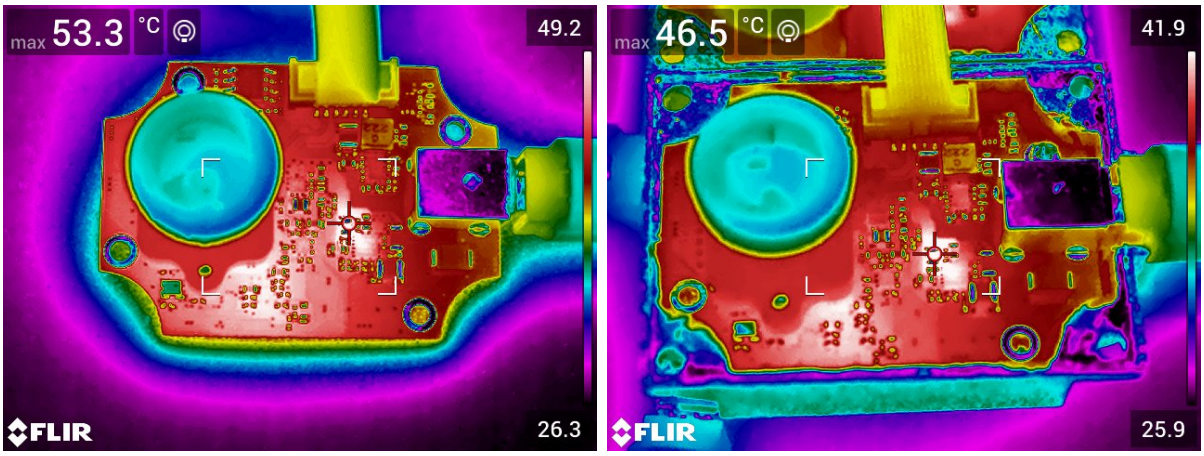

(a) Without heatsink (b) With heatsink

Figure 5.14: Serializer board thermal image

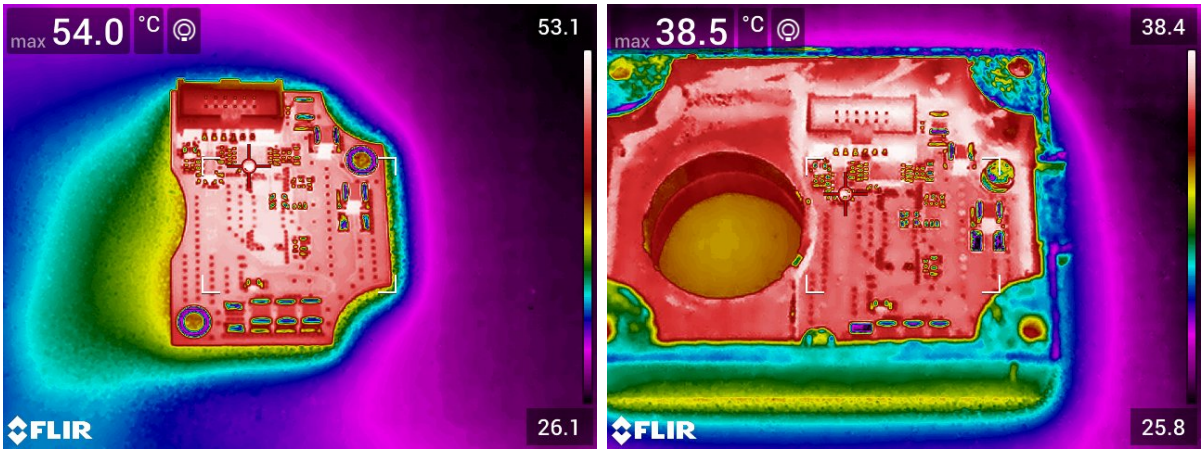

(a) Without heatsink (b) With heatsink

Figure 5.15: Illumination board thermal image

Figure 5.14 and **Figure 5.15** show a significant reduction of the peak temperature, especially at the illumination board.

5.4 Voltage- and current-waveforms

The voltage and current characterization are performed at the highest load, this is the case when using the VCSEL-940nm-illumination at 29.5MHz modulation frequency. The behavior explanation follows the way of current flow. Beginning with the 12V supply current and voltage, and ending at the illumination voltage directly at the VCSEL current limiting resistor.

Starting **Figure 5.16** shows the current flow through the 12V supply voltage beginning at the the 12V power supply and ending at the two illumination and logic DCDCs on the serializer-board. The main current consumption comes from the illumination during the four-sequence integration times.

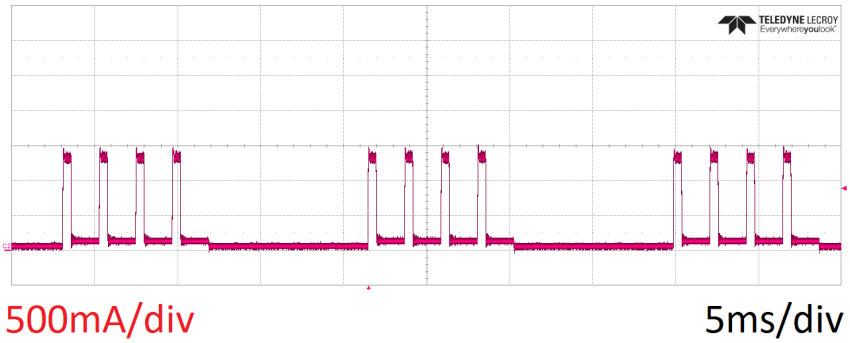

Figure 5.16: Current through 12V supply

Because of this high current, the 12V supply voltage drops by approximately 250mV at the deserializer-board supply input, shown in **Figure 5.17**. This is because the supply regulator needs some time to deliver the needed power. Additional to it, there is also a voltage drop between the supply regulator and the deserialzer, caused by the resistive losses from the connection.

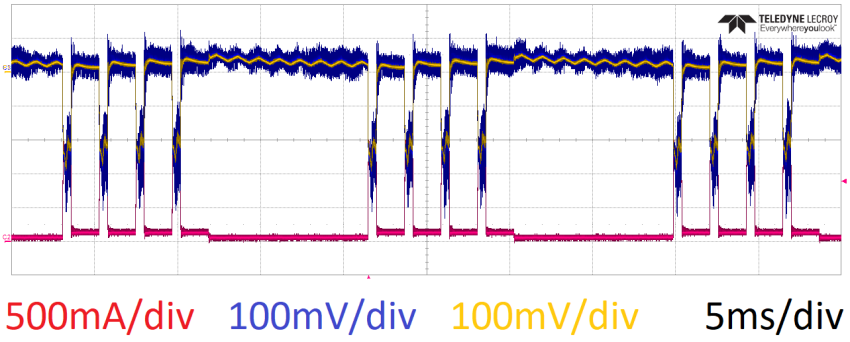

Figure 5.17: 12V supply voltage deserializer-board

In **Figure 5.18** the 12V serializer-board supply voltage shape is printed. The 250mV voltage drop rises on the serializer-board to 900mV. The only reason for this strong increase is the resistance from the connectors and from the 3m long cable.
The remaining 11V are still enough to supply the logic-part 3.6V and the illumination 7V. So there are enough reserves for a further increase of the illumination power.
The current is now measured through the illumination supply. Due to the lower voltage domain the current is increased.

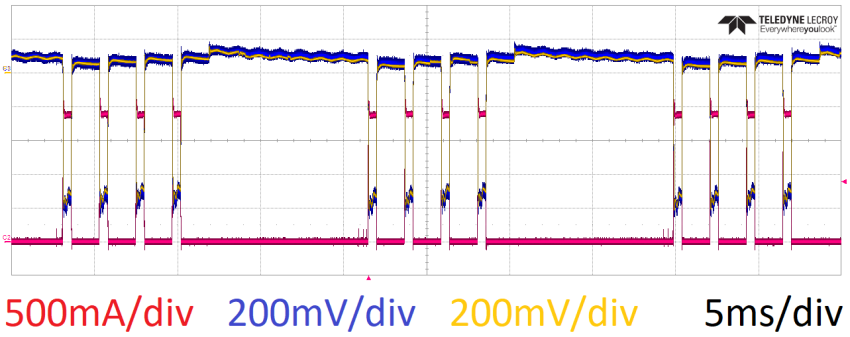

Figure 5.18: 12V supply voltage serializer-board

The propagation of this big voltage drop must be suppressed to the rest of the system. Especially the digital part is sensitive to supply noise.
Between the 12V supply and the digital voltage domains are at least two steps. At first a DCDC converts the voltage to 3.6V. The output of this DCDC is shown in **Figure 5.19a**. It looks like that the output is still very noisy, but a measurement of the noise captured from the oscilloscope probe (see **Figure 5.19b**) shows that the noise is not in the supply rail, but rather captured by the inductive loop, formed by the oscilloscope probe and ground connection.
Nevertheless the voltage drops during the four-sequence measurements, and rises afterward in the range of 20mV peak to peak. This is caused by the inaccuracy of the DCDC.

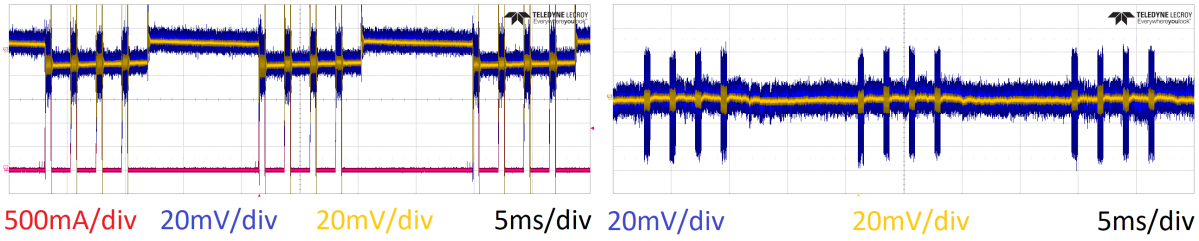

(a) 3.6V logic supply (b) reference noise picture

Figure 5.19: 3.6V logic supply and reference noise measurement

Figure 5.20 shows then the remaining supply ripple of the 3.3V- (a), the 1.8V- (b) and the 1.5V-supply (c). The remaining ripple is in the range of a few mV and has practically no effect on system performance.

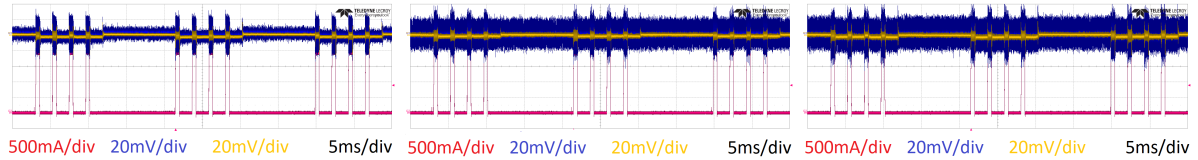

(a) 3.3V supply (b) 1.8V supply (c) 1.5V supply

Figure 5.20: Imager and serializer supply voltages

The next figure, **Figure 5.21** , displays the waveform of the illumination DCDC. To understand this behavior better, it makes sense to look at a picture over more four sequence

cycles and a picture more in detail over one integration period.
When the illumination is turned on, the DCDC is not fast enough to react and the voltage drops by $175mV$. Then the DCDC starts to regulate and is able to keep the voltage at $50mV$ accuracy (**Figure 5.21b**). When the illumination turns off, the DCDC is again not able to react fast enough and charges the output capacitors to $VDD_{Illu} + 100mV$. After this overshoot the DCDC turns off and the attached capacitors discharge until they reach VDD_{Illu} (**Figure 5.21b**).

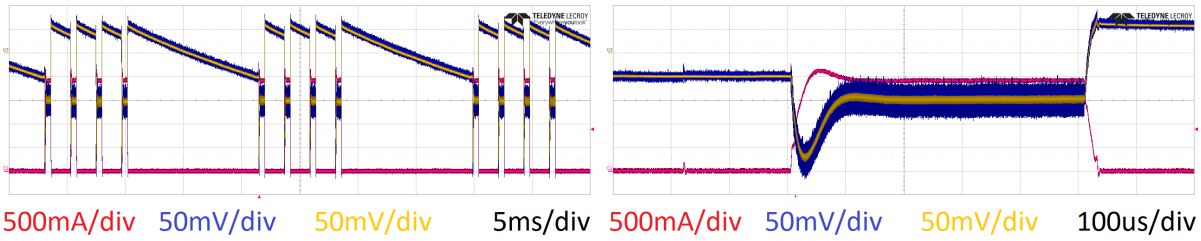

(a) Four sequence (b) One integration period

Figure 5.21: Illumination DCDC output voltage

Figure 5.22 shows the same behavior explained above, measured directly at the illumination current limiting resistor. Due to the resistance between the DCDC and the resistor, the amplitude of the undershoot is much higher. The overshoot is the same, because during this time there is no current which can lead to a resisitive voltage drop.

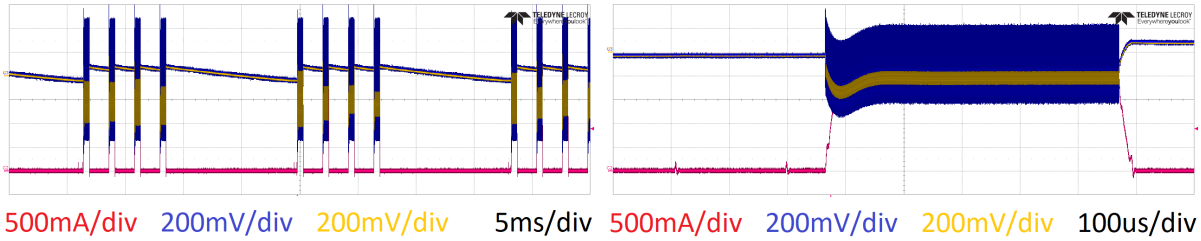

(a) Four sequence (b) One integration period

Figure 5.22: VCSEL supply

Now it is important to know how this supply deviation effects the optical signal. **Figure 5.23** shows the optical power over one integration period. During the turn-on the capacitors are completely charged. Then the power is decreasing until the DCDC delivers the necessary current. Then the power rises again and stays at the level, related to the supply voltage minus the resistive losses of the path.

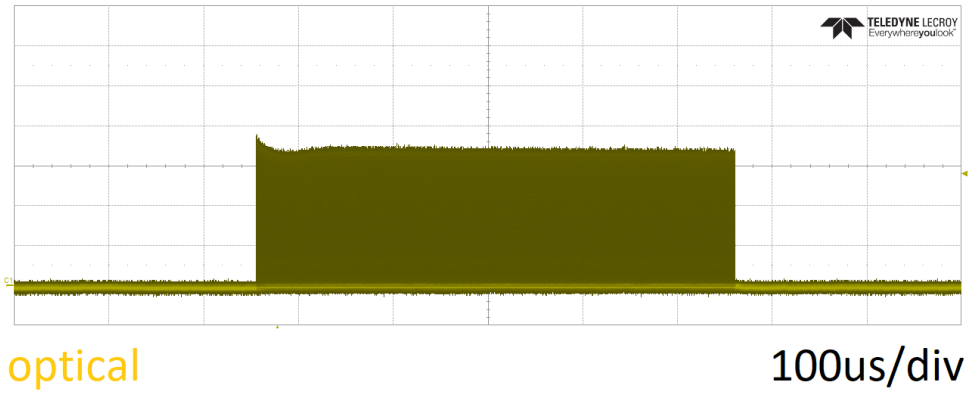

Figure 5.23: Optical signal - one integration period

The drop is not so significant that this causes troubles. If the drop is not tolerable, additional capacitance has to be added on the illumination board to bridge the time needed for the DCDC to react. The additional necessary capacitance is calculated by [Bog17, Page 156]:

$$\begin{aligned} \delta t &= C \times \Delta V \times \frac{V}{P}, \\ C_{Additional} &= \frac{\delta t}{\Delta V \times \frac{V}{P}} = \frac{\delta t}{\Delta V \times \frac{V}{V \times I}} = \frac{\delta t}{\frac{\Delta V}{I}} \\ &= \frac{100us}{\frac{0.2V}{2A}} = 1mF. \end{aligned} \tag{5.3}$$

5.5 Dimensions

The last section of this chapter gives the dimensions from the ToF 3D-camera demonstrator. **Figure 5.24**, **Figure 5.25** and **Figure 5.26** show these dimensions from the different boards and the assembled camera in **Figure 5.27**.

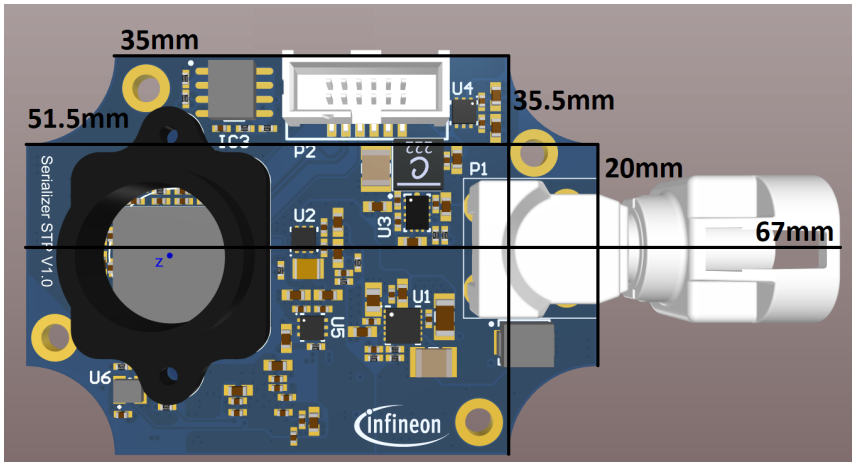

Figure 5.24: Dimension serializer-board

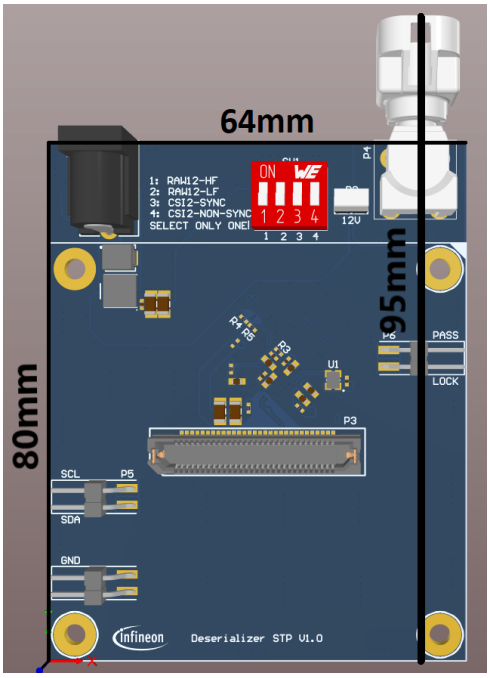

Figure 5.25: Dimension deserializer-board

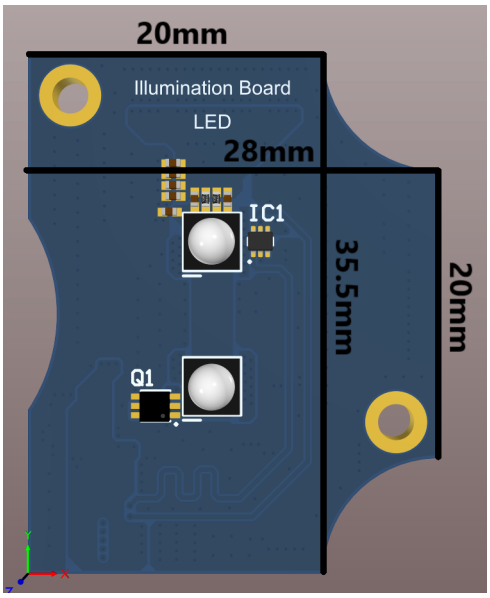

Figure 5.26: Dimension illumination-boards

Due to the integration of the imager on the serializer-board, the reduction of the connection options and LEDS or VCSELs, it was possible to reduce the board areas significantly. The serializer-board shrinks from 51.7cm^2 to 16.3cm^2, the deserializer board from 65.7cm^2 to 51.2cm^2 and the illumination board from 18.4cm^2 to 8.8cm^2.
The reason for the still quite big deserializer board, is that it must be possible to mount the CX3-interface board (40.1cm^2) and the connectors are not fitting under the CX3 board.

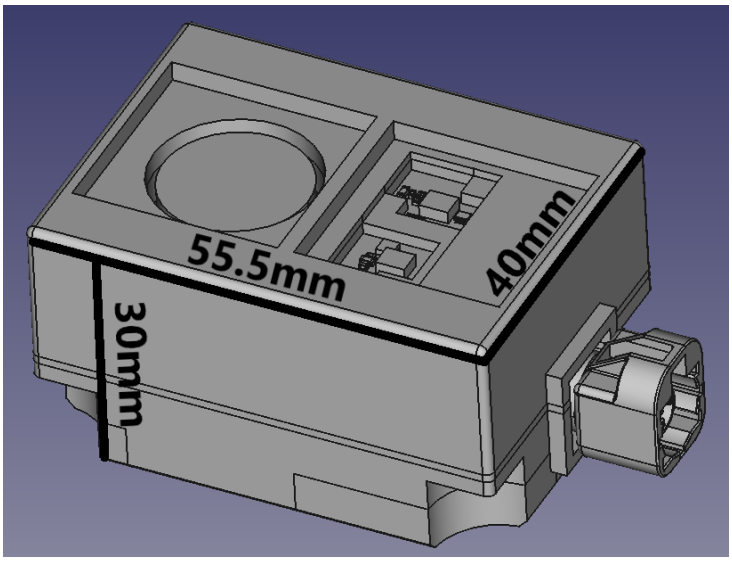

Figure 5.27: Dimension demonstrator-box

The box is designed to be the smallest possible and still mechanical robust solution with proper temperature-conduction. In cross-section the box is only 4mm longer and 4.5mm wider. The height of 30mm results by the skrew-heads, needed for lens mounting, the lens itself (pcb bottom to lens top: 20mm) and the thickness of the optical windows.

6 Conclusion

6.1 Summary and contribution

This master thesis has given an overview of the most common optical distance measurement techniques, Interferometry and Triangulation, with the special case Structured-Light and Time-of-Flight. Then the benefits and drawbacks of these technologies were discussed.

Then Time-of-Flight, the for this thesis used optical distance measurement technique, was described more in detail. Starting with the description of the ToF-system, then the optical signal possibilities for the direct (time) and indirect (phaseshift) ToF measurement. Also the detectors with the corresponding demodulation were explained, this includes the Photo Electric Effect, the Photonic Mixing Device and the Current Assisted Photonic Demodulator. At the end of the theoretical part, the calculation of the phaseshift was derived.

The main outcome of this work is an automotive-grade Time-of-Flight camera demonstrator. This demonstrator fulfills all requirements which were elaborated at the beginning of the thesis. The development started with a proof of concept with the *Texas Instruments Evaluation Kits*. Then the first prototype with a COAX and STP connection option and the first illumination board was built. This board was optimized then to the second modular version with parallel interface.
During the work on the PIF version also a CSI-2 compatible serializer got available. So a version supporting the CSI-2 interface was developed too.
Together with the serializer-deserializer-boards, LED and VCSEL illumination boards were evaluated.
Finally the continuous improving of the demonstrator led to a serializer-deserializer design connected over a two pair STP connector. A simple COAX connector works also, but should be only used for low power devices. It figured out that the first approach with four LEDs or VCSELs is not efficient for a $12V$-power supply. A reduction to two illumination units can reach the same and also higher optical power. For a mechanical robust demonstrator, a box for best temperature conduction and for best optical performance was designed.

The system characterization was performed on a linear translation stage, therefore also a calibration had to be done. Most of the calibration scripts were already developed, but modifications and the calibration of the wiggling error had to be made.
The illumination signal is for the system performance a key parameter, so it was analyzed in perspective of the illumination shape, respectively the FoV, the waveform, power and electrical to optical efficiency. These measurements led to a recommendation for the $850nm$-VCSEL illumination.
Also the power distribution network was analyzed due to its stability and noise performance.

For further serializer-deserializer designs using the *Texas Instruments DS90UB935/36*, an Application Note was written (see **Appendix A**). This Application Note describes the board schematics together with the Bill of Materials, listens and explains the register settings and gives layout recommendations regarding the supply-rails, data interfaces and thermal considerations.

To perform this master thesis it was necessary to get confident with the ToF measurement and the *Infineon IRS1125A*. I learned how to make a proper electric design, in respective to high speed data interfaces, power distribution networks and high switching currents. At least I got familiar with the characterization of ToF-systems.

6.2 Outlook

This topic gives a lot possibilities for further research. The next step will be to adjust the eye-safety circuits from the VCSEL illumination-boards. Maybe this also leads to a possible increase of the optical output power.
For different use cases a change of the FoV makes sense. Therefore more versions with different lenses and VCSELs can be developed.
This demonstrator was only designed for interior use. For automotive driving also an exterior ToF-camera can improve the world sensing in short- to mid-range. For exterior an IP68 certification would be necessary. To increase the maximum optical output power for exterior use it makes sense to increase the supply voltage to $24V$ or $48V$.

References

[Alb07] Martin Albrecht. *Untersuchung von Photogate-PMD-Sensoren hinsichtlich qualifzierender Charakterisierungsparameter und -methoden*. PhD thesis, Universität Siegen, 2007.

[BF86] Glenn Beheim and Klaus Fritsch. Range finding using frequency-modulated laser diode. *Applied Optics*, 25:1439–1442, 1986.

[Bog17] Eric Bogatin. *Signal and Power Integrity*. Pearson, third edition, 2017.

[Car13] David Cardinal. Making gesture recognition work: Lessons from Microsoft Kinect and Leap. `https://www.extremetech.com/extreme/160162-making-gesture-recognition-work-lessons-from-microsoft-kinect-and-leap`, 2013. [Online; accessed 15-October-2019].

[Gru13] Johannes Gruenwald. Investigation of Systematic Errors in Time-of-Flight Imaging. Master's thesis, TU Graz, 2013.

[Inf16a] Infineon. Infineon REAL3 3D Image Sensor bringup platform. User Manual 1.0, Infineon Technologies AG, oct 2016.

[Inf16b] Infineon. REAL3TM IRS1125A. Datasheet 0.1, Infineon Technologies AG, oct 2016.

[Kar09] UNI Karlsruhe. Funktionsweise und Einsatz von Interferometern. `http://www.lehrer.uni-karlsruhe.de/~za134/12Ph2/GFS%20Interferometer/Physik-GFS-Interferometer-Handout.pdf`, 2009.

[Kre16] Martin Krehel. 3D Imaging Technologies Infineon REAL3TM Sensor Family. Whitepaper, Infineon Technologies AG, jul 2016.

[Lan00] Robert Lange. *3D Time-of-Flight Distance Measurement with Custom Solid-State Image Sensors in CMOS/CCD-Technology*. PhD thesis, University of Siegen, 2000.

[LG19] LG. LG G8 ThinQ. `https://www.lg.com/us/mobile-phones/g8-thinq/air-motion`, 2019. [Online; accessed 15-October-2019].

[Mis17] John Misachi. Who Invented The First Camera? `https://www.worldatlas.com/articles/who-invented-the-first-camera.html`, 2017. [Online; accessed 14-October-2019].

[Mor89] I. Moring. Acquisition of three-dimensional image data by a scanning laser rangefinder. *Optical Engineering*, 28(897-905):1439–1442, 1989.

[Onl17] Spiegel Online. CamBoard pico monstar. `https://www.spiegel.de/netzwelt/gadgets/apple-face-id-beim-iphone-x-so-funktioniert-die-neue-gesichtserkennung-a-1170336.html`, 2017. [Online; accessed 15-October-2019].

[Opt19] Edmund Optics. NIR Quarzglasfenster. `https://www.edmundoptics.de/p/25-x-25mm-nir-i-1lambda-fused-silica-window/37319/`, 2019. [Online; accessed 23-October-2019].

[pmd] pmd. CamBoard pico monstar. https://pmdtec.com/picofamily/monstar/. [Online; accessed 15-October-2019].

[Sch99] R. Schwarte. *Principles of 3-D Imaging Techniques*, chapter Handbook of Computer Vision and Applications. Academic Press, 1999.

[SHXH95] R. Schwarte, H. Heinol, Z. Xu, and K. Hartmann. A new active 3D-Vision system based on rf-modulation interferometry of incoherent light. *SPIE 2588, Intelligent Robots and Computer Vision XIV*, 2588, 1995.

[Tex14a] TexasInstruments. Introduction to the Time-of-Flight (ToF) System Design. Users Guide D, Texas Instruments, may 2014.

[Tex14b] TexasInstruments. Sending Power Over Coax in DS90UB913A Designs. Application report, Texas Instruments, June 2014.

[Tex16a] TexasInstruments. DS90UB933-Q1 FPD-Link III Serializer for 1-MP/60-fps Cameras 10/12 Bits,100 MHz. Datasheet Rev. A, Texas Instruments, august 2016.

[Tex16b] TexasInstruments. DS90UB933-Q1EVM Users Guide. Users Guide Rev. A, Texas Instruments, July 2016.

[Tex16c] TexasInstruments. DS90UB964-Q1 Quad FPD-Link III Deserializer Hub. Datasheet Rev. A, Texas Instruments, july 2016.

[Tex16d] TexasInstruments. DS90UB964-Q1EVM Users Guide. Users Guide Rev. A, Texas Instruments, July 2016.

[Tex18a] TexasInstruments. DS90UB935-Q1 FPD-Link III 3-Gbps Serializer With CSI-2 Interface. Datasheet Rev. A, Texas Instruments, july 2018.

[Tex18b] TexasInstruments. DS90UB936-Q1 Dual 3 Gbps FPD-Link III Deserializer Hub With MIPI CSI-2 Outputs. Datasheet Rev. B, Texas Instruments, september 2018.

[Wik17] Wikipedia. Photoelectric effect. https://en.wikipedia.org/w/index.php?title=Photoelectric_effect&oldid=791769392, 2017. [Online; accessed 11-August-2017].

[ZSD96] E. Zimmermann, Y. Salvadé, and R. Dändliker. Stabilized three-wavelength source calibrated by electronic means for high-accuracy absolute distance measurement. *Optics Letters*, 21:531–533, 1996.

Nomenclature

ToF ..... Time of Flight
LiDAR.....Light Detection and Ranging
CW ..... Continuous Wave
SNR ..... Signal to Noise Ratio
LED ..... Light Emitting Diode
EURZ ..... Extended Unambiguity Range Sequence
CAPD ..... Current Assisted Photonic Demodulator
PMD ..... Photonic Mixing Device
CCD..... Charge Coupled Devise
PEE ..... Photo Electric Effect
SRF..... Sensor Response Function
ADC ..... Analog to Digital Converter
ECD ..... Equivalent Circuit Diagram
VCSEL ..... Vertical Cavity Surface Emitting Laser
IR ..... Infrared
ECU.....Electronic Control Unit
MIPI ..... Mobile Industry Processor Interface
CSI ..... Camera Serial Interface
PCB ..... Printed Circuit Board
LVDS ..... Low Voltage Differential Signal
COAX ..... Coaxial Cable
PIF ..... Parallel Interface
FoV ..... Field of View
PoC ..... Power over Coax
I^2C ..... Inter-Integrated Circuit
USB ..... Universal Serial Bus
SoC..... System On a Chip BGA ..... Ball Grid Array
HDRZ ..... High Dynamic Range Sequence
SERDES ..... Serializer and Deserializer
STP ..... Shielded Twisted-Pair
GPIO ..... General Purpose Input/Output
SE.....Single Ended
UART ..... Universal Asynchronous Receiver Transmitter
FPPN ..... Frame Pattern Phase Noise

List of Figures

List of Tables

Appendix:

A: Serializer-Deserializer design guideline

B: Measurement and Characterization results